NUREG/CR-3334
Volume 2
ORNL/TM-8787/V2

ornl

OAK RIDGE NATIONAL LABORATORY

UNION CARBIDE

OPERATED BY
UNION CARBIDE CORPORATION
FOR THE UNITED STATES
DEPARTMENT OF ENERGY

Heavy-Section Steel Technology Program Quarterly Progress Report for April–June 1983

C. E. Pugh

Prepared for the U.S. Nuclear Regulatory Commission
Office of Nuclear Regulatory Research
Under Interagency Agreements DOE 40-551-75 and 40-552-75

Printed in the United States of America. Available from
National Technical Information Service
U.S. Department of Commerce
5285 Port Royal Road, Springfield, Virginia 22161

Available from

GPO Sales Program
Division of Technical Information and Document Control
U.S. Nuclear Regulatory Commission
Washington, D.C. 20555

NUREG/CR-3334
Volume 2
ORNL/TM-8787/V2
Dist. Category RF

Engineering Technology Division

HEAVY-SECTION STEEL TECHNOLOGY PROGRAM QUARTERLY PROGRESS REPORT FOR APRIL-JUNE 1983

C. E. Pugh

Manuscript Completed - October 28, 1983
Date Published - December 1983

Prepared for the
U.S. Nuclear Regulatory Commission
Office of Nuclear Regulatory Research
Under Interagency Agreements DOE 40-551-75 and 40-552-75

NRC FIN No. B0119

Prepared by the
OAK RIDGE NATIONAL LABORATORY
Oak Ridge, Tennessee 37830
operated by
UNION CARBIDE CORPORATION
for the
U.S. DEPARTMENT OF ENERGY
under Contract No. W-7405-eng-26

CONTENTS

LIST OF FIGURES

LIST OF TABLES

PREFACE

The Heavy-Section Steel Technology (HSST) Program, which is sponsored by the Nuclear Regulatory Commission, is an engineering research activity devoted to extending and developing the technology for assessing the margin of safety against fracture of the thick-walled steel pressure vessels used in light-water-cooled nuclear power reactors. The program is being carried out in close cooperation with the nuclear power industry. This report covers the work performed in April-June 1983. The work performed by Oak Ridge National Laboratory (ORNL) and by subcontractors is managed by the Engineering Technology Division. Major tasks at ORNL are carried out by the Engineering Technology Division and the Metals and Ceramics Division. Prior progress reports on this program are ORNL-4176, ORNL-4315, ORNL-4377, ORNL-4463, ORNL-4512, ORNL-4590, ORNL-4653, ORNL-4681, ORNL-4764, ORNL-4816, ORNL-4855, ORNL-4918, ORNL-4971, ORNL/TM-4655 (Vol. II), ORNL/TM-4729 (Vol. II), ORNL/TM-4805 (Vol. II), ORNL/TM-4914 (Vol. II), ORNL/TM-5021 (Vol. II), ORNL/TM-5170, ORNL/NUREG/TM-3, ORNL/NUREG/TM-28, ORNL/NUREG/TM-49, ORNL/NUREG/TM-64, ORNL/NUREG/TM-94, ORNL/NUREG/TM-120, ORNL/NUREG/TM-147, ORNL/NUREG/TM-166, ORNL/NUREG/TM-194, ORNL/NUREG/TM-209, ORNL/NUREG/TM-239, NUREG/CR-0476 (ORNL/NUREG/TM-275), NUREG/CR-0656 (ORNL/NUREG/TM-298), NUREG/CR-0818 (ORNL/NUREG/TM-324), NUREG/CR-0980 (ORNL/NUREG/TM-347), NUREG/CR-1197 (ORNL/NUREG/TM-370), NUREG/CR-1305 (ORNL/NUREG/TM-380), NUREG/CR-1477 (ORNL/NUREG/TM-393), NUREG/CR-1627 (ORNL/NUREG/TM-401), NUREG/CR-1806 (ORNL/NUREG/TM-419), NUREG/CR-1941 (ORNL/NUREG/TM-437), NUREG/CR-2141/Vol. 1 (ORNL/TM-7822), NUREG/CR-2141, Vol. 2 (ORNL/TM-7955), NUREG/CR-2141, Vol. 3 (ORNL/TM-8145), NUREG/CR-2141, Vol. 4 (ORNL/TM-8252), NUREG/CR-2751, Vol. 1 (ORNL/TM-8369/V1), NUREG/CR-2751, Vol. 2 (ORNL/TM-8369/V2), NUREG/CR-2751, Vol. 3 (ORNL/TM-8369/V3), NUREG/CR-2751, Vol. 4 (ORNL/TM-8369/V4), and NUREG/CR-3334, Vol. 1 (ORNL/TM-8787/V1).

SUMMARY

1. PROGRAM ADMINISTRATION AND PROCUREMENT

The Heavy-Section Steel Technology (HSST) Program is an engineering research activity conducted by the Oak Ridge National Laboratory (ORNL) for the Nuclear Regulatory Commission (NRC) in coordination with other research sponsored by the federal government and private organizations. The program comprises studies related to all areas of the technology of materials fabricated into thick-section primary-coolant containment systems of light-water-cooled nuclear power reactors. The principal area of investigation is the behavior and structural integrity of steel pressure vessels containing cracklike flaws. Current work is organized into the following tasks: (1) program administration and procurement, (2) fracture-mechanics analysis and investigations, (3) investigations of irradiated materials, (4) thermal-shock investigations, (5) pressure vessel investigations, (6) stainless steel cladding investigations, and (7) environmentally assisted crack-growth studies.

The work performed at ORNL and under existing research and development subcontracts is included in this report. During the quarter, 11 program briefings, reviews, or presentations were made, and 3 technical reports were published. The meetings included a comprehensive program review before the Vessel Integrity Review Group on June 14, 1983.

2. FRACTURE-MECHANICS ANALYSES AND INVESTIGATIONS

Extensive analyses were performed to determine material parameters and pressure-temperature transients compatible with pressurized-thermal-shock (PTS) test scenarios and with the capability of the PTS test facility at ORNL. The computer program OCA/USA was used to determine stress-intensity factors K_I and times when $K_I = K_{Ic}$, $K_I = K_{Ia}$, and $\dot{K}_I < 0$. An upper-shelf fracture model was implemented in these analyses to examine the scenario in which the crack initiates in cleavage and propagates into a region where the temperatures are sufficiently high for ductile fracture.

In its HSST support program, Battelle-Columbus Laboratories (BCL) carried out work in support of structural tests, crack-reinitiation tests, and crack-arrest studies. In connection with structural test support, TSE-7, PTSE-1, and low-upper-shelf weldment (from ITV-8A) test materials were received by BCL. Crack-arrest testing will be performed on each. Further evidence was obtained suggesting that the reinitiation technique using compact specimens is capable of providing conservative estimates of initiation toughness in thermal-shock cylinders. Further crack-arrest experiments were performed on the retempered thermal-shock material from TSE-6 and involved thicker specimens and positive temperature gradients. The crack-arrest toughness agreed with the thinner-specimen isothermal data obtained earlier. Values of K_a associated with reinitiated cleavage cracks also appear to give good agreement with the balance of the data.

For temperatures above RT_{NDT} + 50°C, the K_a vs T data obey a thermally activated rate-process equation of the kind found for ESSO tests. Finally, impact tests of specimens fabricated from electron-beam weld zones suggest that failure of cracks in duplex specimens to penetrate the test sections is related more to base-metal behavior than to weld zone behavior. The computerized crack-arrest data base task continued with 113 points now included.

The study continued at the University of Maryland on understanding the transition from brittle cleavage at lower temperatures to ductile fracture at high temperatures. During the current report period, fabrication and assembly of the testing fixtures for spring-in-series testing of large-bend specimens of A508 steel were nearly completed. Fractographic and microstructural examinations of specimens of A514 bridge steel fractured during spring-in-series testing at Piccatini Arsenal were started. Some preliminary tests were performed in an effort to resolve the controversy regarding treatment of accumulated plastic displacements in crack-arrest testing. Improvements were made to the SAMCR dynamic fracture code, which substantially enhance its usefulness for modeling and predicting run/arrest phenomena.

3. INVESTIGATION OF IRRADIATED MATERIALS

The main sets of Charpy V-notch (CVN) tests on both unirradiated and irradiated specimens have been completed in the Fourth Irradiation Series cooperative program by ORNL and Materials Engineering Associates (MEA). Scoping tests on unirradiated fracture toughness (1TCS) specimens were also begun. The transition temperature shifts and the upper energy drops determined from statistical analyses of the CVN data were found to be less than the guideline values in the *NRC Regulatory Guide 1.99*. Work continued on high-copper weldment fabrication for the Fifth Irradiation Series, and the prototype 4TCS capsule is scheduled for installation in the Oak Ridge Research Reactor early in the next quarter. The first irradiation experiment of stainless steel cladding (Seventh Irradiation Series) was initiated at the Nuclear Science and Technology Facility reactor and is expected to be completed by the end of July. The CVN and tensile specimens are included.

4. THERMAL-SHOCK INVESTIGATIONS

During this period, thermal-shock experiment TSE-7 was conducted, the ORNL probabilistic fracture-mechanics code OCA-P was modified to include a new flaw-size distribution function and finite-length flaws, and OCA-P was used to analyze several Oconee postulated transients to determine the effect of cladding and the benefit of using certain three-dimensional flaws in lieu of two-dimensional flaws. Material properties and heat treatment studies were performed in support of TSE-7.

5. PRESSURE VESSEL INVESTIGATIONS

Preparations continued along many fronts for the first pressurized-thermal-shock test, PTSE-1. Fabrication of two test vessels was completed, and a series of material characterization tests for PTSE-1 was begun. The major facility construction phase was completed, and testing on the completed systems was undertaken while further facility modification was in progress. An instrumented but unflawed vessel was prepared for preliminary tests (PTSE-0) to determine the test facility operating characteristics and to rehearse pressure-temperature transients for the fracture test PTSE-1.

A new computer code OCA/USA was developed to combine the capabilities of the OCA-II code for linear-elastic fracture analysis and the PTSUSA code for upper-shelf ductile tearing analysis. Improvements to both codes were made to facilitate evaluation of PTS experiments and to incorporate elastic-plastic fracture analysis and ligament tensile instability. OCA/USA is being used in conjunction with the results of material characterization tests for planning PTSE-1.

6. STAINLESS STEEL CLADDING INVESTIGATIONS

Further testing of one-wire-clad plate specimens has been deferred until data on the effects of irradiation have been obtained. A contract to procure three-wire series-arc-clad plates for future study was finalized.

7. ENVIRONMENTALLY ASSISTED CRACK-GROWTH STUDIES

Westinghouse Electric Corporation's Power Systems, Nuclear Technology Division continued studies to characterize the effects of chemistry on the environmentally assisted acceleration of fatigue crack growth. Tests for corrosion fatigue at a high R ratio ($R = 0.7$) were carried out for the round robin being coordinated by the International Cyclic Crack Growth Rate Review Group. Other tests concentrated on better characterizing the effect of materials chemistry on environmental enhancement. The first test for a high-sulfur plate showed crack-growth rates somewhat in excess of the ASME Sect. XI reference growth law at high range of applied stress-intensity factor ΔK. An electrode system has been designed and built for continuous monitoring of water environment.

HEAVY-SECTION STEEL TECHNOLOGY PROGRAM QUARTERLY PROGRESS REPORT FOR APRIL-JUNE 1983*

C. E. Pugh

ABSTRACT

The Heavy-Section Steel Technology (HSST) Program is an engineering research activity conducted by the Oak Ridge National Laboratory (ORNL) for the Nuclear Regulatory Commission. The program comprises studies related to all areas of the technology of materials fabricated into thick-section primary-coolant containment systems of light-water-cooled nuclear power reactors. The investigation focuses on the behavior and structural integrity of steel pressure vessels containing cracklike flaws. Current work is organized into seven tasks: (1) program administration and procurement, (2) fracture-mechanics analyses and investigations, (3) investigations of irradiated materials, (4) thermal-shock investigations, (5) pressure vessel investigations, (6) stainless steel cladding investigations, and (7) environmentally assisted crack-growth studies.

Analyses were performed to determine material parameters and pressure-temperature transients compatible with potential pressurized-thermal-shock experiments. Subcontractors continued studies on crack arrest, crack reinitiation, fracture transition, and environmentally assisted crack growth. Charpy tests were performed for both irradiated and unirradiated specimens (state-of-the art welds) in the Fourth Irradiation Series. Irradiation of the first two capsules containing Charpy and tensile specimens of one-wire stainless steel cladding was begun. Thermal-shock experiment TSE-7 was conducted, and properties for the TSE-7 test material were determined. Preparations for the first pressurized-thermal-shock experiment (PTSE-1) continued. Construction of the test facility was completed; analyses of potential test histograms were performed; fabrication of the two vessels for use in the shakedown test and the PTSE-1 was completed, and the vessels were delivered to ORNL; and vessel instrumentation, thermocouple thimble fabrication, data acquisition system preparation, and other facility apparatus development have been carried out.

---

*Conversions from SI to English units for all SI quantities are listed on a foldout page at the end of this report.

1. PROGRAM ADMINISTRATION AND PROCUREMENT

C. E. Pugh

The Heavy-Section Steel Technology (HSST) Program, a major safety program sponsored by the Nuclear Regulatory Commission (NRC) at the Oak Ridge National Laboratory, is concerned with the structural integrity of the primary systems [particularly the reactor pressure vessels (RPVs)] of light-water-cooled nuclear power reactors. The structural integrity of these vessels is ensured by (1) designing and fabricating RPVs according to standards set by the code for nuclear pressure vessels, (2) detecting flaws of significant size that occur during fabrication and in service, and (3) developing methods of producing quantitative estimates of conditions under which fracture could occur. The program is concerned mainly with developing pertinent fracture technology, including knowledge of (1) the material used in these thick-walled vessels, (2) the flaw-growth rate, and (3) the combination of flaw size and load that would cause fracture and thus limit the life and/or the operating conditions of this type of reactor plant.

The program is coordinated with other government agencies and with the manufacturing and utility sectors of the nuclear power industry in the United States and abroad. The overall objective is a quantification of safety assessments for regulatory agencies, for professional code-writing bodies, and for the nuclear power industry. Several activities are conducted under subcontract by research facilities in the United States and through informal cooperative effort on an international basis. Three research and development subcontracts are currently in force.

Administratively, the program is organized into seven tasks, as reflected in this report: (1) program administration and procurement, (2) fracture-mechanics analysis and investigations, (3) investigations of irradiated material, (4) thermal-shock investigations, (5) pressure vessel investigations, (6) stainless steel cladding investigations, and (7) environmentally assisted crack-growth studies.

During this quarter, 11 program briefings, reviews, or presentations were made by the HSST staff at technical meetings and at program reviews for the NRC staff or visitors. This includes a comprehensive program review that was given before the Vessel Integrity Review Group on June 14 in Oak Ridge. Three technical reports were published[1-3] during the quarter.

References

1. G. D. Whitman et al., *Heavy-Section Steel Technology Quart. Prog. Rep. October-December 1982*, NUREG/CR-2751, Vol. 4 (ORNL/TM-8369/V4), Union Carbide Corp. Nuclear Div., Oak Ridge Natl. Lab.

2. A. Sauter, R. D. Cheverton, and S. K. Iskander, *Modification of OCA-I for Application to a Reactor Pressure Vessel with Cladding on the Inner Surface*, NUREG/CR-3155 (ORNL/TM-8649), Union Carbide Corp. Nuclear Div., Oak Ridge Natl. Lab., May 1983.

3. J. G. Merkle and R. E. Johnson, *Example Calculations Illustrating Methods for Analyzing Ductile Flaw Stability in Nuclear Pressure Vessels*, NUREG-0939, Union Carbide Corp. Nuclear Div., Oak Ridge Natl. Lab., May 1983.

2. FRACTURE-MECHANICS ANALYSIS AND INVESTIGATIONS

2.1 Computational Methods for Analysis of PTS Experiments

B. R. Bass* R. H. Bryan
J. W. Bryson J. G. Merkle

Extensive computational analyses have been performed to determine material parameters and optimum pressure-temperature transients compatible with proposed pressurized-thermal-shock (PTS) test scenarios and with the capability of the PTS test facility.[1,2] Both linear and nonlinear material models have been employed, as well as two- and three-dimensional (2-D and 3-D) finite-element representations of crack geometries. Computational economy required application of certain techniques suitable for parameter studies involving the analysis of a large number of transients. These techniques have been incorporated into the OCA/USA computer program, which represents an enhanced version of the OCA-I (Ref. 3) program. Essential features of the OCA/USA program, including applications to the PTS test configuration, are described below.

The computer program OCA/USA is structured around the OCA-I code, with enhancements for 3-D crack analysis as well as limited inelastic and upper-shelf capabilities. The OCA-I program assumes an infinitely long crack geometry and uses superposition techniques to calculate stress-intensity factors for time-dependent combined pressure and thermal loadings. For each crack depth, the computed stress-intensity factors K_I, the initiation factors K_{Ic}, and the arrest factors K_{Ia} are interpolated to determine the times in the transient at which $K_I = K_{Ic}$, $K_I = K_{Ia}$, and $dK_I/dt = 0$. To obtain improved estimates of K_I values for planning PTS transients, the 3-D superposition technique for finite-length surface cracks described in Ref. 4 was implemented in OCA/USA. This option was motivated by results from direct 3-D calculations performed on finite-length cracks of interest in the PTS studies using the ADINA-ORVIRT computer system (cracks with surface length $2b = 1000$ mm and a range of crack-depth-to-wall ratios of $0 < a/w \leq 0.6$, in a cylinder with wall thickness $w = 147$ mm and inner radius $R_i = 343$ mm). These calculations indicated that for deeper cracks, the K_I value for the infinitely long crack significantly overestimates the maximum K_I value for the finite-length surface crack of the same maximum depth (for certain test transients, $K_{I_{2-D}}$ exceeded $K_{I_{3-D\ max}}$ by 15% for $a/w = 0.5$).

Figure 2.1 compares results from the 3-D superposition technique of OCA/USA with those from the direct 3-D ADINA (Ref. 5)-ORVIRT (Ref. 6) analyses for the parameters of the PTS transient shown. The surface cracks considered have depth-to-thickness ratios of $a/w = 0.1$ and 0.6, and the OCA/USA results are for infinitely long cracks with the same a/w ratios. The latter results illustrate the discrepancy between infinite crack and finite crack models for deeper cracks in this series.

---

*Computer Sciences Division, Union Carbide Corporation-Nuclear Division (UCC-ND).

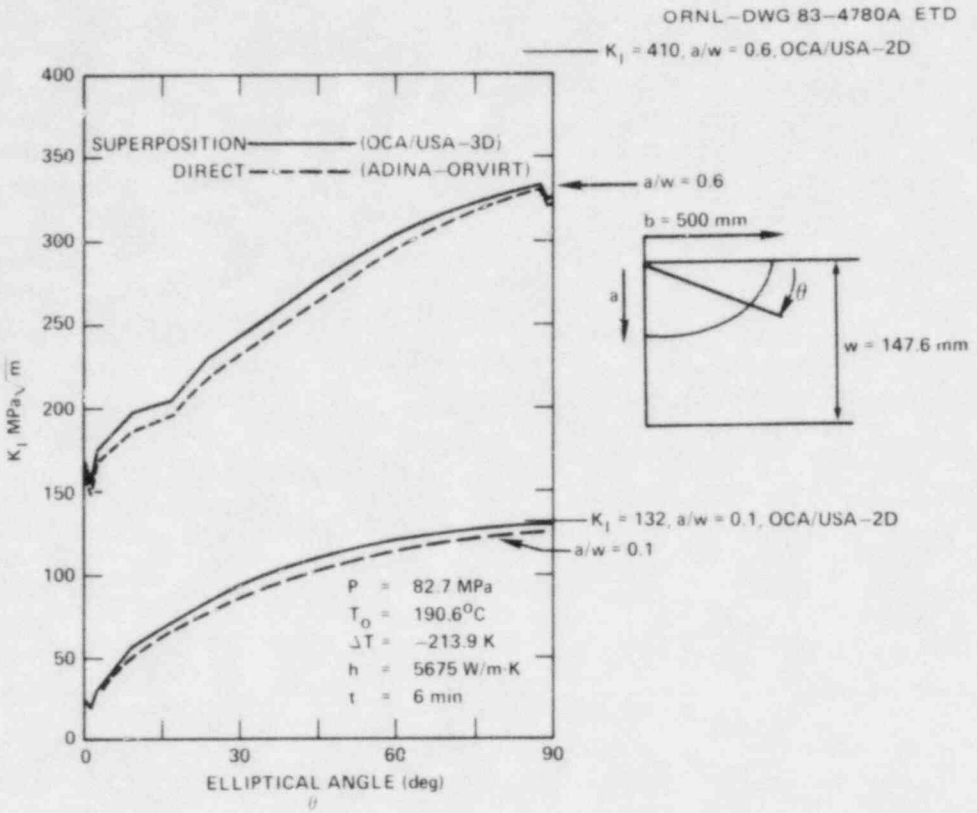

Fig. 2.1. Comparison of OCA/USA 3-D superposition with 3-D direct analysis of finite-length cracks on outer surface of cylinder.

Another enhancement of OCA/USA was motivated by a proposed PTS test scenario in which the crack initiates in cleavage and propagates into a region where temperatures are sufficiently high for completely ductile fracture. To incorporate ductile behavior into the OCA/USA analysis, an upper-shelf fracture model[7] was developed and implemented in the program. The model assumes the existence of a temperature T_D, above which ductile fracture prevails and below which fracture is entirely by the cleavage mode. Continued growth of a crack in the region $T > T_D$ is assumed controlled by a tearing resistance J_R, which generally is a function of incremental crack growth and crack-tip temperature. The technique converts K_I (subjected previously to a plastic zone size correction) to J_I and computes stable and unstable upper-shelf points based on the relationship between J_I and J_R. Several applications of this model are presented in Ref. 7.

Another consideration in the PTS transient is that the upper shelf be reached at a crack depth/pressure combination that precludes tensile instability of the remaining ligament. At the unstable crack depth corresponding to the ligament fully yielded in tension, stretching of the ligament causes large increases in crack-mouth opening displacement (CMOD). The model[8] implemented in OCA/USA for this problem assumes a deep continuous surface crack with complete ligament yielding without strain hardening. Because the crack is deep, a strip-yield type model was adopted so

that yielding occurs only on the plane ahead of the tip. Based on a completely yielded ligament, J_I is calculated for a range of crack depths at each time step in the transient. In addition, the crack depth corresponding to ligament instability is also determined. To evaluate the reliability of this yielded ligament model, direct thermo-elastic-plastic analyses were performed using a representative multilinear strain-hardening curve and reported in Ref. 9.

For the PTS transient shown in Fig. 2.1, K_I values computed by OCA/USA for the infinitely long crack model are plotted in Figs. 2.2 and 2.3. These are composite curves, constructed by the program at each crack depth

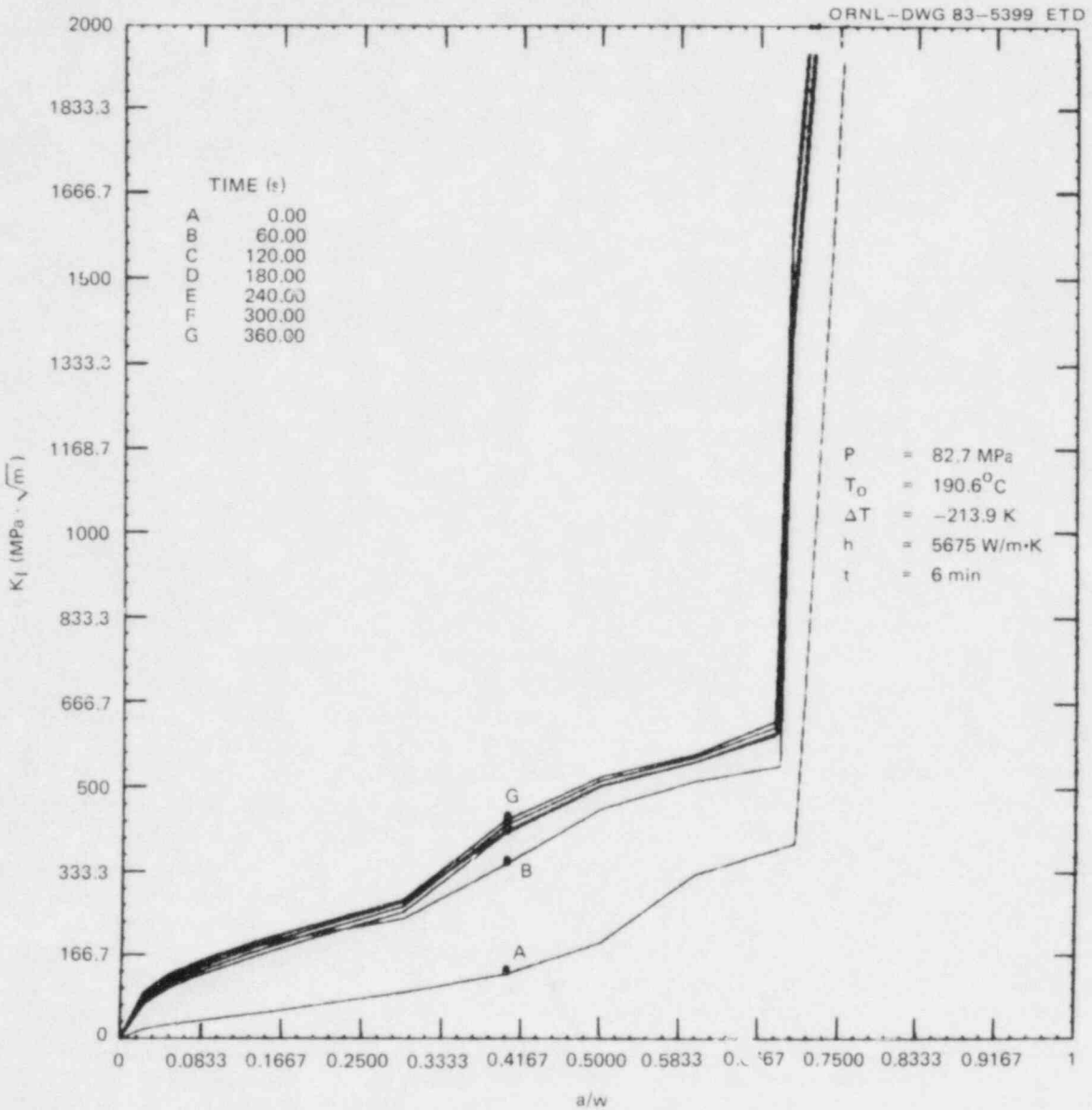

Fig. 2.2. Composite K_I variation with crack depth for infinitely long crack on outer surface of cylinder.

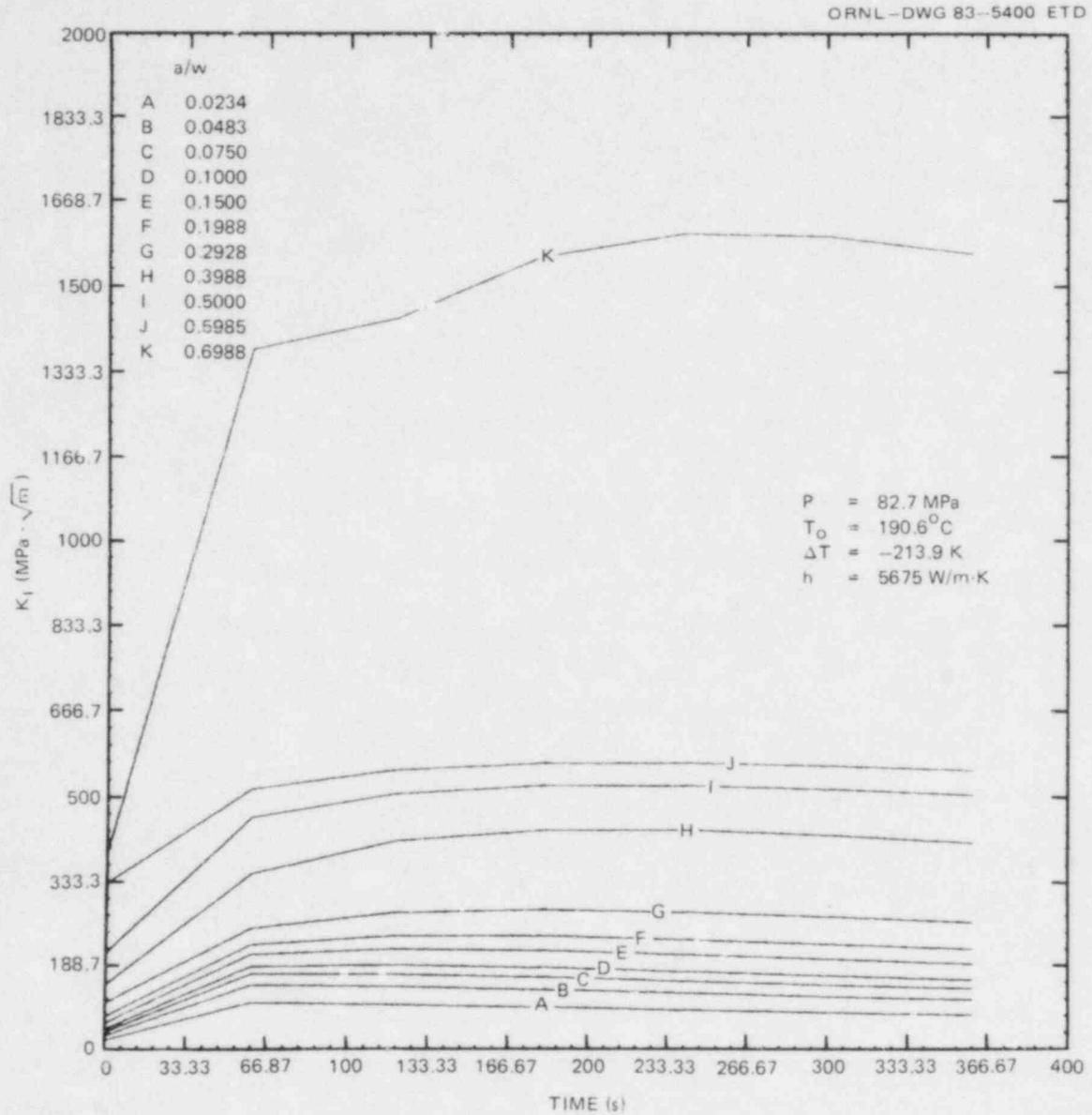

Fig. 2.3. Composite K_I variation with time for infinitely long crack on outer surface of cylinder.

from the larger K_I value calculated in two analyses: the ideally plastic ligament analysis and the superposition analysis with plastic zone size correction. The sharp break in the curves of Fig. 2.2 indicates the point of impending tensile instability of the remaining ligament.

2.2 BCL HSST Support Program*

A. R. Rosenfield† C. W. Marschall†
T. A. Bishop† J. K. McCoy†
F. T. Freuler† P. N. Mincer†
S. W. Rust†

2.2.1 Task 1: Administration – Introduction and summary

The objective of the Battelle-Columbus (BCL) Heavy-Section Steel Technology (HSST) Support Program is to develop small-scale test procedures to provide data for steels used in overcooling experiments at Oak Ridge National Laboratory (ORNL). The program consists of four research tasks, and the progress in each is reported below.

2.2.2 Task 2: Overcooling-experiment support

Work was initiated to obtain crack-arrest data on a low-upper-shelf energy weld from the ORNL Intermediate Test Vessel ITV-8A. The piece weld received at BCL has been designated as Piece V8A-D and has dimensions ~390 mm long by 170 mm wide by 150 mm thick. Originally, it was thought that the low-toughness automatic-submerged-arc weld extended for the entire length of the piece so that all of the material, except for a 19-mm-thick discard piece at the flame-cut end, could be used for preparing crack-arrest specimens. However, it was determined subsequently that less than half the length of the piece was welded automatically; the remainder included a length of manual weldment and a length of base metal. Thus, the number of crack-arrest specimens that could be machined was fewer than expected.

The CVN upper-shelf energy of the weld in the width-longitudinal (WL) orientation was reported by ORNL to be 57 J (42 ft-lb) (Ref. 10). With respect to fracture appearance, 50% shear was observed at about 50°C and 100% shear at about 100°C (Ref. 10). At 150°C, the yield strength was about 400 MPa (Ref. 10) in a direction perpendicular to the weld centerline, and J_{Ic} was ~43 kJ/m (Ref. 11) ($K_{Ic} \approx 97$ MPa·$\sqrt{m}$) in both the width-transverse (WT) and WL orientations [Babcock and Wilcox (B&W) orientation code].

In addition to Piece V8A-D, ORNL also furnished to BCL two pieces of a B&W characterization weld seam, V872, similar in composition and properties to V8A-D. These additional pieces were furnished for BCL's use in development of fabrication and testing procedures.

Piece V8A-D was cut to obtain a total of 16 crack-arrest specimens, following the cutting plan shown in Fig. 2.4. The specimen sizes, orientations, and proposed test temperatures are listed in Table 2.1. It was discovered by grinding and etching that only blanks 12, 13, 14, 15, and 16, plus a 19-mm-thick piece to the left of blanks 15 and 16, contained

---

*Work sponsored by HSST Program under UCC-ND Subcontract 85X-17624C between UCC-ND and BCL.

†BCL, Columbus, Ohio.

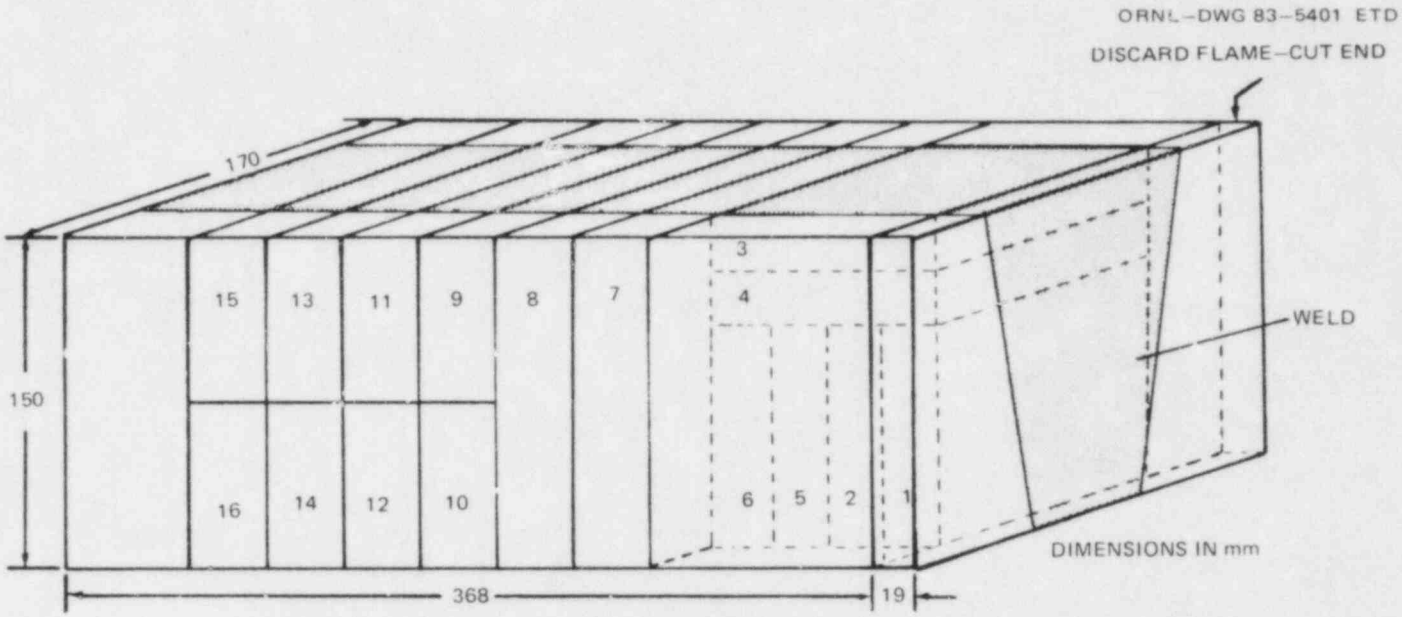

Fig. 2.4. Cutting pattern used to obtain crack-arrest specimens from low-upper-shelf energy weld piece V8A-D.

Table 2.1. Cutting plan for low-upper-shelf weld Piece V8A-D

Pieces	Specimen type[a]	Crack direction	Approximate dimensions[b] (mm)	Proposed test temperature (°C)
1, 2	BWCCA	Radial	100 x 100 x 25	RT_{NDT}
3, 4	BWCCA	Longitudinal	100 x 100 x 25	RT_{NDT}
5, 6	BWCCA	Radial	100 x 100 x 25	RT_{NDT} + 20
7, 8	BWCCA	Radial	100 x 100 x 35	RT_{NDT} + 40
9, 10	DCCA	Radial	150 x 150 x 35	RT_{NDT} + 60
11, 12	DCCA	Radial	150 x 150 x 35	RT_{NDT} + 80[c]
13, 14	DCCA	Radial	150 x 150 x 35	RT_{NDT} + 100[c]
15, 16	DCCA	Radial	150 x 150 x 35	RT_{NDT} + 120[c]

[a] BWCCA refers to brittle-weld compact crack-arrest specimens; DCCA refers to duplex compact crack-arrest specimens.

[b] Dimensions shown may have to be reduced slightly, depending on the actual cross section of the piece.

[c] These temperatures are tentative and are included for planning; the highest temperatures employed will depend on results obtained at somewhat lower temperatures.

the low-toughness weld metal. Thus, the most recent plans are to fabricate three 100 x 100 x 15 mm duplex compact crack-arrest (DCCA) specimens from the piece at the left end of the blank. These will be tested at RT_{NDT} and RT_{NDT} + 20°C. Blanks 12–16 will be used to fabricate five 150 x 150 x 35 mm DCCA specimens for testing at RT_{NDT} + 40°C and above.

BCL has, on earlier occasions, experienced problems with defects in electron-beam welds used in making duplex crack-arrest specimens from weldments. Recent Japanese investigations have shown that the quality of electron-beam welds sometimes can be improved by oscillating the beam forward and backward along the weld path.[12] The usefulness of this technique for this task was investigated through the use of 117-mm-long by 38-mm-wide by 35-mm-thick blanks that were cut from weld seam V872. BCL had weldments made under four different conditions at Youngstown Welding and Engineering Company. The electron beam was oscillated in three of the welds, but not in the fourth. All pieces were welded from both sides, using beam-penetration depths that were slightly greater than one-half the sample thickness. Each specimen was radiographed in two orientations to check for defects. The results shown in Table 2.2 indicate that oscillating the beam at 100 Hz produced a weld with markedly less porosity than was obtained without beam oscillation. Beam oscillations at either 100 or 1000 Hz with a table speed of 510 mm/min produced welds with less porosity than welds made without beam oscillations, but they had more porosity than welds made with a table speed of 380 mm/min. Additional electron-beam welding trials will be carried out on weld V872 to further optimize the use of the beam-oscillation technique. Depending on specimen fabrication activities in other tasks, the actual welding of duplex specimens from Piece V8A-D could be delayed until August.

Table 2.2. Results of trial electron-beam welds on samples of characterization weld V872

Sample No.	Table speed (mm/min)	Beam oscillation frequency (Hz)	Remarks
1	380	0	Normal welding conditions; significant porosity present in weld
2	380	100	Very little porosity evident
3	510	100	Porosity slightly greater than in sample 2
4	510	1000	Porosity similar to sample 3

2.2.3 Task 3: Crack initiation

Procedures are evolving to maximize the number of data obtainable from a single specimen. By use of the reinitiation technique, it is now possible to obtain one initiation (K_Q) and two arrest (K_a) values from the same test piece. Comparisons have been made for consistency between compact-specimen reinitiation data and full-scale test results, including cross comparisons of the arrest data using several techniques. A problem remains in deciding how to account for the unbroken ligaments in evaluating the stress intensity associated with reinitiation.

The reinitiation method of estimating K_{Ic} (Refs. 13 and 14) has two distinct advantages. First, because reinitiation toughness is obtained following a crack-arrest test, the two crack jumps of a reinitiation specimen can provide one K_Q and two K_a values. Second, reinitiation experiments eliminate costly and time-consuming fatigue precracking.

The major problems are that the effects of experimental variables (such as precrack conditions) are not clearly established and that no independent verification of the method has been carried out. It has also been found that reinitiation toughness values associated with arrested cleavage cracks are lower than those associated with dimpled rupture.

Figure 2.5 summarizes the available data. The BCL compact-specimen data are those reported earlier[13,14] plus the new data listed in Table 2.3. (Note that the table does not include data from duplex samples where the precrack arrested in the weld zone. For those specimens, the only usable result of the reinitiation experiment is the final K_a value.) The data in Fig. 2.5 and Table 2.3 include a single result on a 50.8-mm-thick specimen in which cleavage reinitiation was achieved at RT_{NDT} + 85°C. If the initiation upper shelf is judged to be the point where the ASME K_{Ic} curve reaches 220 MPa·$\sqrt{m}$, cleavage in this specimen was unexpected; but it reinforced the suggestion that arrested cleavage cracks are more potent than are stably growing dimpled ruptures.

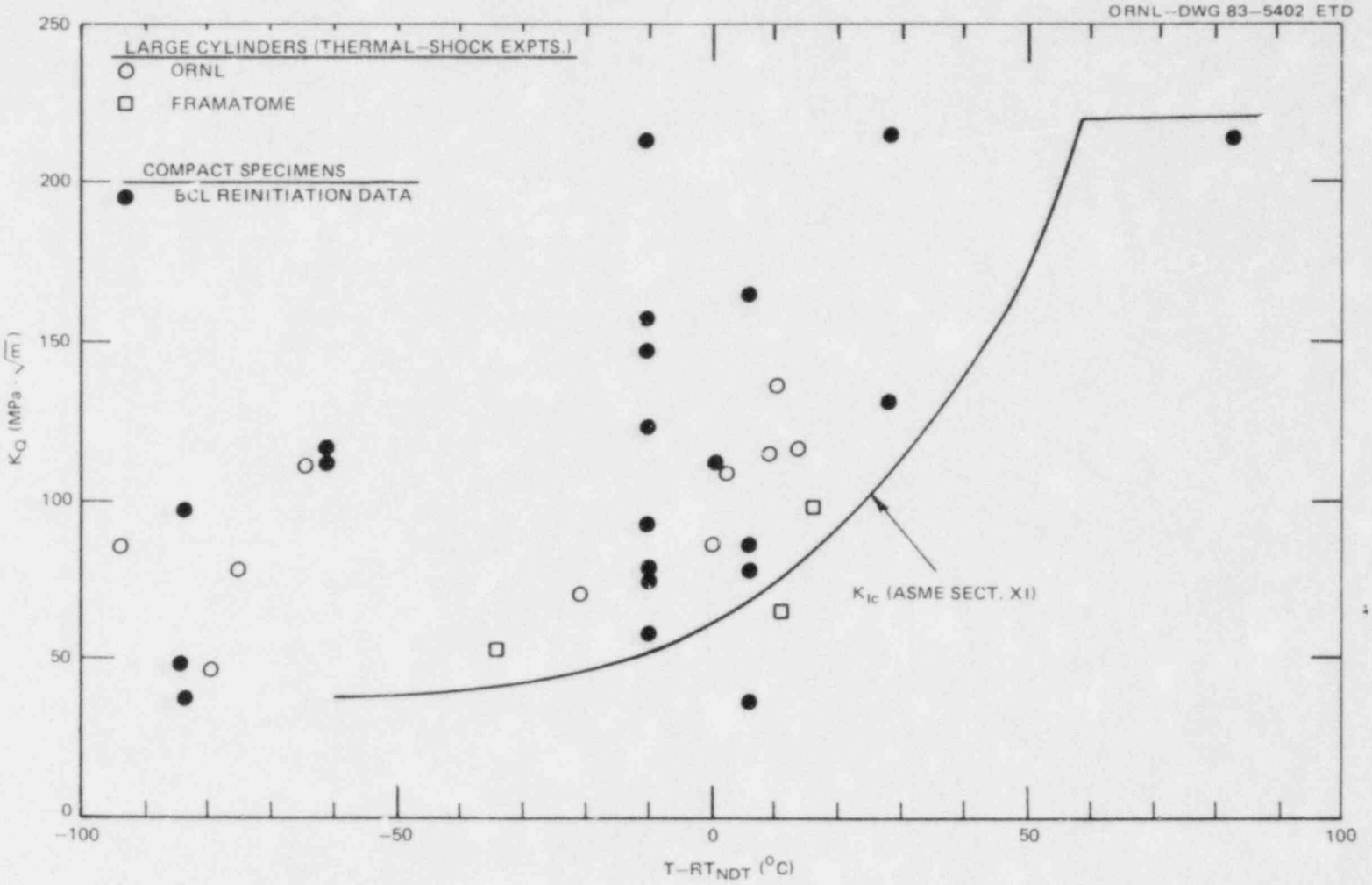

Fig. 2.5. Comparison of crack-initiation toughness resulting from thermal shock with reinitiation of arrested cleavage cracks in compact specimens.

Table 2.3. Reinitiation of arrested cleavage cracks: retempered TSE-6 forging designated TSE-6R

Specimen No.	Pretest		Reinitiation					
	Test temperature (°C)	K_a (MPa·$\sqrt{m}$)	Test temperature (°C)	Displacement (mm)		Crack length[a] (mm)		K_Q[b] (MPa·$\sqrt{m}$)
				−0.25w location	0.303w location	a_p/w	a_e/w	
4	23	205	0	2.57	1.25	0.853	0.813	216
6	39	134	−28	1.66	0.77	0.881	0.767	111
8	53	207	0	1.11	0.48	0.873	0.695	130
16[c]	56	150	54	2.13	0.93	0.828	0.706	212

[a] a_p = physical crack length, a_e = effective crack length, w = specimen width.

[b] Calculated from a_e.

[c] Specimen was 50.8 x 197.6 x 203.2 mm; all other specimens were 34.9 x 148.2 x 152.4 mm.

The large-cylinder data in Fig. 2.5 are from the ORNL thermal-shock series (TSE-4, -5, -5A, and -6)[16,26] and from a recently reported Framatome result.[17] Although the scatter in the compact data is greater than that for the large cylinders, the small-specimen results appear capable of providing a lower-bound estimate using relatively few specimens.

This result, combined with the arrest data reported below, provides encouragement for continued use of the reinitiation technique. The procedure to be employed will be to do a crack-arrest test, heat tint the specimen, reinitiate at a temperature about 40°C lower, and heat tint again. The second heat tint will be done at a temperature lower than the first. This procedure will be used on TSE-7 and PTSE-1 material.

As was mentioned previously, an additional problem has arisen in the interpretation of the reinitiation results. This has to do with accounting for the presence of unbroken ligaments bridging the faces of the arrested crack. Initially, BCL suggested that ligaments cause the effective crack length to be less than the physical crack length because they act as pinching forces.[13] However, physical examination of broken specimens has revealed that those that are heavily ligamented are also those with effective crack lengths most in excess of the physical crack length. A quantitative analysis of this problem has been developed by Milella,[18] who suggested that the effect of ligaments can be analyzed in terms of compliance. With the aid of a detailed examination of test records, he was able to deduce the "lost" compliance arising from ligaments. He also concluded that the effective crack length of a ligament-containing specimen in a displacement-controlled system is larger than the physical crack length. This conclusion follows from the realization that if the unbroken ligaments were severed, the crack would have to advance if the stress intensity were to remain constant under fixed-grip conditions.

Milella's method requires that the load on the specimen be calculated from the load on the wedge, using an estimate of the coefficient of friction between the wedge and split pins. Such information is available from cyclic loading, a procedure not used in the reinitiation experiments. Further investigation of this problem with a view towards procedure modification is planned.

2.2.4 Task 4: Crack arrest

During the last report period, K_{Ia} data were obtained at temperatures corresponding to the onset of the upper shelf in the CVN impact test. During this quarter, attention turned to crack-arrest experiments using a positive temperature gradient. New isothermal experiments also were carried out. All specimens were of the duplex contoured-side-groove design.[14] Loading was accomplished using inverted split pins.[19]

The temperature gradient was imposed by wrapping the end of the specimen's test section with electrical-resistance heating tape while cooling the starter-section end with granulated dry ice. As is shown in Fig. 2.6, gradients on the order of 1.5°C/mm were achieved. This is three to ten times the steepness in typical ESSO tests[20,21] and is necessitated by the much smaller crack path available in the compact specimen.

Two other points are indicated on Fig. 2.6. The upper curve, representative of three samples, was designed so that the entry point of the

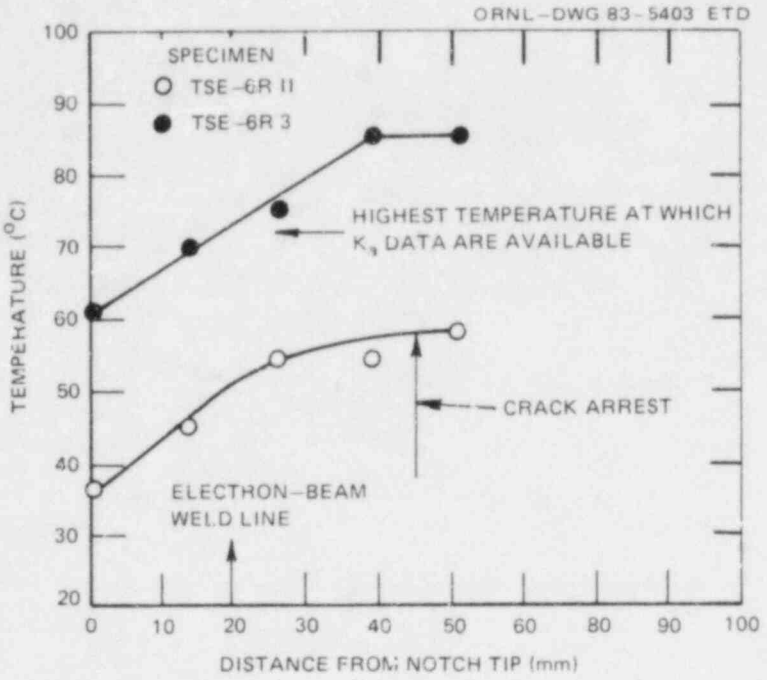

Fig. 2.6. Temperature profiles in crack-arrest tests of specimens with temperature gradients.

crack into the test section was at a temperature about equal to the highest temperature at which crack arrest had been obtained in an isothermal test (71°C). All three of these tests resulted either in weld cracking or arrest at the weld line. The second point concerns the specimen tested at lower temperatures. Here, arrest occurred after the crack had propagated through the region of positive temperature gradient and had reached an essentially isothermal region.

A group of larger specimens has also been tested with the aim of extending the isothermal test temperature higher. Their dimensions were the same as those of specimens used on the Cooperative Test Program. Two of those specimens resulted in weld-zone arrest at the highest temperature where data had been obtained successfully using smaller specimens. A third specimen was tested at the arrest temperature of the gradient specimen and produced K_a values very similar to it, both after initiation and after reinitiation.

Table 2.4 summarizes the data obtained during this quarter on the retempered TSE-6 forging designated 6R. Figure 2.7 contains those data, as well as those reported last quarter. The new data tend to lay along the K_{IR} curve at room temperature and above ($RT_{NDT} \approx -29°C$). Figure 2.7 also reflects the suggestion made regarding multiple data from a single specimen. Many of the reinitiation data reflect salvage of specimens where arrest occurred initially in the electron-beam weld zone. However, there were two specimens, 6R-6 and -8,[14] where K_a both obtained after initiation and reinitiation was augmented by a reinitiation K_Q. The third specimen where this happened, 6-R4, was very heavily ligamented, and the

Table 2.4. Additional crack-arrest data for retempered TSE-6 forging designated TSE-6R

(Duplex specimens, contoured side grooves, and inverted split-pin loading)

Specimen No.	Test temperature (°C)	Displacement (mm)		Crack length (mm)		Stress intensity (MPa·√m)	
		Initiation	Arrest	Initiation	Arrest	Initiation K_O	Arrest K_a
6R-1	94	1.73	1.84	40.6	[a]	275	[a]
-1[b]	22	1.02	1.11	63.1	107.8	180	84
-2	[c]	1.46	1.51	40.6	[a]	233	[a]
-2[b]	24	0.97	0.99	60.3	100.4	169	86
-3	[c]	[d]	[d]	[d]	[d]	[d]	[d]
-3[b]	-1	1.33	1.40	55.7	113.9	259	85
-6	39	1.73	1.88	40.6	94.0	276	134
-6[b]	-28	1.66	1.66	94.0	111.9	119	74
-11	57[c,e]	1.95	2.06	41.2	86.2	309	170
-12	[c]	1.58	1.67	40.6	[a]	252	[a]
-12[b]	24	0.94	0.98	59.9	103.3	117	81
-15[f]	72	1.67	1.82	54.0	[a]	252	[a]
-15[b,f]	39	1.59	1.68	80.9	140.1	250	118[g]
-16[f]	56	1.69	1.85[g]	54.5	126.6	254	166
-16[b,f]	54	2.13	2.13	126.6	140.2	191	150
-19[f]	74	1.75	1.84	54.3	[a]	263	[a]
-19[b,f]	40	1.30	1.38	81.2	143.8	204	90

[a] Arrested in weld zone.

[b] Reinitiation of arrested crack.

[c] Temperature gradient imposed on specimen.

[d] Crack in electron-beam weld.

[e] Temperature at point of crack arrest.

[f] Specimens were 50.8 x 197.6 x 203.2 mm; all other specimens were 34.9 x 148.2 x 152.4 mm.

[g] Estimated arrest displacement; clip gage came out of seating blocks.

crack possibly branched. For this reason, the points are shown in parentheses on the graph and are not considered further.

A comparison also was made between these data and a relation for temperature dependence appearing in the Japanese literature.[21,23] Susukida et al.[21] have plotted ESSO data as if crack arrest were a thermally activated process:

$$K_a = K_{ao} \exp [-A/T] \qquad (2.1)$$

where K_{ao} and A are material parameters, T being absolute temperature. Susukida et al.[21] found that Eq. (2.1) was obeyed above NDT for ASTM A533B steel with A ≈ 3100 K. Nakano[22] showed a similar relation for combined compact and ESSO data for temperatures straddling RT_{NDT} for A533B. However, Nakano's slope was only 640 K. Figure 2.8 shows that the BCL data can be described by two line segments, each obeying Eq. (2.1). The high-temperature slope was drawn to equal that of Susukida et al.,[21] but the

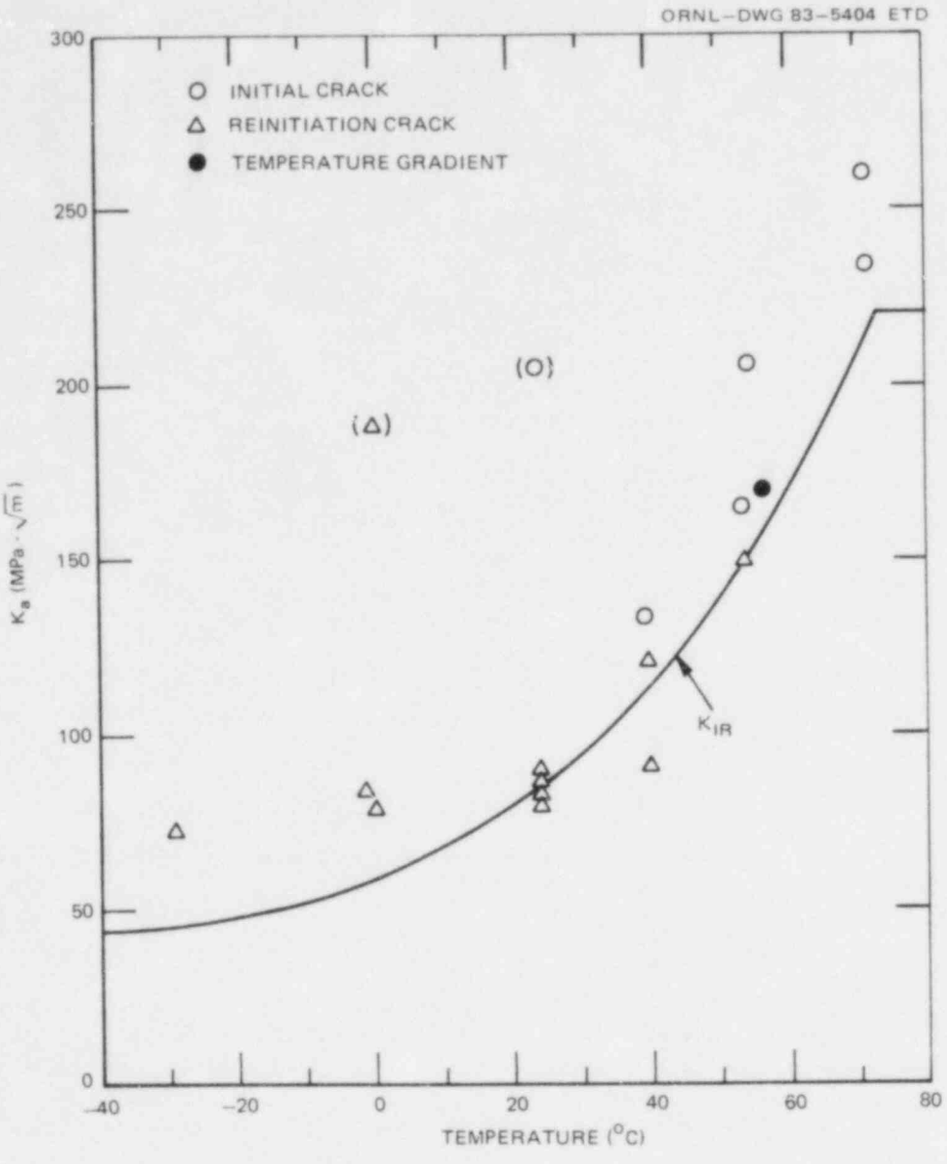

Fig. 2.7. Crack-arrest data for TSE-6R forging.

low-temperature slope is only half of Nakano's. The agreement with Eq. (2.1) is surprisingly good and suggests that some variant of it may be useful in formulating K_a vs T relations. However, the reasons for the variation in slope among investigators needs further examination. Because it is also not clear how to incorporate differences in transition temperature into the thermally activated approach, Eq. (2.1) was not used to correlate the large quantities of varied data that are considered in the following data base section.

Additional experiments were carried out to determine whether high weld zone toughness in duplex specimens contributes to the difficulties

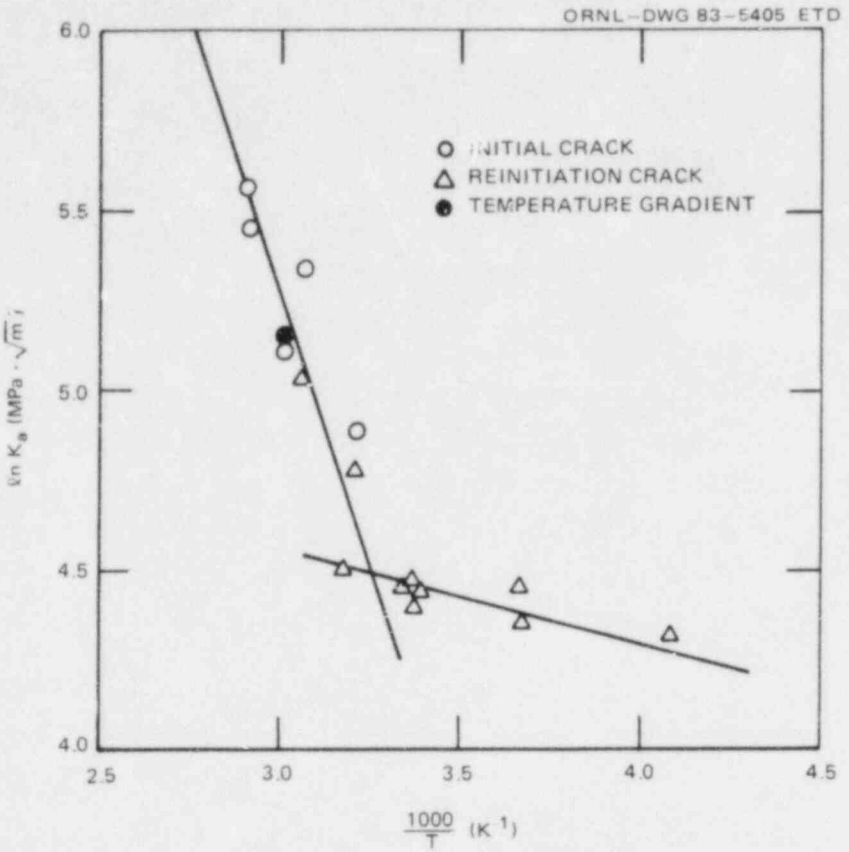

Fig. 2.8. Thermal-activation plot of crack-arrest data for retempered TSE-6R forging.

of penetrating into the test sections at high test temperatures. A modified CVN specimen, in which the crack path traverses the weld zone, was described in the previous report.[14] The absorbed impact energy was found to be roughly independent of temperature between 20 and 150°C for TSE-6 steel, where great difficulty was experienced in penetrating into the test section. New data were obtained on TSE-6R steel, where a high crack-arrest-test success rate was achieved. The results are shown in Fig. 2.9. The data for TSE-6R at 71°C represent different welds and suggest some scatter due to weld procedure. The sharp rise in energy between 71 and 93°C for TSE-6R may explain why penetration was not achieved for that heat treatment at 93°C. However, overall TSE-6R weld zones appear as tough as, or tougher than, TSE-6 weld zones. Thus, the overall conclusion obtained by comparing unsuccessful TSE-6 with successful TSE-6R is that the lack of crack penetration arises from test section toughness and not from weld zone characteristics.

2.2.5 Task 5: Data base

The methods of collecting, tabulating, and analyzing the available K_{Ia} data have been described in previous quarterly reports. Several data

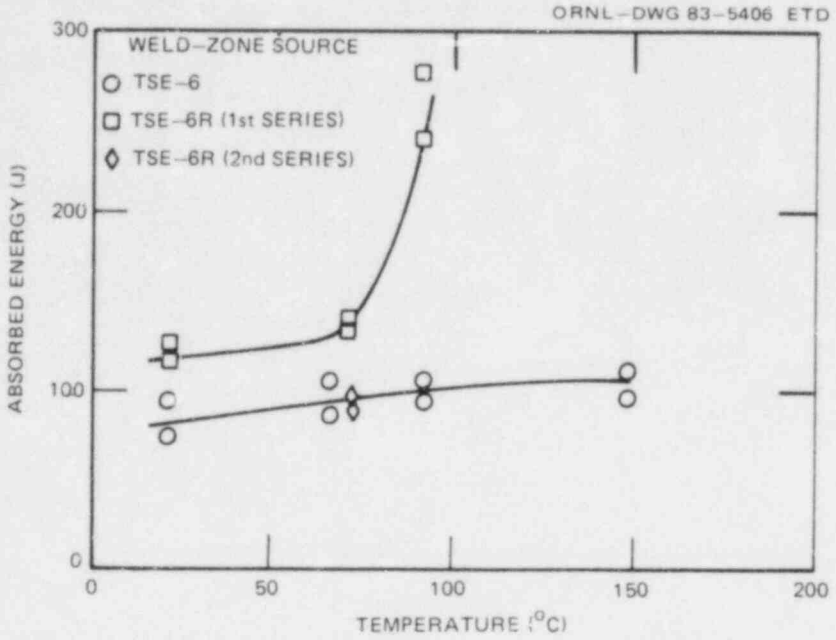

Fig. 2.9. Impact energies of weld zones cut from duplex crack-arrest specimens.

sets were analyzed using a temperature-dependent Weibull formulation in which the failure probability P is given by

$$P = 1 - \exp\left\{-\left[K_{Ia}/\beta(T)\right]^{\alpha(T)}\right\}, \qquad (2.2)$$

with α and β being temperature-dependent parameters. The main result in the last report is illustrated by a comparison of the ORNL TSE data and the corresponding BCL small-specimen data (Fig. 2.10). Although based on a limited number of points, the graph shows reasonably good agreement between the two laboratories, both in the central tendency (63rd percentile) and the lower bound (5th percentile). However, the limited data base resulted in serious discrepancies in the confidence limits on the fifth percentile.

During the current quarter, the data input and statistical computer programs were linked together, and some initial production runs were made. A total of 113 points was selected to represent a variety of data sources and test procedures, as listed in Table 2.5. Two new analyses were made: (1) all data, and (2) all U.S. wedge-loaded brittle-weld compact-specimen data. The tabulated data are available separately by request to BCL.

Results for the largest sample (113 points) are given in Fig. 2.11. The calculated fifth percentile is shown at the lower edge of the points to represent an estimated lower bound of these data. The 95% confidence limits on this percentile curve are quite narrow over most of the temperature range, being +5–10 MPa·$\sqrt{m}$ up to RT_{NDT} + 30°C. The confidence interval then broadens continually as temperature increases, reaching $\pm$34 MPa·$\sqrt{m}$ at RT_{NDT} + 85°C. This broadening reflects both the smaller

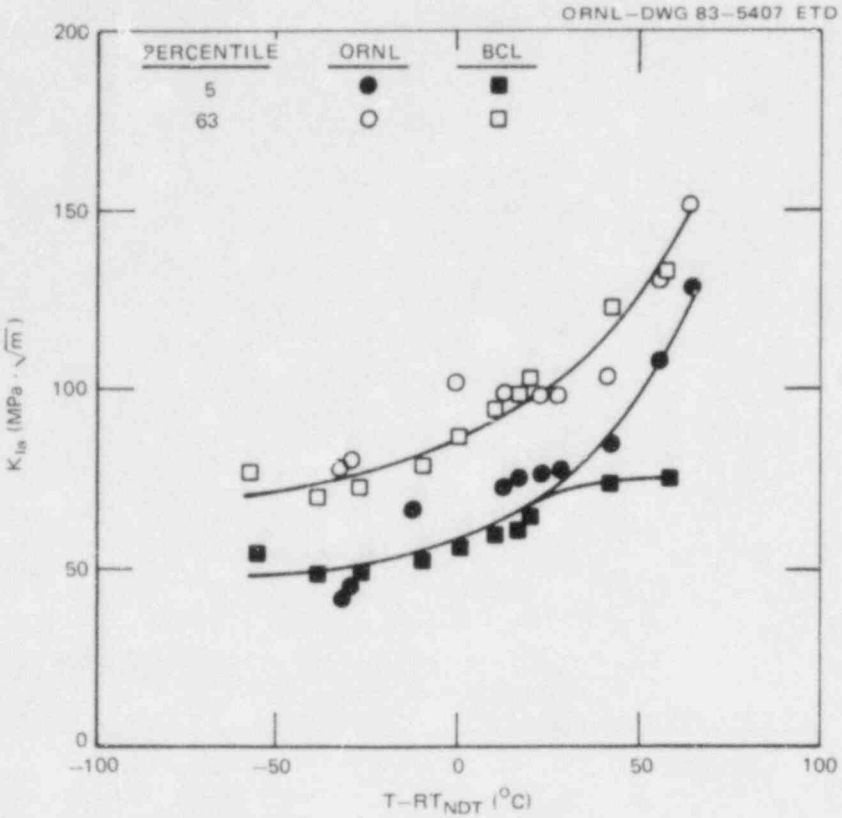

Fig. 2.10. Comparison of statistically calculated percentiles of crack-arrest data from ORNL and BCL.

Table 2.5. Classification of data analyzed

Specimen design	Number of specimens	Laboratories
Wedge loaded		
Brittle-weld compact	80 (66)[a]	BCL, MRL, Kawasaki
Duplex double-cantilever beam	5	BCL
Machine loaded		
Contoured double-cantilever beam	14	MRL
ESSO	4	Kawasaki
Thermal shock		
Thermal-shock cylinder	10[b]	ORNL
	113 (66)[a]	

[a]The number in parentheses indicates specimens for which raw data were available and for which results were computer-calculated at BCL.

[b]Number listed is total number of jumps from four cylinders.

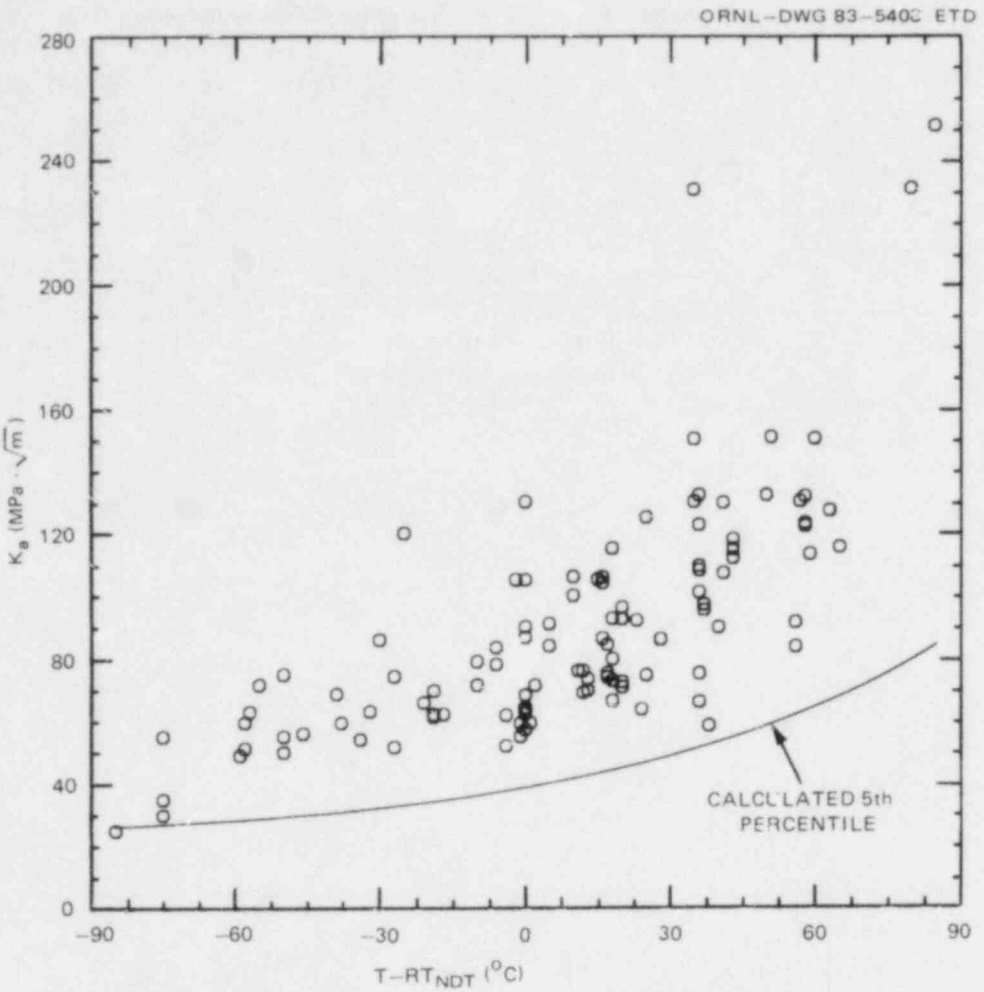

Fig. 2.11. BCL crack-arrest data bank indicating estimated fifth percentile.

number of samples and the broader scatter in the raw data at higher temperatures.

While Fig. 2.11 might be considered an update of the ASME K_{IR} curve, several cautions are in order.

1. The BCL data bank has not been completely computerized. The points on Fig. 2.11 represent an estimated 20 to 30% of those existing currently.
2. No welds are included in Fig. 2.11.
3. For purposes of calculation, all data were considered equally valid. When the ASTM Task Group on Crack Arrest Testing produces a draft standard, the statistical program will be rerun using only specimens that pass its criteria.
4. The fifth percentile was chosen arbitrarily to represent the "lower bound" of the data. Appropriate choices of percentile and confidence criteria need to be made.

Pending resolution of these points, the lower bound in Fig. 2.11 should be considered only illustrative.

Results for all three data sets are compared in Figs. 2.12 and 2.13. Figure 2.12 is a plot of the central tendency as characterized by the β parameter of Eq. (2.2), while Fig. 2.13 is a plot of the relative breadth of the distribution as characterized by the α parameter. A small value of α reflects broad scatter, and it has been shown that $\alpha \sim \bar{x}/s$, where $\bar{x}$ is the mean and s is the standard deviation of a Weibull distribution.[33]

In Fig. 2.12, the temperature dependence of β is seen to be similar for all three data sets. There is a tendency for the middle-size set (compact specimens only) to lie slightly below the other set, but the significance of this observation is not clear.

While the differences in central tendency were slight, Fig. 2.13 shows that the differences in scatter between sets are considerable. The partial BCL data (25 data points), representing the initial data on TSE-4,

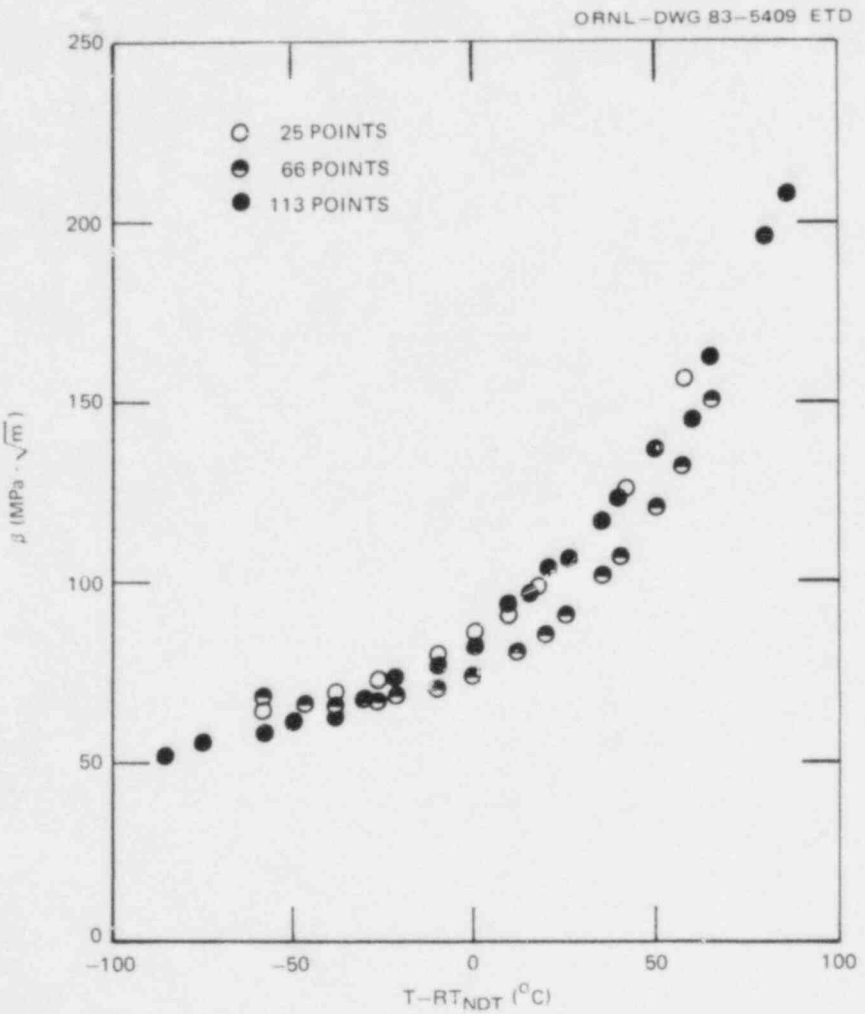

Fig. 2.12. Temperature dependence of β, 63rd percentile of crack-arrest-toughness distribution function.

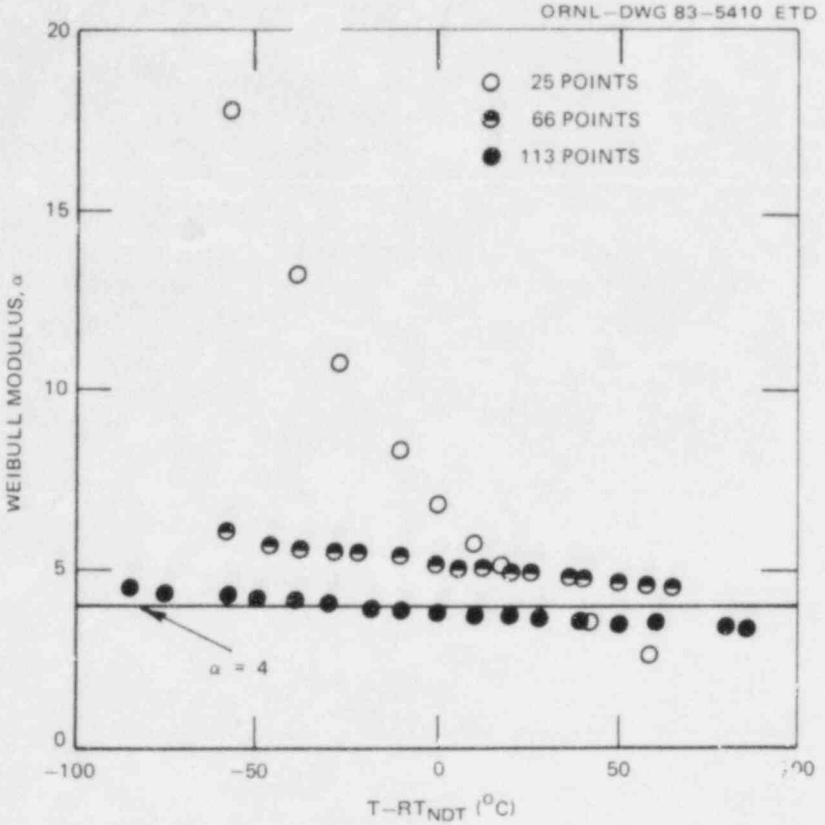

Fig. 2.12. Temperature dependence of Weibull modulus of crack-arrest-toughness distribution function.

-5, -5A, and -6 steels, have a very narrow distribution at low temperatures. The distribution broadens considerably as the temperature is raised, with α falling below four at the two highest temperatures. Addition of the other compact-specimen data (half-filled points) broadens the distribution below RT_{NDT} and narrows it slightly above RT_{NDT}. The further addition of data from other specimen designs (filled points) uniformly broadens the distribution.

The half-filled points are represented by α values close to five, while $\alpha \approx 4$ for the filled points. These values are interesting in view of a recent theory by Wallin et al.[24] They argue that the α value is always four for crack initiation by cleavage. This viewpoint can be rationalized by recognizing that a full development of weakest-link statistics adds a volume term to the exponent and replaces the K term of Eq. (2.2) with a critical stress. The volume referred to is that of the plastic zone, which varies as K^4 (at constant thickness), while the stress term is independent of K. The α values close to four for K_a data suggest that the micromechanism of crack propagation may be similar to that for initiation: fracture of hard particles slightly ahead of the crack followed by cleavage of the intervening region. While this suggestion is, of course, speculative, data analysis would be considerably simplified if the existence of a unique temperature-independent α value could be demonstrated.

2.3 Finite-Element Analyses of ESSO Tests*

M. F. Kanninen† J. Ahmad†
C. R. Barnes†

2.3.1 Introduction

The objective of this task is to assess the validity of wide-plate tests (ESSO, Double Tension) to provide reliable upper-shelf crack-arrest toughness data for use in thermal-shock analyses. The effort includes:

1. a literature search for existing wide-plate test data containing enough information to enable dynamic finite-element interpretation of the test results,
2. a limited number of elastodynamic finite-element analyses of wide-plate tests, and
3. recommendations for suitable instrumentation of the test specimens.

2.3.2 Work accomplished

The literature search was completed. It was found that the work of Kanazawa and Machida contains sufficient data to allow a complete dynamic fracture-mechanics interpretation of results. Both generation and application phase finite-element computations were performed using the FRACTDYN code. It was found that while the experimental measurements made by the procedure developed by Kanazawa et al. appear to be accurate, some discrepancies exist in the analytical interpretation of the measurements.

A preliminary set of recommendations for instrumenting the test specimens for future experiments was also completed.

2.3.3 Work in progress

During this quarter attempts were made to resolve the discrepancies between the analytical results reported by Kanazawa and Machida and those obtained at BCL. A possible source appears to be the inaccuracy in reading the plot of crack velocity vs time data reported by Kanazawa and Machida. Professor S. Machida has been contacted to obtain, if possible, a more accurate description of these data. Once these data are available, a re-evaluation of the analytical results will be made.

2.3.4 Work planned for next quarter

Final evaluation of both analytical and experimental procedures will be completed, and recommendation for proper instrumentation of test specimens will be finalized. The final report on this task will be submitted.

---

*Work sponsored by HSST Program under UCC-ND Subcontract 85X-17624C between UCC-ND and BCL.

†BCL, Columbus, Ohio.

2.4 Investigation of Damping and of the Cleavage-Fibrous Transition in Reactor-Grade Steel*

W. L. Fourney† K. Ogawa†
G. R. Irwin† R. J. Sanford†
R. Chona† C. W. Schwartz†
X-J. Zhang†

2.4.1 Introduction

The research at the University of Maryland is aimed at increasing the understanding of run/arrest behavior of cracks in nuclear reactor pressure vessel steels. The studies emphasize the behavior of various steels in the transition temperature range. That is to say, scanning electron microscope (SEM) and metallographic studies are being conducted to investigate the transition from pure ductile fracturing at high temperatures to brittle cleavage at lower temperatures. In particular, the attempts are to assess what is responsible for the conversion of slow fibrous fracturing into rapid cleavage.

The approach includes the examination of the specimen halves tested in very compliant loading machines. Single- and double-width Charpy testing is also used to evaluate fracture toughness and to determine the temperature above which slow fibrous fracturing could be expected for the steels under investigation. This research into transition behavior is aimed at formulating a mechanistic model that could be used to aid the understanding of this complicated transition behavior.

Dynamic calculations are also being performed with a dynamic finite-element computer code (SAMCR) to predict run/arrest events in standard specimen geometries and thermal-shock cylinders. Crack-arrest studies are also supported by the testing of transparent and opaque models covered with photoelastic coatings.

2.4.2 Cleavage-fibrous transition studies

Fabrication and assembly of testing fixtures for spring-in-series testing of large-bend specimens of A508 steel is nearing completion. The material has an elevated yield strength and should be similar to the A508 material used in TSE-6 at ORNL. The 3-point loaded bend specimens have a thickness (B) of 60 mm, a depth (W) of 102 mm, and a loading span (S) of 406 mm. The titanium alloy spring plate is designed to provide nearly 2.54-mm midspan deflection at the expected largest fracture loads. The spring plate stiffness is relatively large to encourage rapid load recovery if abrupt increments of crack extension occur and cause load drops.

An initial group of fractured specimens from spring-in-series tests of a 38.1-mm-thick bridge steel plate of A514 steel has been received from

---

*Work sponsored by HSST Program under UCC-ND Subcontract 7778 between UCC-ND and the University of Maryland.

†Department of Mechanical Engineering, University of Maryland, College Park.

a testing program at Picatini Arsenal. The yield strength of the A514 steel is about 730 MPa. Completion of the A508 and A514 tests, along with comparison to CVN fractures and fractographic examinations, will provide supporting data for conclusions regarding loss of cleavage with increases in temperature.

Fractography and microstructure. SEM examinations of fracture surfaces, including stereo-pair photographs and topological measurements, have assisted in a better understanding of cleavage fracture mechanisms. During the current reporting period sections taken along the fracture and normal to the fracture surface have been examined. The two matching fracture surfaces are cleaned, coated with a nickel coating, and sectioned along the same line. In this manner, the fracture topologies of the upper and lower fracture surfaces can be compared. In addition, the microstructure beneath the fracture surfaces can be observed.

Figure 2.14 shows SEM photographs of both fracture surfaces for a 25.4-mm-thick side-grooved compact specimen of A533B steel fractured at 4°C by the Naval Ship Research and Development Center (NSRDC) (Annapolis) using a spring-plate. After nickel plating, these surfaces were sectioned along the corresponding lines E and E'. These lines are parallel to the direction of fracturing and pass close to the probable cleavage initiation site A. Vertical section views of both sides are shown in Fig. 2.15. Details of the large late-breaking region on the right in Fig. 2.15 were shown in previous progress reports. Attention was drawn to small cleavage cracks, probably associated with cleavage undercutting, which were opened by plastic strain during fibrous separation of the late-breaking region. Another group of small cleavage cracks in the section view of the upper fracture is indicated in Fig. 2.15 and will be discussed later.

Figure 2.16 shows a higher magnification of the portion of Fig. 2.15 adjacent to the fatigue precrack. A late-breaking region, smaller than that noted previously, is indicated by an arrow. A trace of the upper fracture surface topology is superimposed. Except for the two late-breaking regions mentioned, the upper and lower fracture contours can be closed with little mismatch. Along the regions where closure of the upper and lower contours shows little mismatch, frequent interruptions to the spread of cleavage facets can be seen. However, these fibrous ridges and late-breaking regions are on a very fine scale. Evidently the cleavage-dominated portion of the separation occurred with minimal plastic strain. Indications of large plastic deformation were restricted to the close neighborhood of the larger late-breaking ligaments.

Enlarged views of the small cleavage cracks, indicated on Fig. 2.15, are shown in Figs. 2.17(*a*) and (*b*). From previous work at BCL, when small cracks of this nature are traced, they are consistently found to be connected with the main fracture surface. For the larger cracks shown in Fig. 2.17(*a*), this is obvious because the crack surfaces have a small nickel coating. The tight cleavage crack shown in Fig. 2.17(*b*) penetrated into adjacent ferrite grains with interruptions at the grain boundaries and represents the normal appearance of cleavage in the material prior to distortion from subsequent plastic strain.

Initial fractographic examinations have been made of three fracture surfaces of A514 steel from spring-in-series tests at Picatini Arsenal. The testing temperatures were −29, −18, and 4°C. The result at 4°C is of special interest because that test temperature may be nearly high enough

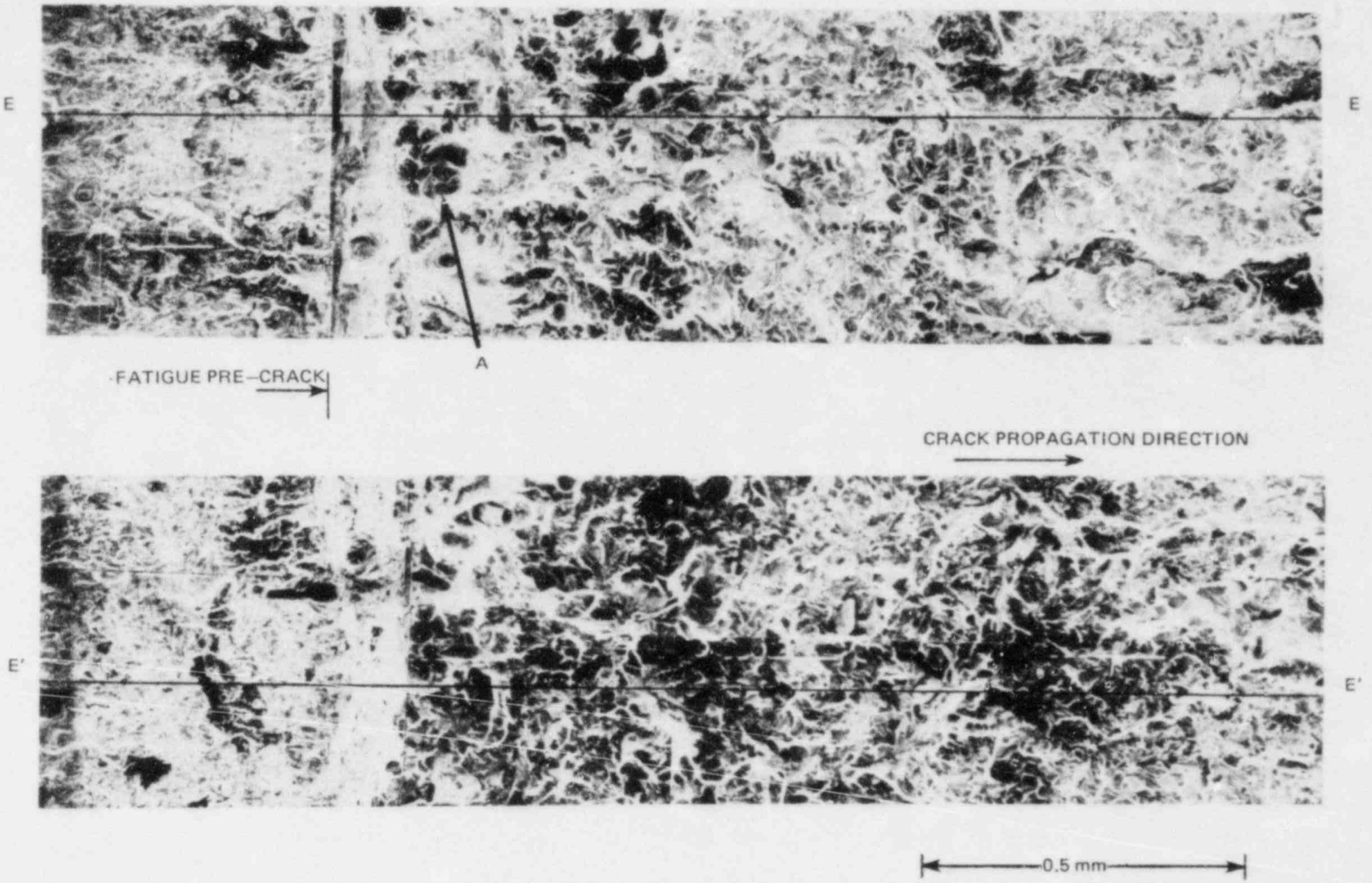

Fig. 2.14. SEM photographs of both fracture surfaces of A533B steel compact specimen tested at 4°C. (Test TL-24 from NSRDC, Annapolis.)

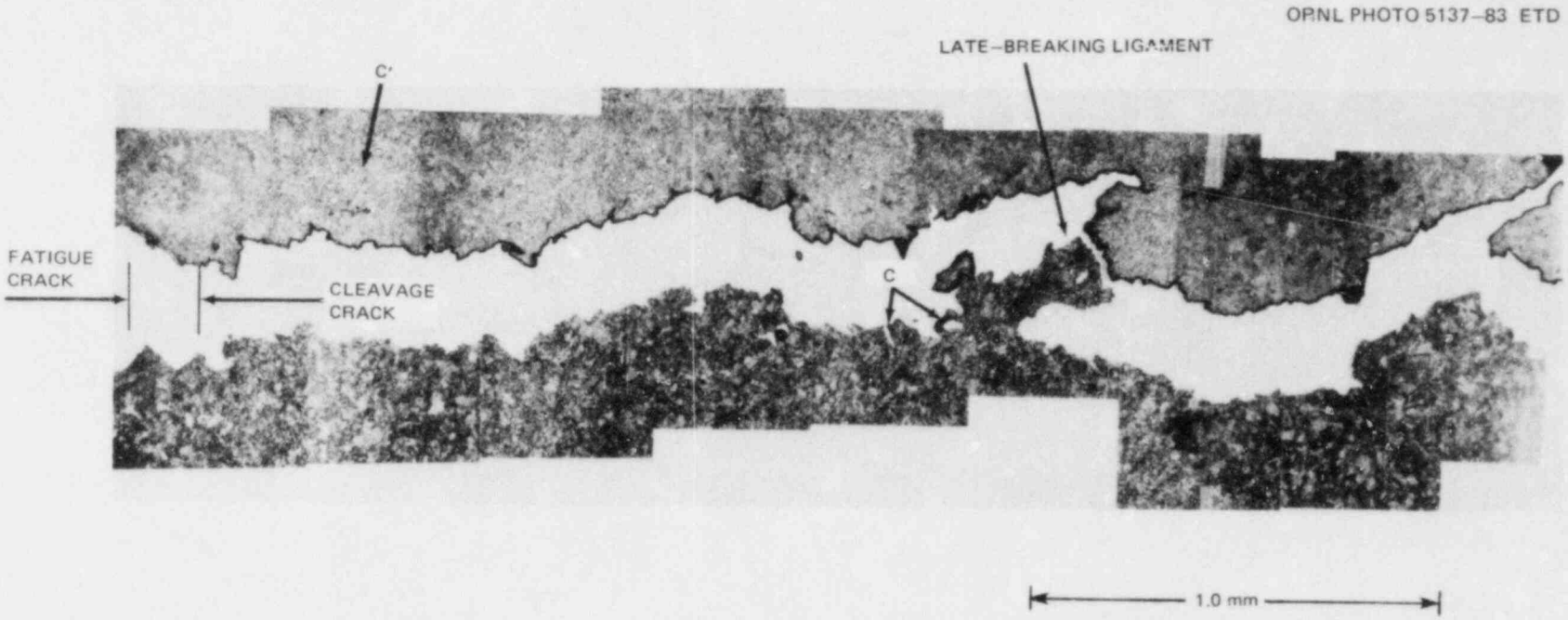

Fig. 2.15. Low-magnification section views along lines E-E and E'-E' normal to fracture surfaces shown in Fig. 2.14, showing deformed cleavage cracks (C) near large late-breaking ligament and smaller cleavage cracks (C'). (Original reduced 6%)

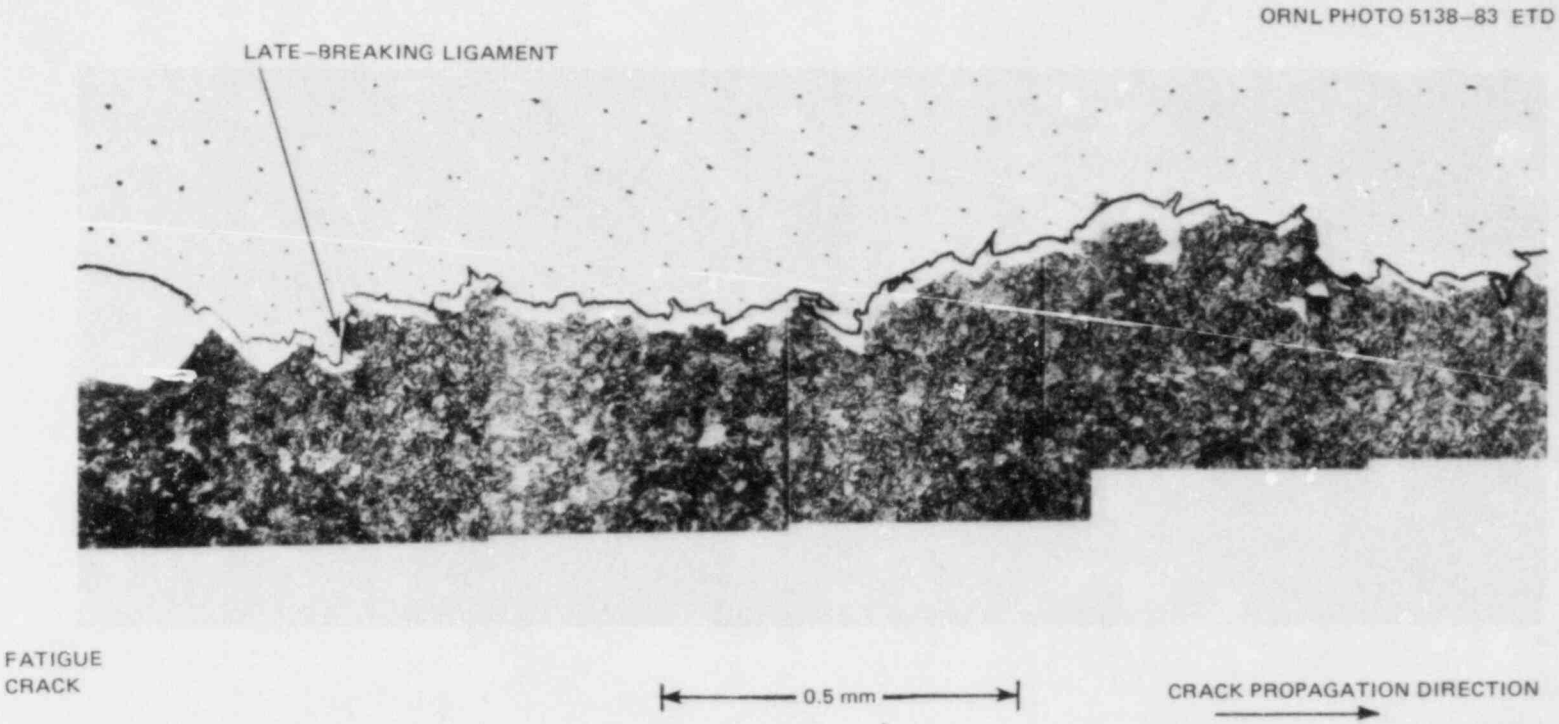

Fig. 2.16. Higher-magnification view of left-hand region of lower-section view in Fig. 2.15. A trace of the upper-surface contour is superimposed to show the matching of the upper and lower fracture surfaces.

ORNL PHOTO 5139-83 ETD

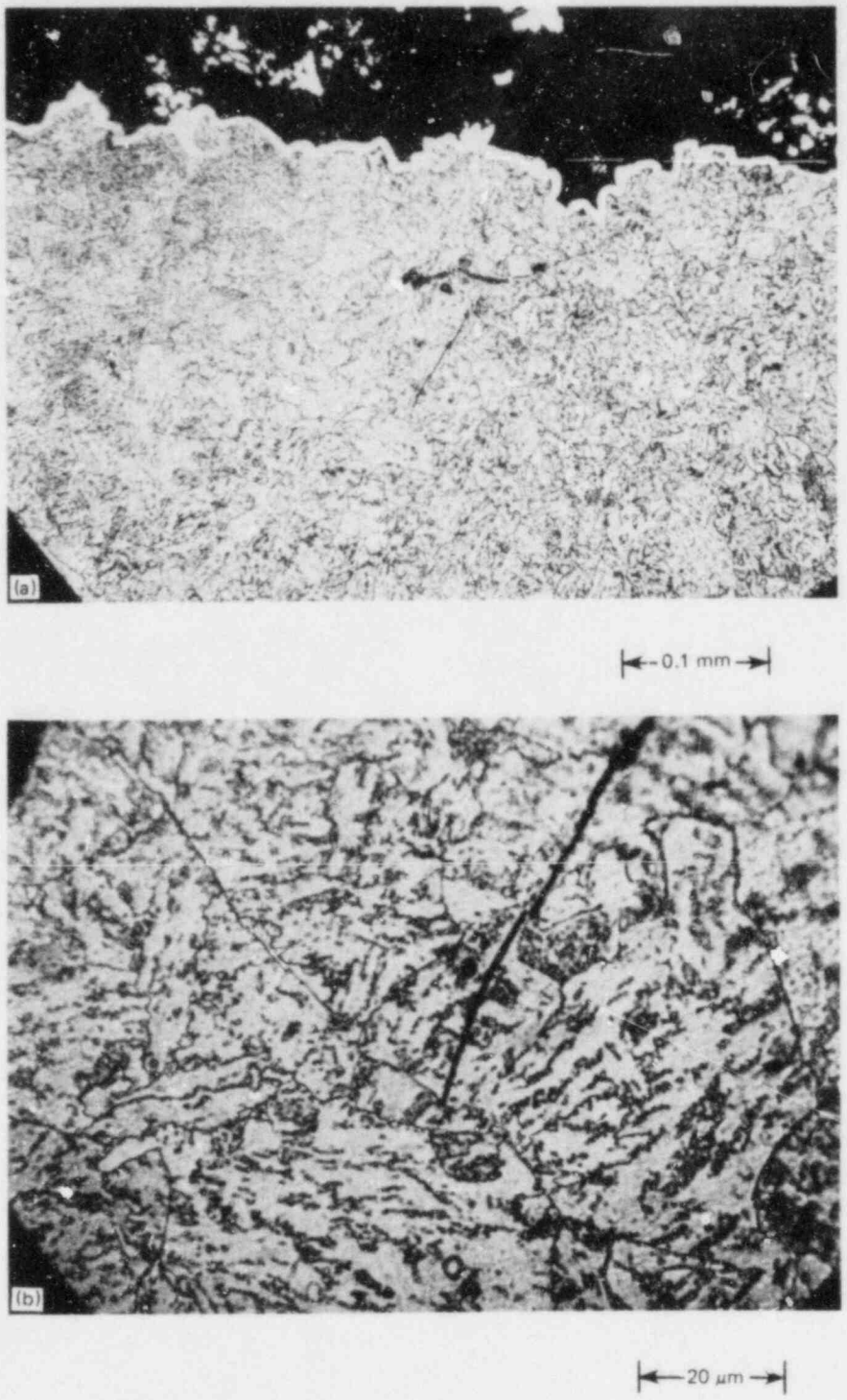

Fig. 2.17. Low- and high-magnification views of small cleavage cracks in region indicated by C′ in Fig. 2.15. (*a*) Low magnification and (*b*) high magnification.

for loss of cleavage. Figure 2.18(*a*) shows the general appearance of the fracture surface. Initial crack extension began in a fibrous manner and was accompanied by the opening of a vertical split. Beyond the maximum load point, the speed of crack extension caused initiation of regions of cleavage-dominated fracturing on each side of the vertical split. The edge of the vertical split then acted like a large and rather stiff late-breaking region, causing termination of cleavage and a return to fibrous crack extension.

Figures 2.18(*b*) and (*c*) show selected portions of the regions of change from fibrous-to-cleavage and cleavage-to-fibrous modes of crack extension, respectively. A degree of graduality in these changes is similar to the graduality of the fibrous-to-cleavage change observed in a spring-in-series fracture of A533B steel tested at 54°C.[25]

2.4.3 Plastic zone studies

The correct manner of handling a sizable plastic zone around the initial starter notch is presently of some interest with regard to crack-arrest testing. The presence of this plastic zone influences the measured CMODs and consequently affects the calculated values of K_0 and K_a. An unresolved question is how much of the plastic displacement should be included. A series of experiments has been conducted to gain some insight into this problem. Compact tension specimens fabricated from 6.4-mm-thick 7075 aluminum were used, with a 1-mm-thick birefringent coating (Photoelastic PS-1) bonded onto one face. The specimens all had a width w of 152 mm and a sawcut "crack," terminating in a drilled hole, to give an a/w of 0.42. A total of four tests were conducted using this geometry, which is shown in Fig. 2.19.

The specimen used in Test I of the series was loaded in steps to 47 kN and then completely unloaded in steps. The load vs CMOD record is shown in Fig. 2.20. Each step in the load-displacement record corresponds to a point where the loading was stopped to allow the photoelastic fringe pattern to be photographed and the strain gage readings to be taken at locations 12.7 and 25.4 mm ahead of the crack tip along the crack line. The strain gage measurements are shown in Fig. 2.21. The nonlinearity of the loading cycle strain measurements clearly indicates the presence of some plastic deformation ahead of the crack tip, and this can be confirmed from the fringe patterns shown in Figs. 2.22(*a*) and (*b*), which correspond to maximum load (P ~ 47 kN and K ~ 120 MPa·$\sqrt{m}$) and zero load (after unloading), respectively. The plastic zone size, $2r_Y$, can be calculated as being of the order of 20 mm for this case. A circle of this diameter has been marked on Fig. 2.22(*b*). Note that the fringe pattern of Fig. 2.22(*b*) does not represent the plastic zone itself, but rather shows the self-equilibrated redistribution of the elastic stress field that is produced by the presence of a small yielded region ahead of the crack tip.

The specimen was then removed from the testing machine and the slot extended to an a/w of 0.7 by saw-cutting with a jeweler's slitting saw of 0.25-mm thickness. Care was taken to remove only small amounts of material at a time to minimize the introduction of thermal stresses into either the aluminum or the coating material. A continous stream of coolant was also used for the same reason. The residual stress pattern remaining

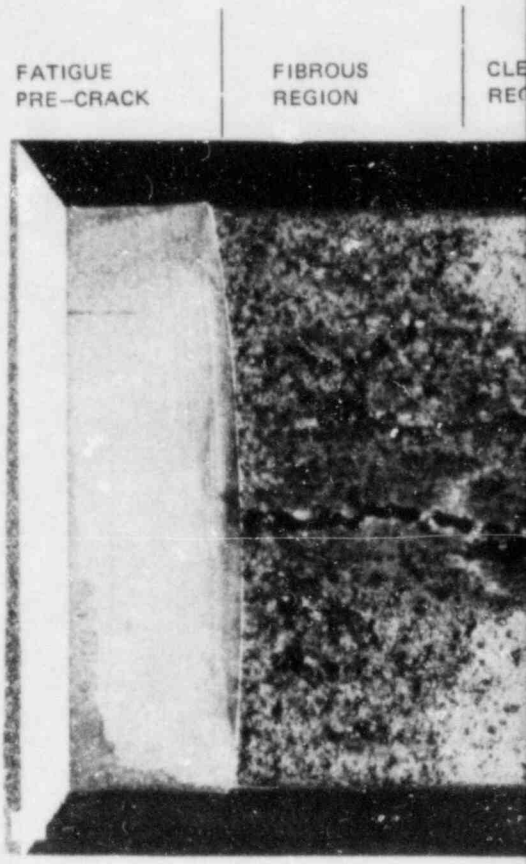

Fig.
4°C at Pic
surface, (
fibrous tr

ORNL PHOTO 5140-83 ETD

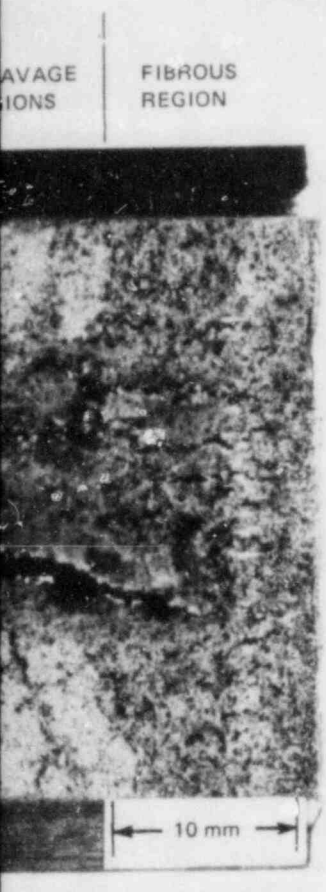

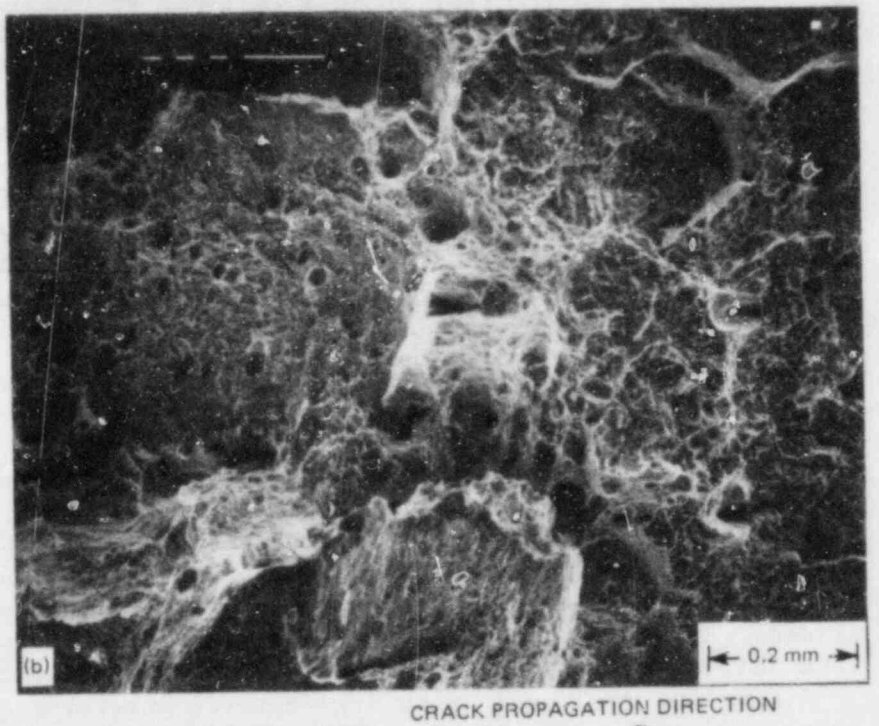

CRACK PROPAGATION DIRECTION

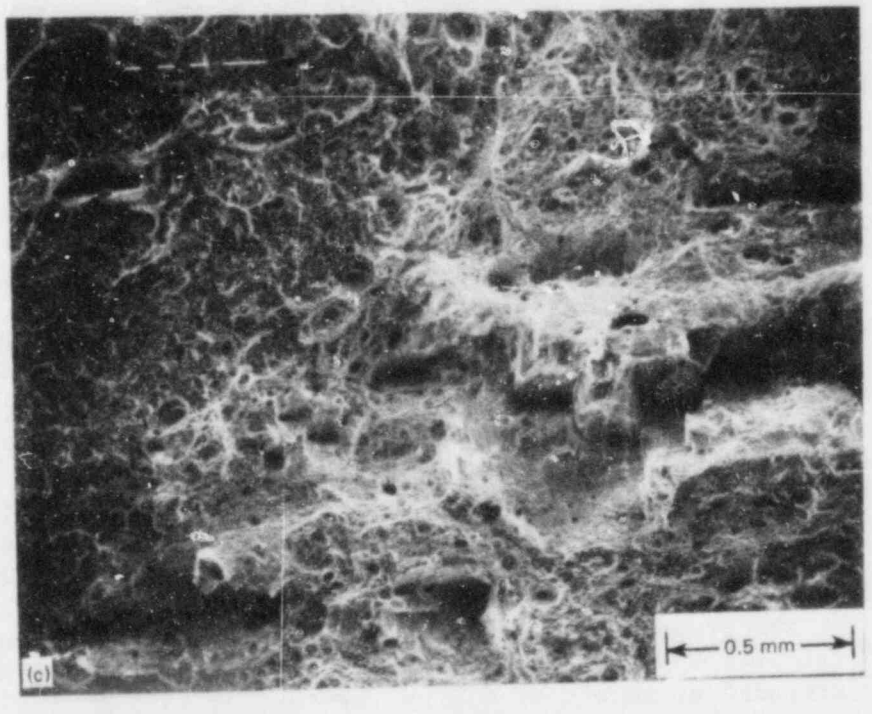

.18. Fracture appearance of A514 steel bend specimen tested at catini Arsenal. (*a*) Low-magnification photograph of fracture) fibrous-to-cleavage transition region, and (*c*) cleavage-to-nsition region.

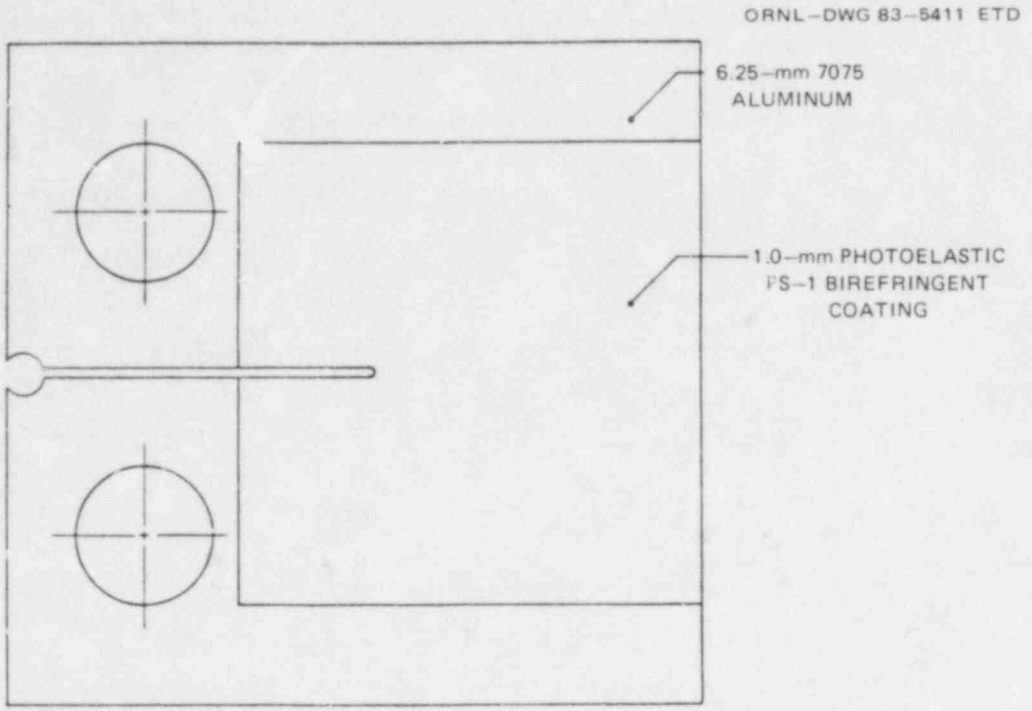

Fig. 2.19. Compact tension specimen used for plastic zone studies.

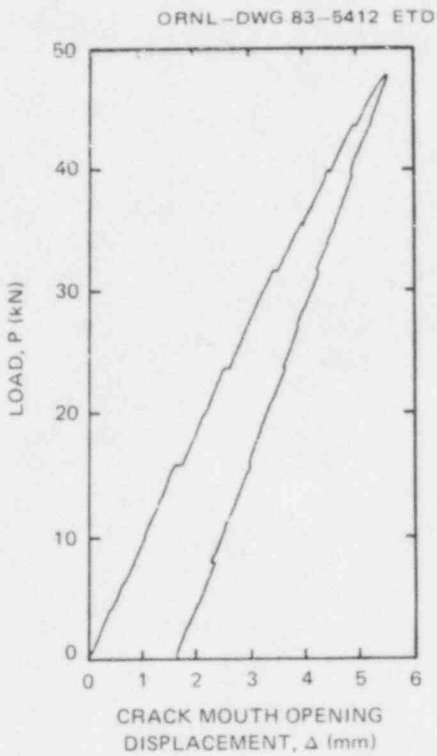

Fig. 2.20. Load vs CMOD record for Test I.

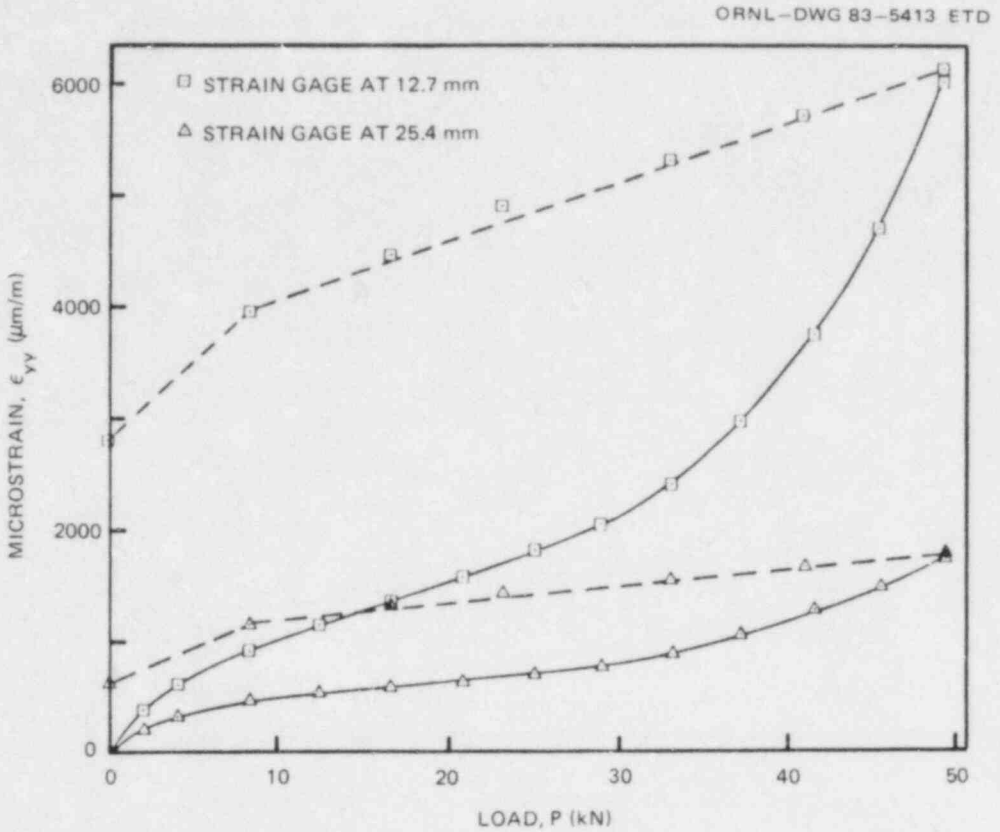

Fig. 2.21. Microstrain measured 12.7 and 25.4 mm ahead of crack tip during loading and unloading of specimen for Test I.

in the coating after slot extension was photographed (see Fig. 2.23). The only visible effect of the initial plastic zone is a low-order residual fringe pattern related to the permanent stretch in the plastic zone and comparable in size to the $2r_y$ value of 20 mm. The absence of most of the fringes of Fig. 2.22(*b*) indicates relief of the yielded region due to slot extension. The load-displacement record for this test (Fig. 2.20) shows that, after discounting the relaxation displacements, a permanent opening of 0.48 mm was present after unloading. (The maximum opening was 48 mm.) Optical measurements before and after slot extension indicated a recovery of 0.36 mm of opening displacement, giving a final residual opening of 0.12 mm.

This test sequence was repeated with another specimen, but with two important differences. Firstly, loading was continuous to eliminate any relaxation stair-steps in the load-displacement record, such as those seen in Fig. 2.20. Secondly, the specimen was unloaded to about 10 kN and the crack wedged open with a drill rod prior to saw-cutting. This was prompted by a desire to avoid taking the yielded region from tension to compression, which seemed to have occurred in Test I. (Note the change in slope in the unloading strain records at approximately this load in Fig. 2.21.) The residual fringe pattern after extending the crack by saw-cutting and removing the drill rod is shown in Fig. 2.24. Once again, no

ORNL PHOTO 5141–83 ETD

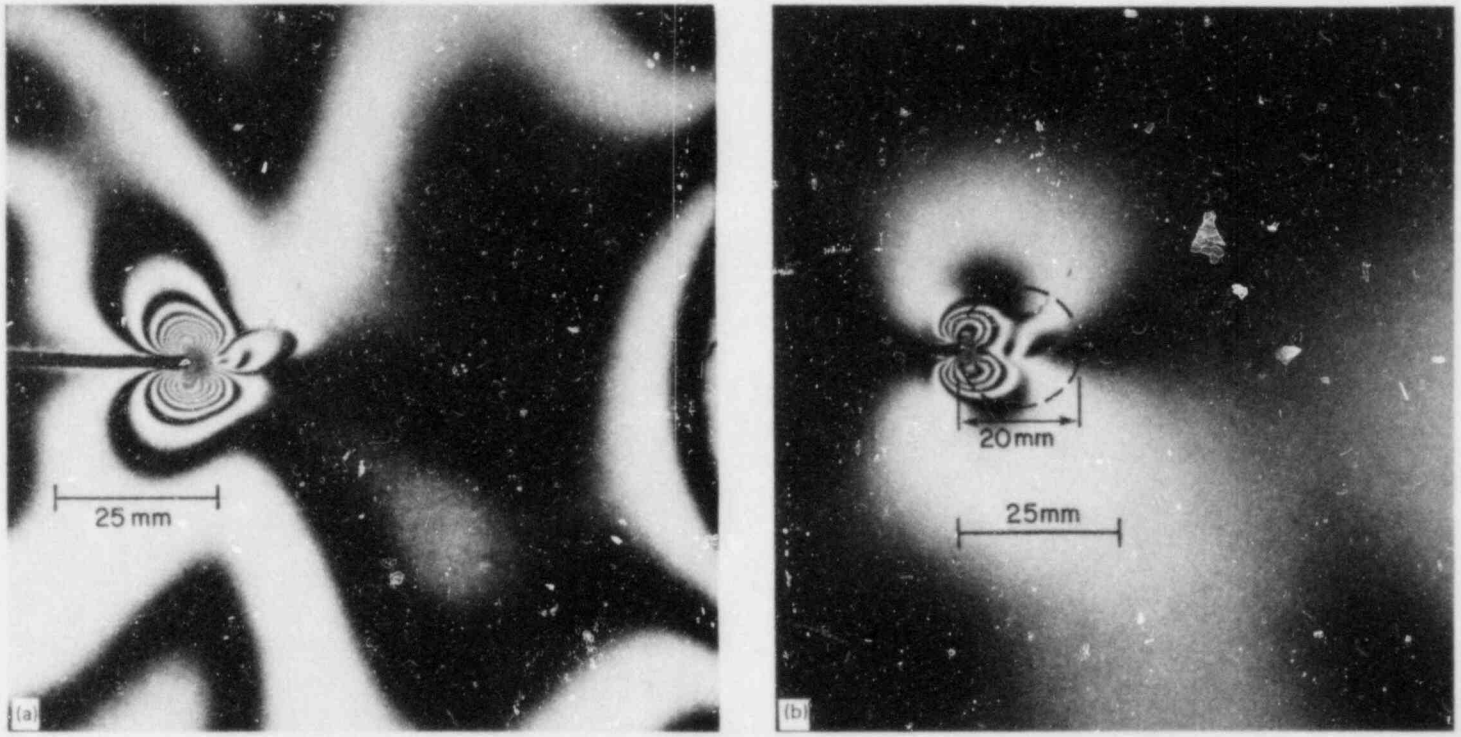

Fig. 2.22. Photoelastic fringe patterns in birefringent coating for Test I. (*a*) At maximum load and (*b*) after unloading to zero load.

ORNL PHOTO 5142-83 ETD

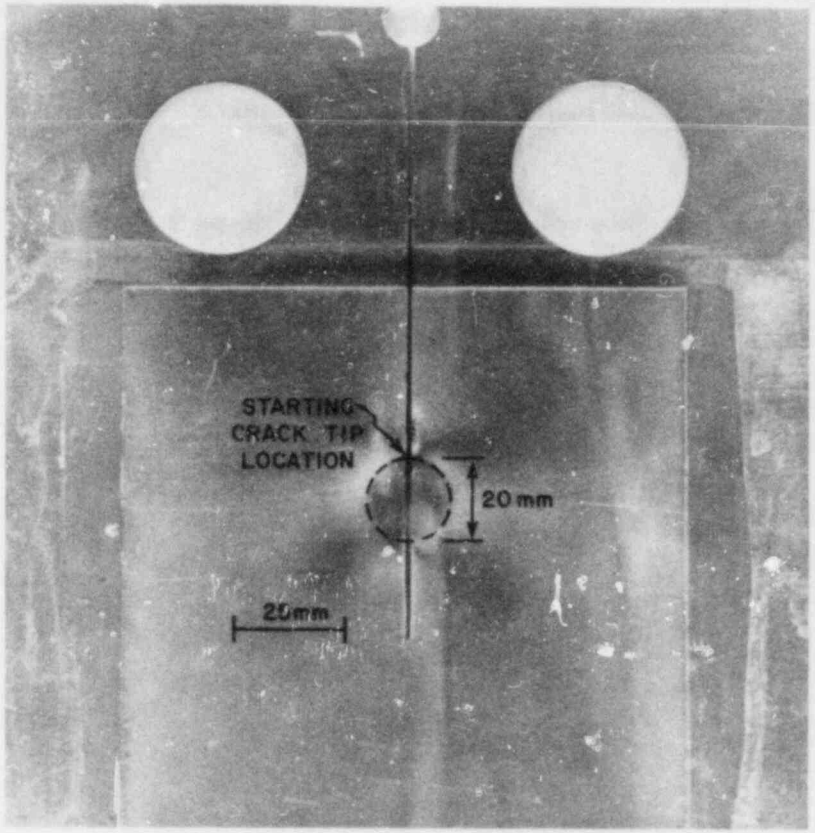

Fig. 2.23. Residual fringe pattern in birefringent coating after slot extension for Test I.

ORNL PHOTO 5143-83 ETD

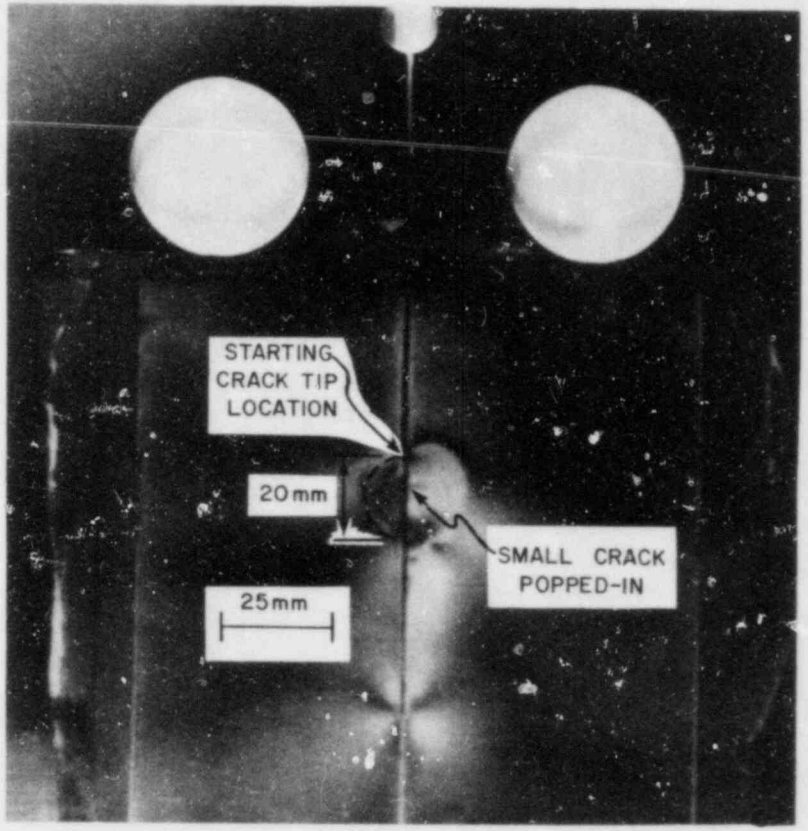

Fig. 2.24. Residual fringe pattern in birefringent coating after slot extension for Test II.

visible residual stress pattern can be seen in the birefringent coating, other than the low-order fringe in the left half of the specimen, comparable in size with the $2r_\gamma$ of the original plastic zone. (The fringe pattern in the right half of the specimen is the result of a small off-axis crack that popped in during loading.) Optical measurements prior to loading and after completion of the test sequence indicated a final residual CMOD of 0.15 mm, which compares well with the result of 0.12 mm obtained from Test I. Note that the CMOD at maximum load and the associated plastic displacement could not be measured because of the small crack that popped in.

A fine (0.25-mm-thick) jeweler's saw was used to extend the crack in each of Tests I and II. This procedure differs from the run of a crack during a run/arrest event because the removal of material by the saw blade allows for the closure of the crack to an extent that would not be possible in a crack-arrest test due to impingement of the mating fracture surfaces. Tests III and IV were therefore performed to study this effect. Specimens of the type described earlier were used, with 20% side grooves on the one side and the coating on the other side split with the 0.25-mm saw. Both specimens were loaded to failure; this occurred at loads of the order of 30 kN and K-values of about 90 MPa$\cdot\sqrt{m}$, which corresponds to a $2r\gamma$ of 11 mm. The residual fringe patterns photographed after the run of the crack in Tests III and IV are shown in Figs. 2.25 and 2.26, respectively. The residual patterns are similar to those obtained with Tests I and II, indicating the possibility of similar behavior with regard to opening displacements also.

Care must be taken when trying to apply these preliminary results to the proposed crack-arrest test procedure. Firstly, the plastic zone sizes in the specimens tested were relatively small ($2r_\gamma$ values of 11 and 19 mm) when compared with the lateral dimensions of the specimen (w = 152 mm). Secondly, the results obtained from Tests III and IV, in which the crack ran through the specimen, have to be interpreted in a qualitative fashion, because photographs of the residual fringe pattern prior to crack propagation could not be recorded and residual plastic opening displacements could not be measured. We therefore intended to pursue this investigation further during the coming quarter, with a view towards using larger plastic zones and perhaps taking flash photographs of the propagating crack-tip fringe patterns.

2.4.4 Dynamic run/arrest calculations

Improvements to the SAMCR code. Substantial progress towards improving our 2-D dynamic finite-element code, SAMCR, has been made during the current report period. Sources of particular concern in the computer code results have been identified previously[26-28] as being the oscillations with time in the computed K-values, the discontinuous changes in K that were associated with the shift of the J-integral contour as the crack tip completed its advance from one node to the next, and the rather long time required for K to decay from its starting value. No evidence of such phenomena has been seen in the many plastic model tests conducted in our dynamic photoelastic studies of run/arrest fracturing, and it was felt that the computational results were a consequence of some flaw in the computer

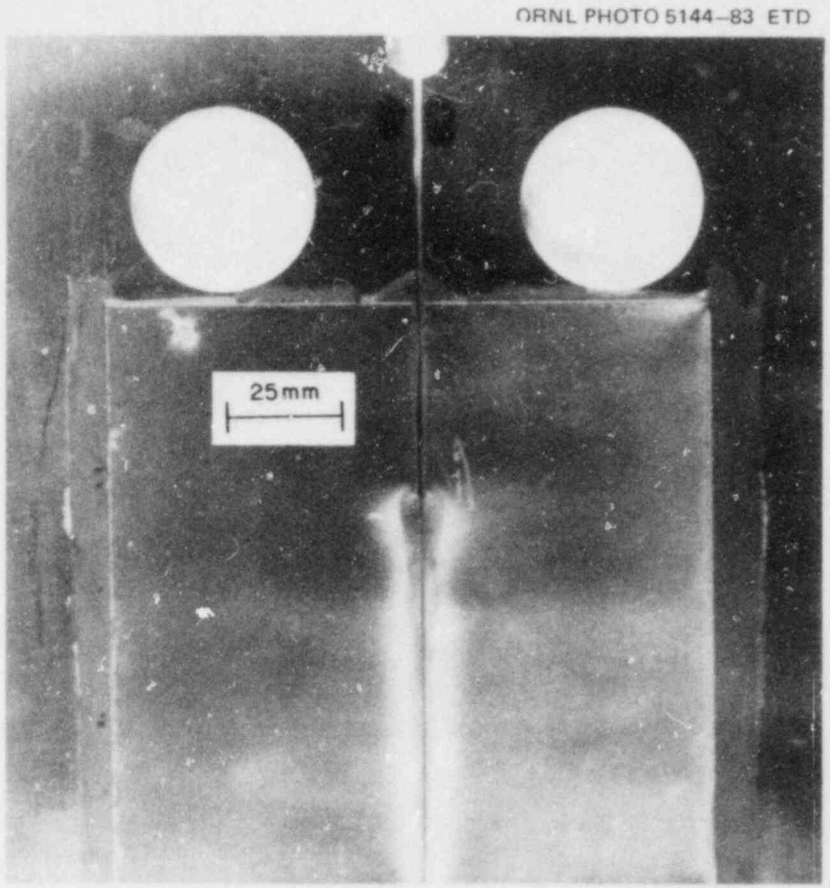

Fig. 2.25. Residual fringe pattern in birefringent coating after run of crack in Test III.

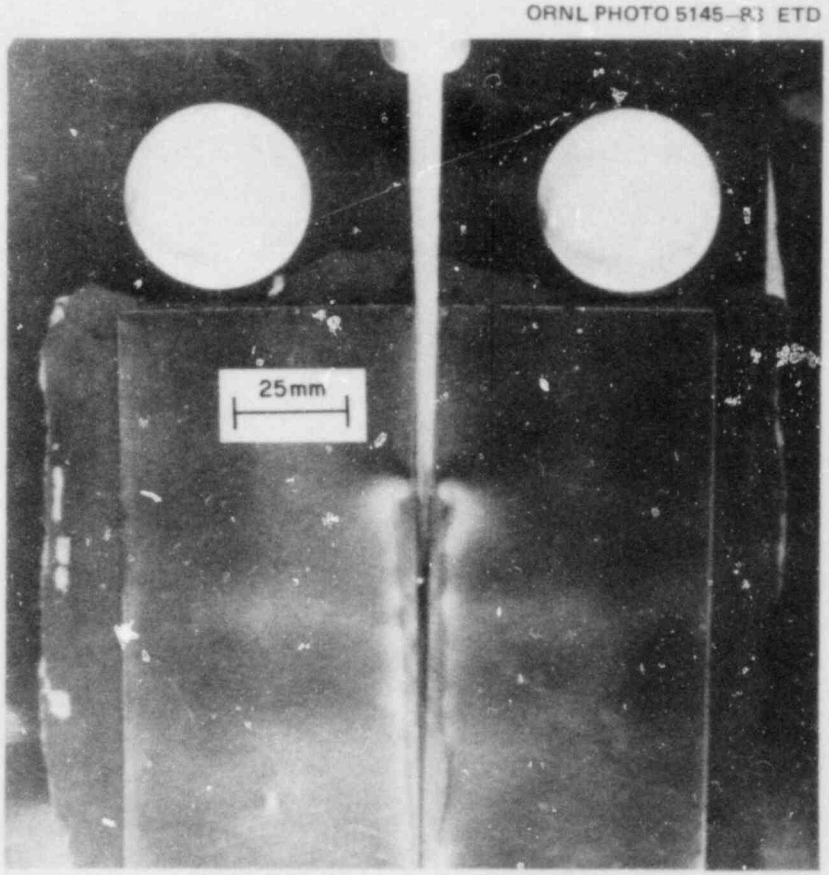

Fig. 2.26. Residual fringe pattern in birefringent coating after run of crack in Test IV.

code algorithms or the manner in which the propagation of the crack was being modeled.

Previous results from our continuing critical appraisal of the formulations used in SAMCR and other computer codes had led to modifications to SAMCR: (1) the use of element stiffness corrections to control keystone mode deformations,[26] (2) changes in the J-contour geometery used,[27] and (3) the use of small amounts of viscous damping in both bulk and keystone modes.[28] The computed K vs time data obtained from the modeling of one dynamic photoelastic test following these improvements are shown in Fig. 2.27 for the first 150 μs of crack propagation. (These results were originally reported in ORNL/TM-8787/V1.) Although these results represented a substantial improvement over those obtained previously, they display a strong underlying oscillation, as well as some abrupt changes in K (though of a much greater diminished magnitude than before). The period of the K-oscillation is of the order of 15 to 20 μs, which compares closely with the transit time of the crack tip from one node to the next. This suggested a closer examination of the J-integral algorithm and the algorithm governing the internode crack propagation.

Three further improvements have therefore been made to the SAMCR code: (1) a change in the calculation of the net nodal force at the node that is immediately behind the crack tip and currently being released, (2) a more continuous transition from the partially released to the fully released condition for the released node, and (3) the use of a "continuously moving" J-contour – that is, a linearly interpolated J-value obtained using contours centered on the nodes immediately ahead of and immediately behind the crack tip.

Figure 2.28 shows the results from the revised analysis for K as a function of time for the same test whose results were presented in Fig. 2.27. The predicted drop in K after crack initiation more closely follows that observed experimentally;[29] discontinuous changes in K are now completely eliminated, and the level of any oscillations is of a degree to be expected in any dynamic analysis of this type.

An extensive series of verification analyses involving dynamically loaded uncracked plates and plates with nonpropagating fractures has been performed using the revised code. These changes in combination with those listed previously have improved the performance of the code substantially. However, we are continuing detailed sensitivity studies and comparisons between analytical, numerical, and experimental results for further development and enhancement of the SAMCR code.

Comparisons between photoelastic experiments and SAMCR results. The revised formulation of SAMCR has been used to predict run/arrest behavior in wedge-loaded modified compact tension (MCT) specimens fabricated from Homalite 100. The specimens all had a width w of 203 mm, a thickness of 12.7 mm, and an initial crack length of a/w = 0.44. Computer runs were made with low, intermediate, and high values of initial stress-intensity factor K_Q to model three experiments for which data had previously been obtained using dynamic photoelasticity. The same three tests had been analyzed with SAMCR (Ref. 29), and the intermediate test was being used for the different trials with SAMCR reported in the past several quarterly reports.

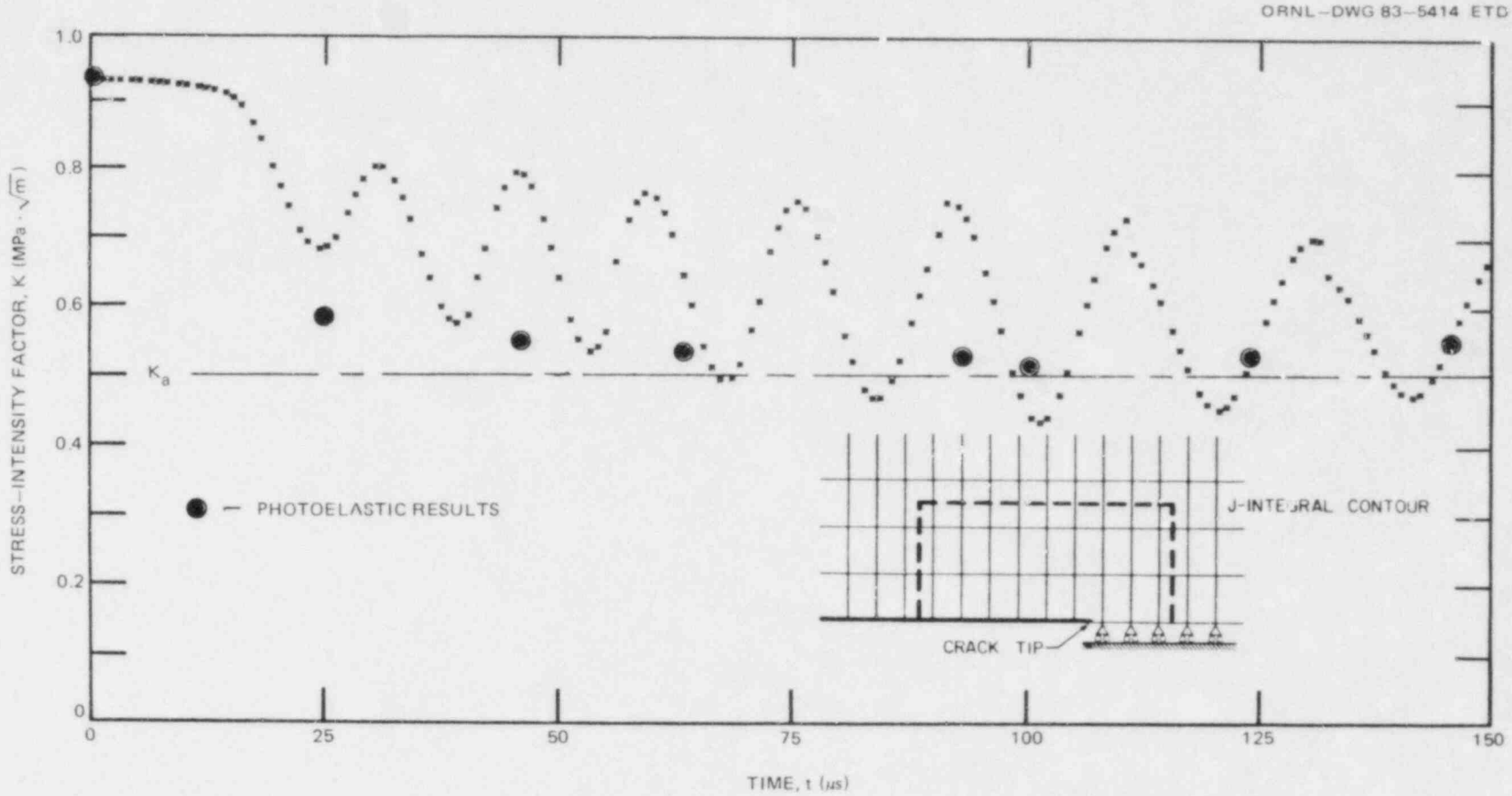

Fig. 2.27. Stress-intensity factor as function of time for Homalite 100 MCT test using version of SAMCR with stiffness corrections, viscosity, and J-contour shown.

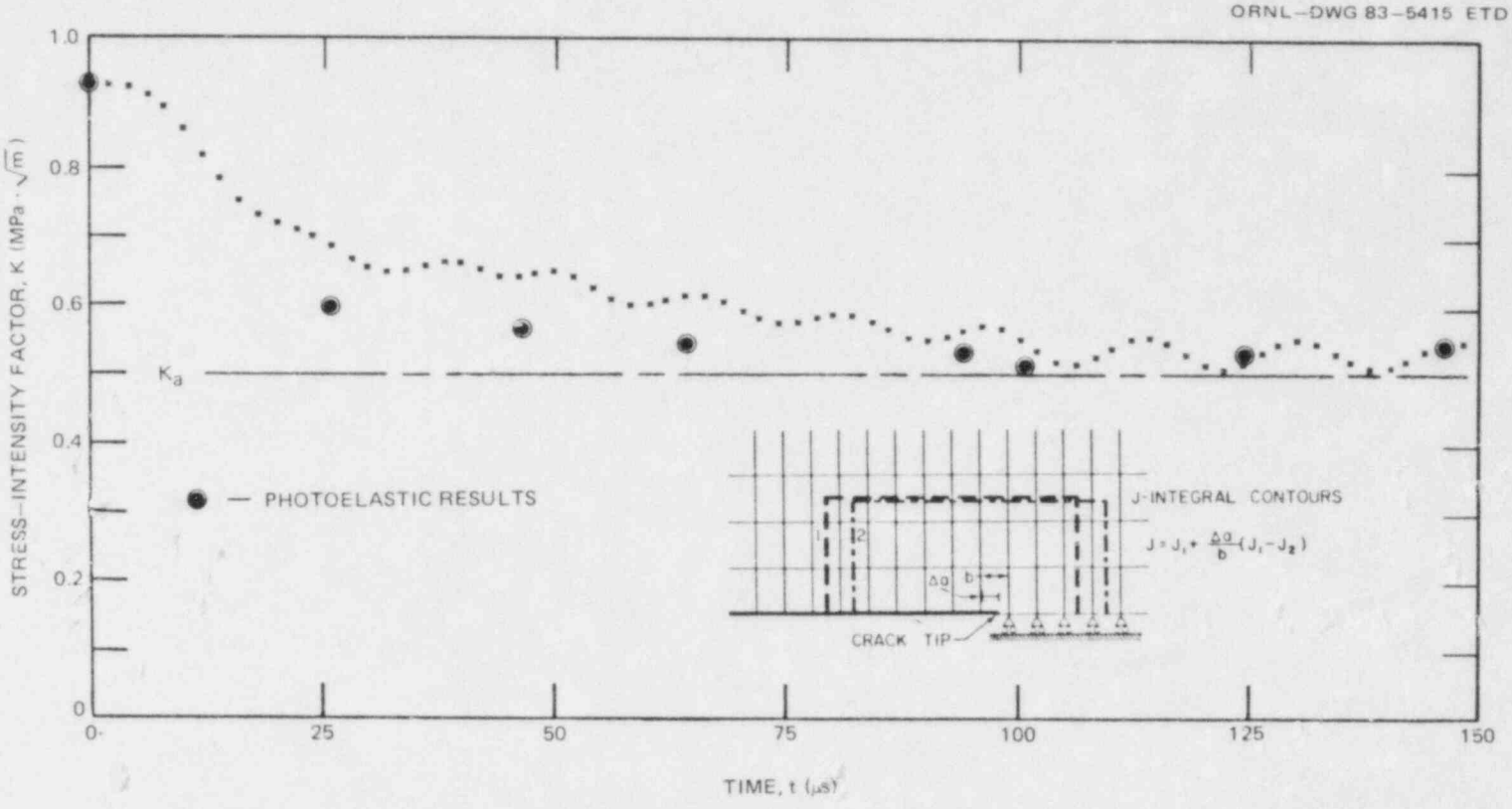

Fig. 2.28. Stress-intensity factor as function of time for same test as Fig. 2.27, analyzed using SAMCR with additional improvements in treatment of nodal force release and continuously moving J-contour.

The analysis results for all three tests are quite similar and only the lowest K_Q test (Test P9) will be discussed in detail. Figures 2.29–2.31 show, respectively, K vs time, crack extension vs time, and energies vs time for this test, over a time span of 500 μs. These results compare well with the experimental measurements superposed in Figs. 2.29 and 2.30.

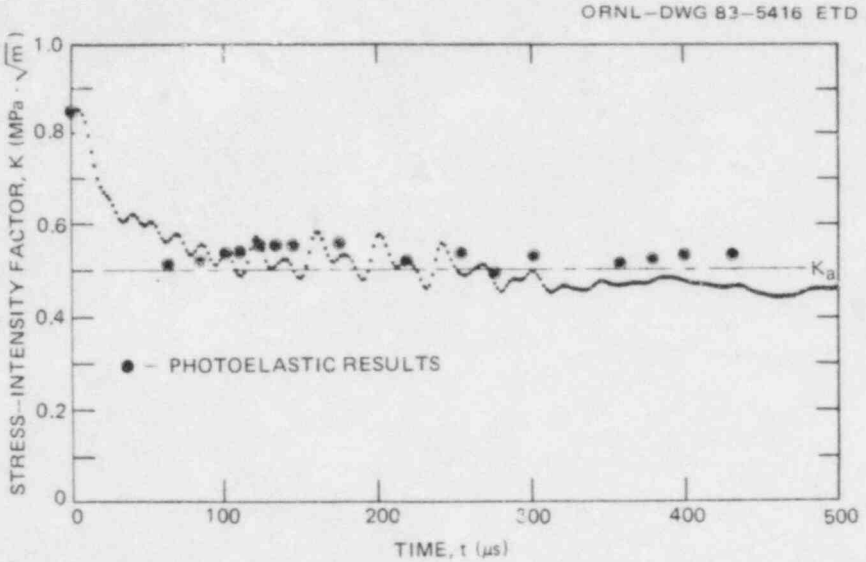

Fig. 2.29. Predicted and experimental values of K as function of time for Test P9.

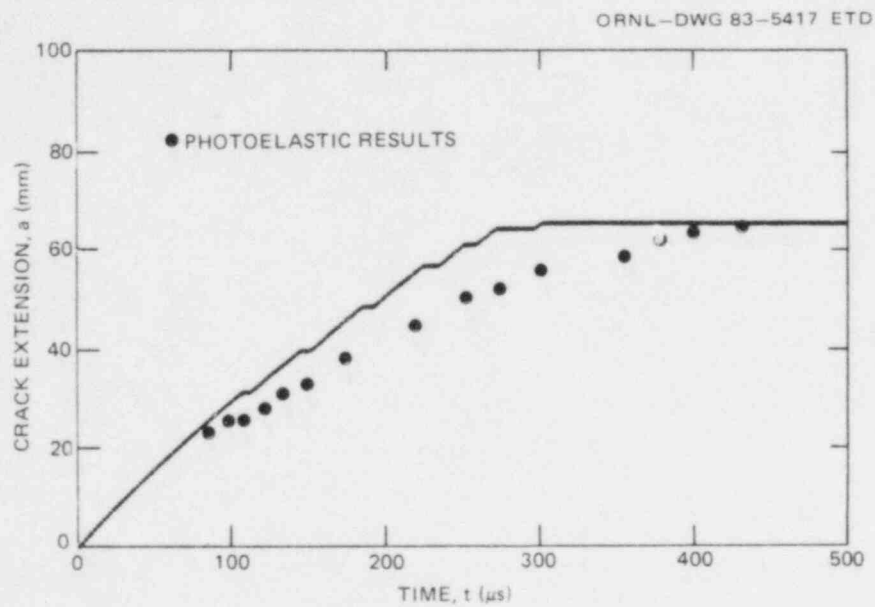

Fig. 2.30. Predicted and experimental crack extension as function of time for Test P9.

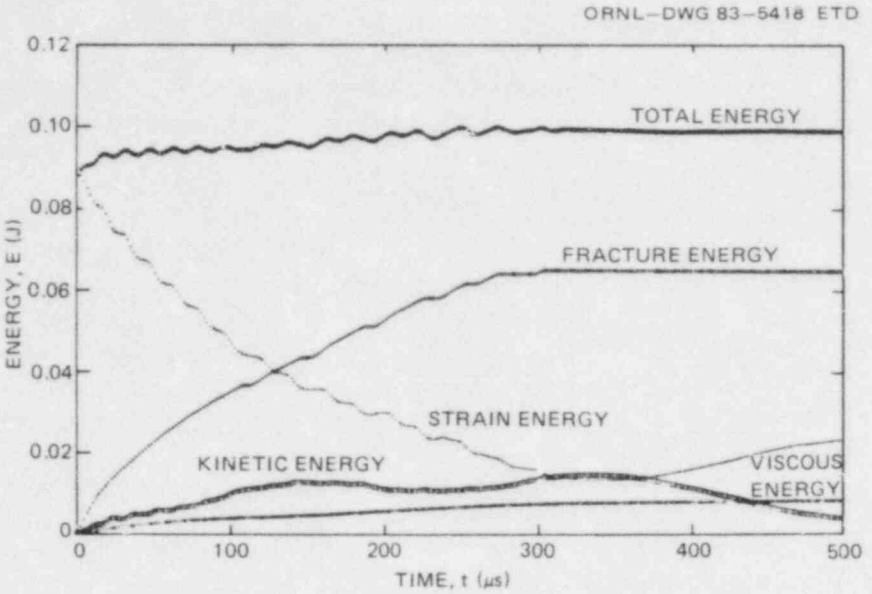

Fig. 2.31. Strain, fracture, kinetic, viscous, and total energies as functions of time for Test P9.

Some minor differences merit further comment. The computed K-value (Fig. 2.29) drops quickly from the initiation level but not quite as rapidly as the experimental data. At the other end of the propagation phase, arrest does not occur as a single event but rather as a series of short run/arrest segments, followed by a much longer arrest that is typically of 150- to 200-μs duration in a computational time span of 500 μs. Table 2.6 shows the comparison between predicted and observed crack extension for the three tests analyzed. Predicted crack jumps differed from the measured values by <7% for all three cases.

Sensitivity studies. Several parameters governing the internal details of the calculations in the computer code have been identified in

Table 2.6. Comparison of observed and predicted crack extension for wedge-loaded Homalite 100 MCT specimens

Test	Wedge-load (kN)	Crack jump (mm)		Ratio of predicted to observed jump (%)
		Observed	Predicted	
P9	0.51	67.3	65.5	97.5
P7	0.56	79.5	74.2	93.4
P10	0.65	86.1	89.9	104.0

this and previous progress reports. These include the geometry selected for the J-contour, the level of viscous damping, and the exact form of the force decay function for the node being released. The effects of varying these parameters on the code results have been examined to some degree.

It has been found that the SAMCR results are relatively insensitive to the details of the J-contour, the viscosity level, and the restrained nodal force decay function. The maximum difference in crack jump, for example, was found to be <5%. Arrest time did show a greater sensitivity to the specified viscosity with a maximum difference of about 20%. The slight oscillations still present in the computed K-values were also found to vary somewhat with viscosity level and force decay function, as would be expected. Detailed results from verification analyses and sensitivity studies are too lengthy for discussion in a progress report, but they will be included in a topical report on the SAMCR code.

Some interesting results were obtained when the computations for the wedge-loaded MCT specimens were carried out to times of the order of 1500 μs, which is of course much longer than the run/arrest time of 400 μs typical of the experimental tests used for comparison. After arresting for time periods of the order of 150 to 200 μs, the code results predicted a reinitiation resulting in an additional increment of crack extension late in the event.

The reasons for this additional segment of predicted crack extension are not immediately clear. Such behavior was not observed experimentally in the tests being modeled, for which the fracture surfaces of the specimens clearly showed a single run/arrest sequence. An examination of the computed K-values in the reinitiation phase showed that these rarely exceeded K_a by more than 7.5%. It is generally agreed that an elevation in K of 5 to 10% is necessary for reinitiation of an arrested crack; this requirement is not included in the present code. Also, polymeric materials such as Homalite 100 display a sensitivity of elastic modulus to strain rate. The use of a strain-rate dependent modulus would lower K-values obtained from J-calculations by up to 10%, which would eliminate this late reinitiation from the computational results. The current version of SAMCR does not account for strain-rate effects in the J-to-K conversion and does not allow for elevation of initiation toughness after a long arrest period.

We are currently pursuing comparisons between computer code results and crack-arrest experiments for 4340 steel MCT specimens; additional verification and sensitivity studies; the incorporation of thermal effects for TSE-support analysis; and the analysis of geometries such as the single-edge-notch, which is similar to the specimen proposed for ESSO-type testing.

References

1. R. W. McCulloch, "OCA Parametric Study for PTSE-1," *Heavy-Section Steel Technology Program Quart. Prog. Rep. October-December 1982*, NUREG/CR-2751, Vol. 4 (ORNL/TM-8369/V4), Union Carbide Corp. Nuclear Div., Oak Ridge Natl. Lab.

2. J. W. Bryson and R. W. McCulloch, "Comparisons of 3-D and 2-D Computed K-Values for Outside Surface Flaws in an ITV for Combined Pressure-Thermal Loading," *Heavy-Section Steel Technology Program Quart. Prog. Rep. October-December 1982*, NUREG/CR-2751, Vol. 4 (ORNL/TM-8369/V4), Union Carbide Corp. Nuclear Div., Oak Ridge Natl. Lab.

3. S. K. Iskander et al., *OCA-I, A Code for Calculating the Behavior of Flaws on the Inner Surface of a Pressure Vessel Subjected to Temperature and Pressure Transients*, NUREG/CR-2113 (ORNL/NUREG-84), Union Carbide Corp. Nuclear Div., Oak Ridge Natl. Lab., August 1981.

4. D. G. Ball et al., "Superposition Methods in Three-Dimensional Computational Fracture Mechanics," *Heavy-Section Steel Technology Program Quart. Prog. Rep. October-December 1982*, NUREG/CR-2751, Vol. 4 (ORNL/TM-8369/V4), Union Carbide Corp. Nuclear Div., Oak Ridge Natl. Lab.

5. K. J. Bathe, *ADINA — A Finite-Element Program for Automatic Dynamic Incremental Nonlinear Analysis*, Report 82448-1, Massachusetts Institute of Technology, Cambridge, Mass., September 1975 (revised December 1978).

6. B. R. Bass and J. W. Bryson, *Applications of Energy Release Rate Techniques to Part-Through Cracks in Plates and Cylinders, Volume 2. ORVIRT: A Finite Element Program for Energy Release Rate Calculations for 2-D and 3-D Crack Models*, NUREG/CR-2997, Vol. 2 (ORNL/TM-8527/V2), Union Carbide Corp. Nuclear Div., Oak Ridge Natl. Lab., February 1983.

7. R. H. Bryan and J. G. Merkle, "Upper-Shelf Arrest Analysis Based on J_R-Controlled Tearing," *Heavy-Section Steel Technology Program Quart. Prog. Rep. January-March 1983*, NUREG/CR-3334, Vol. 1 (ORNL/TM-8787/V1), Union Carbide Corp. Nuclear Div., Oak Ridge Natl. Lab.

8. J. G. Merkle, "Elastic-Ideally Plastic Pressurized Thermal Shock Analysis for a Deep Continuous External Longitudinal Crack in a Cylinder," *Heavy-Section Steel Technology Program Quart. Prog. Rep. January-March 1983*, NUREG/CR-3334, Vol. 1 (ORNL/TM-8787/V1), Union Carbide Corp. Nuclear Div., Oak Ridge Natl. Lab.

9. J. W. Bryson, J. G. Merkle, and B. R. Bass, "Fully Plastic Ligament Study of an ITV for Combined Pressure-Thermal Loading Using ADINA-ORVIRT," *Heavy-Section Steel Technology Program Quart. Prog. Rep. January-March 1983*, NUREG/CR-3334, Vol. 1 (ORNL/TM-8787/V1), Union Carbide Corp. Nuclear Div., Oak Ridge Natl. Lab.

10. R. H. Bryan, Oak Ridge National Laboratory, and W. J. Stelzman, Oak Ridge National Laboratory, private communication, April 19, 1983.

11. H. A. Domian and R. J. Futato, "J-Integral Test Results of HSST-ITV8A Low Upper Shelf Weld," Babcock and Wilcox Company, Alliance, Ohio; submitted to ORNL February 1983.

12. M. Nakanishi et al., "Electron Beam Welding of Heavy Section Steel Plates," *Transactions, Iron and Steel Inst. of Japan* 23, 71–80 (1983).

13. A. R. Rosenfield and P. N. Mincer, "Reinitiation of an Arrested Cleavage Crack," *Engineering Fracture Mechanics* (in press).

14. A. R. Rosenfield et al., "BCL HSST Support Program," *Heavy-Section Steel Technology Program Quart. Prog. Rep. January–March 1983*, NUREG/CR-3334, Vol. 1 (ORNL/TM-8787/V1), Union Carbide Corp. Nuclear Div., Oak Ridge Natl. Lab.

15. R. D. Cheverton et al., "Application of Crack Arrest Theory to a Thermal Shock Experiment," pp. 392–421, in *Crack Arrest Methodology and Applications: A Symposium*, ASTM STP 711 (1980).

16. R. D. Cheverton et al., "Fracture Mechanics Data Deduced from Thermal Shock and Related Experiments with LWR Pressure Vessel Material," *Aspects of Fracture Mechanics in Pressure Vessels and Piping*, ASME Publ. PVP 58, 1–15 (1982).

17. A. Pellissier-Tanon et al., "Crack Initiation and Arrest in a SA508 CL3 Cylinder Under Liquid Nitrogen Thermal Shock Experiment," *SMIRT-VII Proceedings*, Chicago, Illinois (1983).

18. A. R. Rosenfield et al., *Critical Experiments, Measurements, and Analyses to Establish a Crack Arrest Methodology for Nuclear-Pressure-Vessel Steels*, NUREG/CR-1887 (BMI-2071), 1981.

19. W. L. Fourney, "Investigation of Damping and of the Cleavage-Fibrous Transition in Reactor-Grade Steel," *Heavy-Section Steel Technology Program Quart. Prog. Rep. October–December 1981*, NUREG/CR-2141, Vol. 4 (ORNL/TM-8252/V4), Union Carbide Corp. Nuclear Div., Oak Ridge Natl. Lab.

20. Y. Nakano and M. Tanaka, "Crack Arrest Toughness of Structural Steels Evaluated by Compact Test," *Trans. Iron and Steel Inst. of Japan* 22, 147–53 (1982).

21. H. Susukida et al., "Fracture Toughness of Heavy Section Steel for Nuclear Reactor Pressure Vessel Steel," *Trans. Iron and Steel Inst. of Japan* 17, 497–505 (1982).

22. Y. Nakano, "Stress Intensity Factors During Brittle Crack Propagation and at Arrest in ESSO Specimens," *Zairyo* 31, 204–09 (1982); tr. Language Services, Knoxville, Tennessee.

23. P. Stanley et al., "A Design Exercise for a Ceramic Turbine Disc Subjected to Centrifugal Stresses," *J. Strain Anal. and Engr. Design* 13, 103–13 (1978).

24. K. Wallin et al., "Theoretical Scatter in Brittle Fracture Toughness Results Described by the Weibull Distribution," paper to be presented at the European Conference on Fracture (1983).

25. K. Ogawa et al., "Microstructural Aspects of the Fracture Toughness Cleavage-Fibrous Transition for Reactor Grade Steel," ASTM 15th National Symposium on Fracture Mechanics, College Park, Md., July 1982, ASTM STP (in press).

26. W. L. Fourney, "Investigation of Damping and of the Cleavage-Fibrous Transition in Reactor-Grade Steel," pp. 49–55 in *Heavy-Section Steel Technology Program Quart. Prog. Rep. July-September 1982*, NUREG/CR-2751, Vol. 3 (ORNL/TM-8369/V3), Union Carbide Corp. Nuclear Div., Oak Ridge Natl. Lab.

27. G. D. Whitman and R. H. Bryan, pp. 50–55 in *Heavy-Section Steel Technology Program Quart. Prog. Rep. October-December 1982*, NUREG/CR-2751/Vol. 4 (ORNL/TM-8369/V4), Union Carbide Corp. Nuclear Div., Oak Ridge Natl. Lab.

28. W. L. Fourney et al., "Investigation of Damping and of the Cleavage-Fibrous Transition in Reactor Grade Steel," *Heavy-Section Steel Technology Program Quart. Prog. Rep. January-March 1983*, NUREG/CR-3334, Vol. 1 (ORNL/TM-8787/V1), Union Carbide Corp. Nuclear Div., Oak Ridge Natl. Lab.

29. G. R. Irwin et al., *Photoelastic Studies of Damping, Crack Propagation and Crack Arrest in Polymers and 4340 Steel*, NUREG/CR-1455, Union Carbide Corp. Nuclear Div., Oak Ridge Natl. Lab., May 1980.

3. INVESTIGATION OF IRRADIATED MATERIALS

R. K. Nanstad

3.1 Fourth HSST Irradiation Series

R. G. Berggren T. N. Jones
R. K. Nanstad

The cooperative testing program[1] on specimens from the first three capsules of the Fourth Heavy-Section Steel Technology (HSST) Irradiation Study is continuing. In this program, Charpy V-notch (CVN) impact tests and fracture toughness tests on 1TCS specimens are divided between two facilities, Oak Ridge National Laboratory (ORNL) and Materials Engineering Associates (MEA). The main sets of CVN tests on both unirradiated (control) and irradiated specimens have been completed by the two facilities. The CVN tests of the few "unassigned" specimens will be conducted after completion of a statistical study of the results obtained to date. Scoping tests on unirradiated fracture toughness (1TCS) specimens were started. The main body of fracture toughness tests should be completed in the next quarter.

The fourth capsule of the Fourth HSST Irradiation Study contains materials supplied by the Federal Republic of Germany (FRG). A proposed test program has been submitted to the FRG, and testing should begin soon after consensus is reached on the test program.

Some statistical analyses of the CVN impact tests (unirradiated and irradiated) on materials (chemical compositions previously reported[1]) from the first three capsules have been conducted by the method presented previously.[2] In this method of analysis, (1) the transition region and upper-shelf region of unirradiated specimen data are separately fitted to linear functions, and (2) the differences between irradiated specimen data and the straight-line function for unirradiated specimen data are the input to a fitting procedure using an equation with a linear copper content term and a power function of neutron fluence term. The results are presented in Table 3.1. While all transition temperature shifts and upper-shelf energy drops in Table 3.1 are less than the "guideline" values of the U.S. Nuclear Regulatory Commission (NRC) *Regulatory Guide 1.99*, Rev. 1 (Ref. 3), several things should be considered in using these data: (1) the "observed" results are statistical best fits, while the guideline (*Regulatory Guide 1.99*) values are essentially lower-bound values; (2) the tolerances in Table 3.1 are 1-σ tolerances on the determination of transition temperature shift and upper-shelf energy drop and are not tolerances on individual test results; and (3) the radiation-induced changes are based on best fits of the unirradiated specimen data, and tolerances are associated with those data. If we use a 2-σ criterion, the transition temperature shifts for plate HSST-02 and weld 70W could exceed the guideline values. While statistical analyses of radiation-induced property changes can, and should, be better than "eyeball" analyses, care must be exercised in applying results of such analyses.

Table 3.1. Charpy property degradation of low-copper welds and plate produced by irradiation at 288°C to 2.0 x 10^{19} neutrons/cm^2 compared with the predictions of *Regulatory Guide 1.99*

Material	Content (wt %)		Transition temperature shift (°C)		Upper-shelf energy change (%)	
	Cu	Ni	Observed	Guideline	Observed	Guideline
Plate HSST-02	0.14	0.67	78 ± 4	83	−14 ± 2	−28
Weld 68W	0.040	0.13	14 ± 3	39	−3 ± 4	−22
Weld 69W	0.120	0.10	51 ± 4	71	0 ± 6	−31
Weld 70W	0.056	0.63	37 ± 6	39	+0.5 ± 3	−22
Weld 71W	0.046	0.63	15 ± 7	39	+12 ± 4	−22

Three of the submerged-arc welds showed essentially no decrease of upper-shelf energy, and the fourth gave an increased upper-shelf energy after irradiation. Statistical analyses conducted to date indicate that this observation is real. However, we cannot presently provide a verified physical explanation for a radiation-induced increase of upper-shelf energy.

Hyperbolic tangent functions were fitted to both unirradiated and irradiated specimen results and are presented in Figs. 3.1–3.5. The curve fitting of unirradiated specimen results was previously presented.[4] The curve fits for irradiated specimen results were not corrected for variations in fast neutron fluence. Some of the individual results appear to exceed the guideline values, but further statistical analysis is required. We are continuing the statistical analysis efforts to obtain confidence limits that account for several uncertainties inherent in the experimental procedures and materials.

3.2 Irradiation-Induced K_{Ic} Curve Shift

R. G. Berggren R. K. Nanstad

This study (Fifth HSST Irradiation Study) was presented in previous reports.[5,6] A purchase order for fabrication of the 94 ft of 8-3/4-in.-thick weldments for this irradiation study was placed with Combustion Engineering (CE), Chattanooga. The plate and one composition (0.35% Cu) of weld wire were delivered to CE. Plate cutting and edge preparation for welding are in progress. A test weld has been fabricated to verify welding procedures and mechanical properties of the material, but testing is not complete.

Assembly of a prototype 4TCS capsule was completed. This capsule will be operated in the poolside facility of the Oak Ridge Research Reactor (ORR) to obtain data on operational parameters of the capsule and

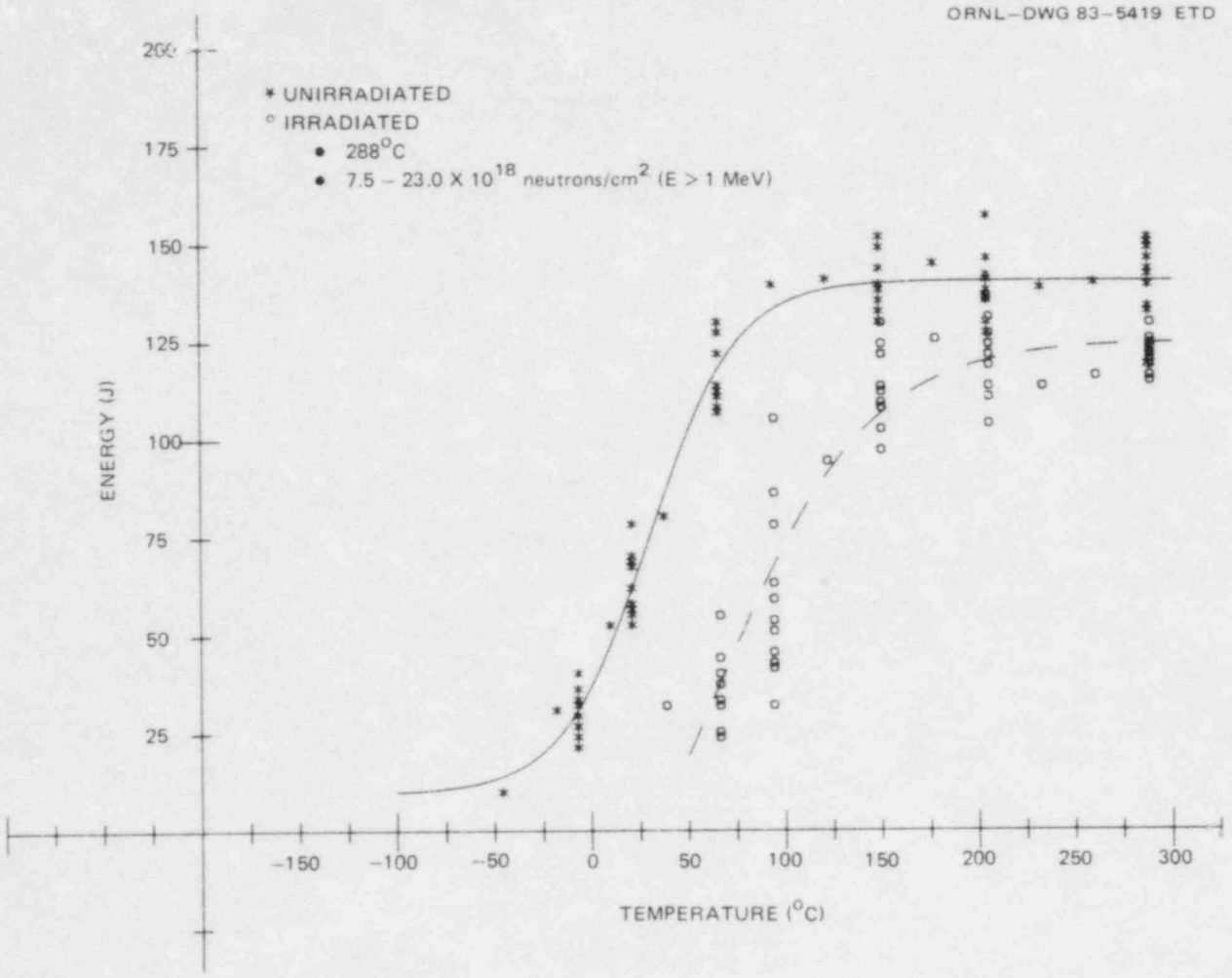

Fig. 3.1. Charpy V-notch impact energy for HSST plate 02, A533 grade B class 1 steel.

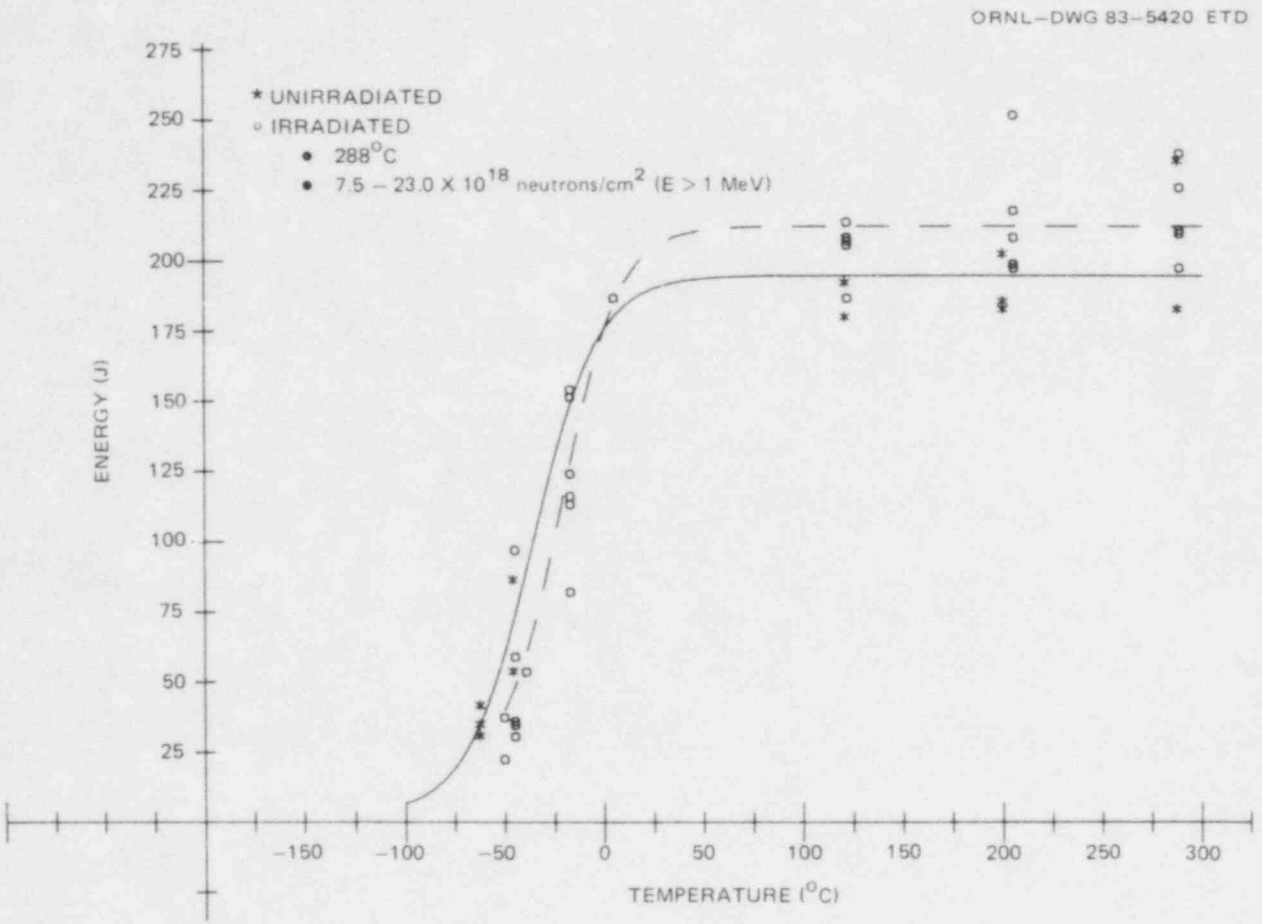

Fig. 3.2. Charpy V-notch impact energy for HSST 68W weld metal.

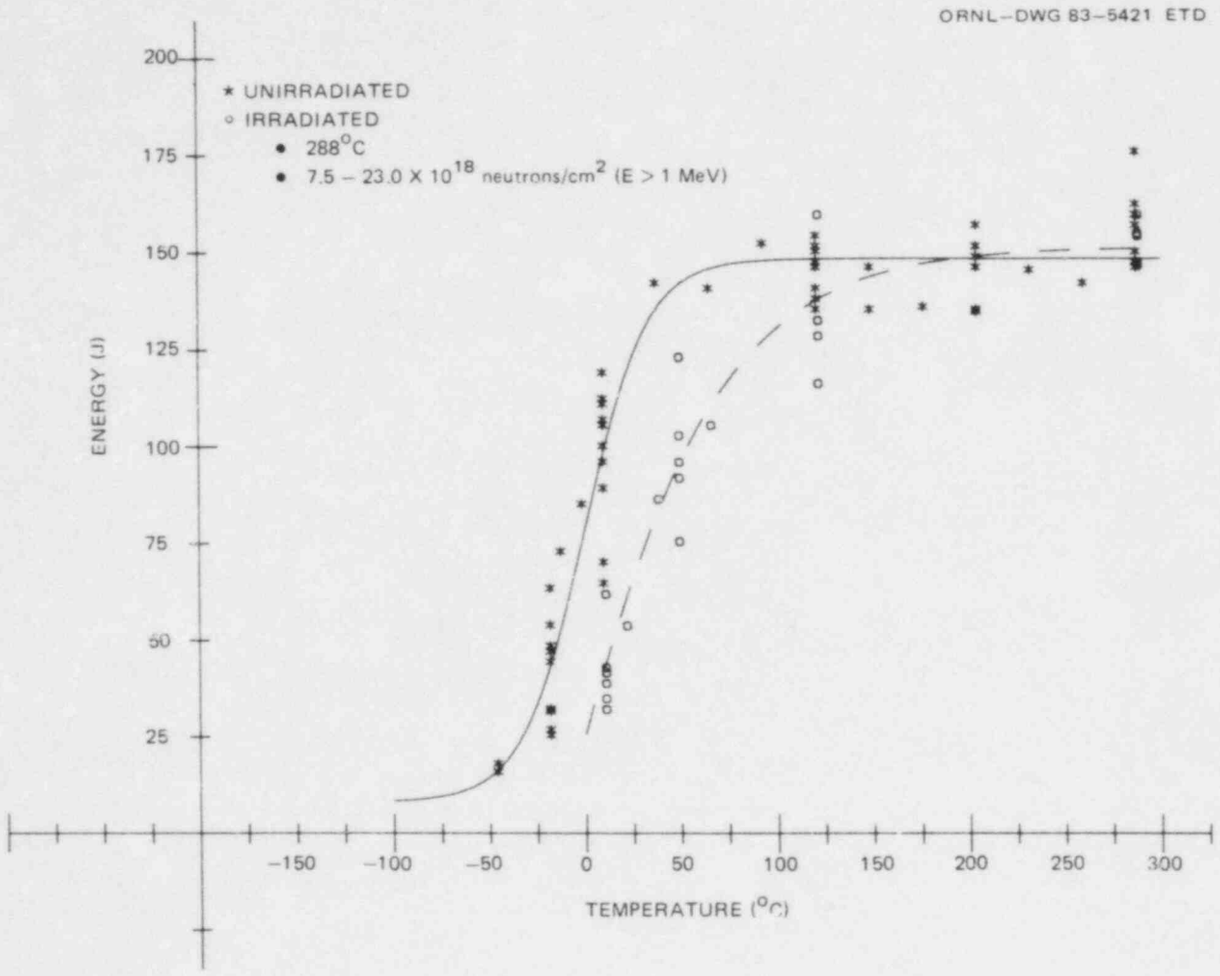

Fig. 3.3. Charpy V-notch impact energy for HSST 69W weld metal.

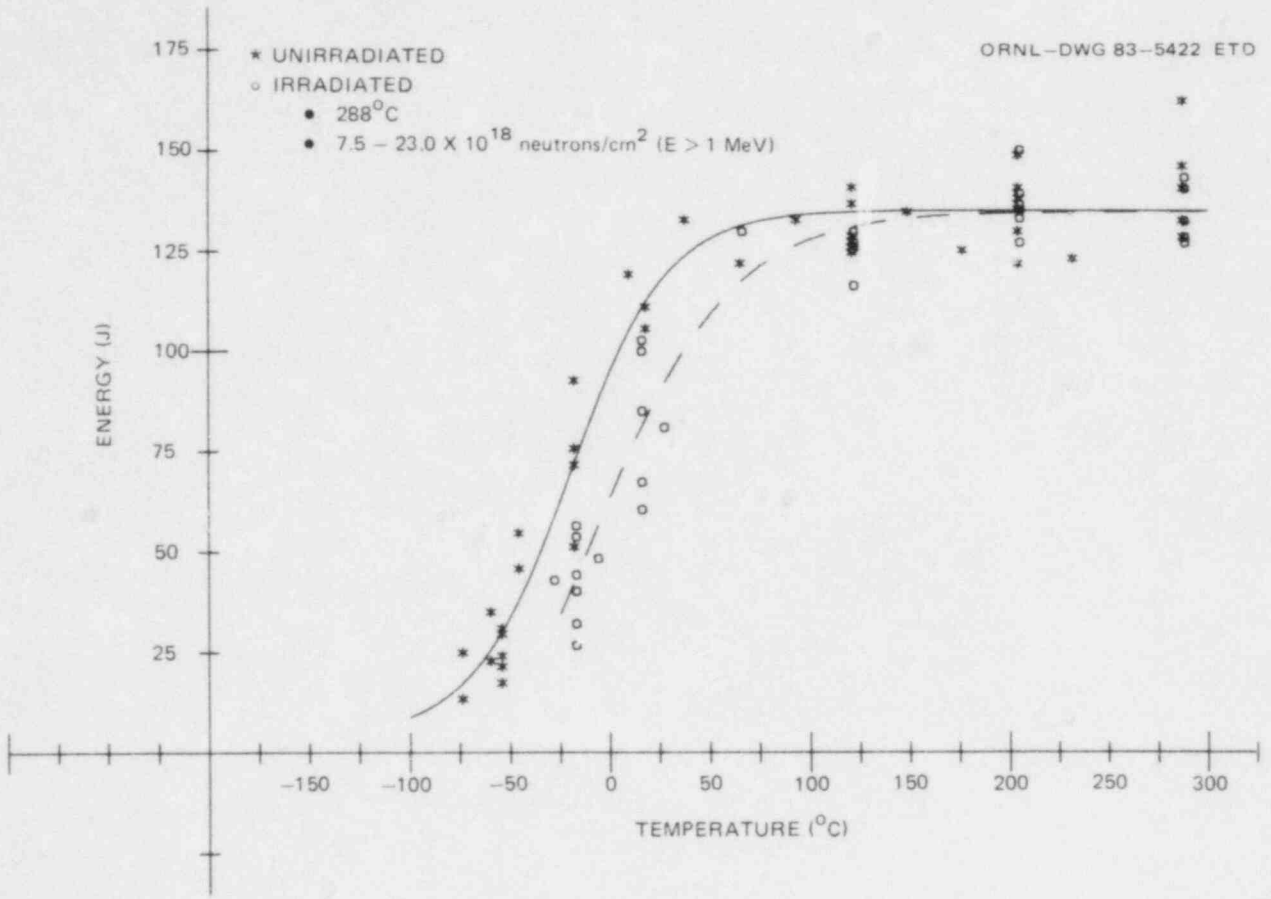

Fig. 3.4. Charpy V-notch impact energy for HSST 70W weld metal.

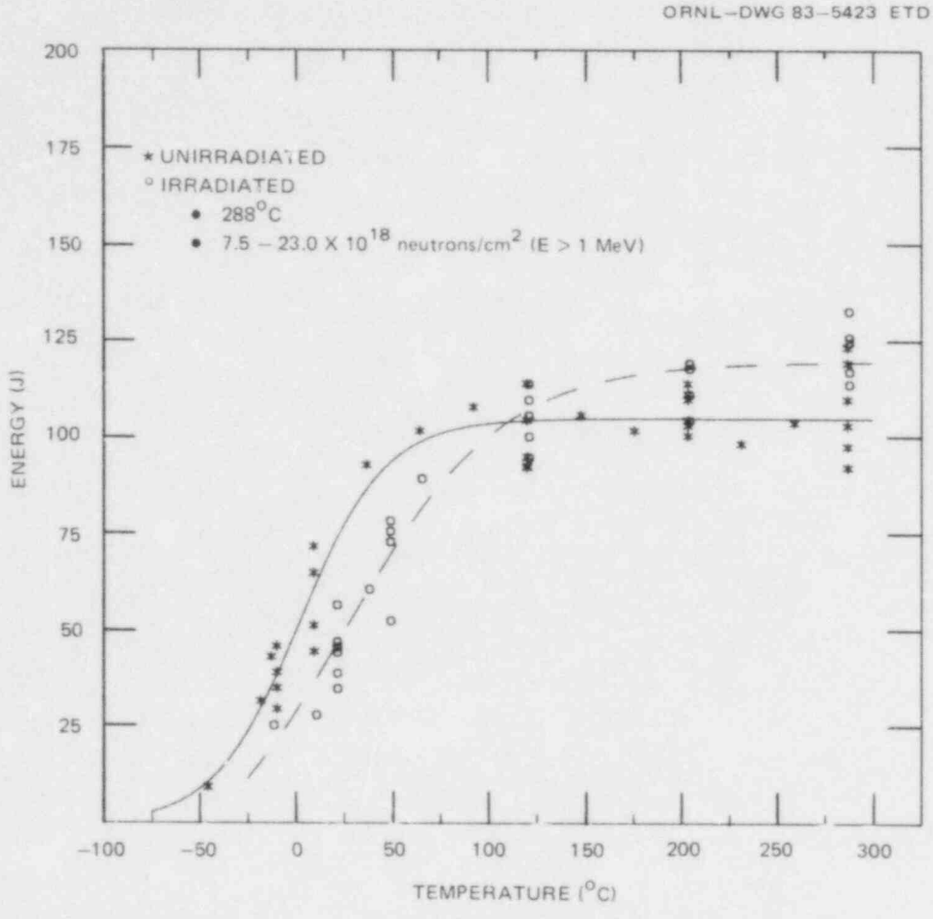

Fig. 3.5. Charpy V-notch impact energy for HSST 71W weld metal.

associated instrumentation and to finalize design parameters. In addition to measurements in the prototype capsule, temperatures will be recorded at various points on the gamma shields and reactor core box to determine the adequacy of natural-convective cooling. We have prepared for addition of forced-convective cooling if necessary. We will also determine the reactor reactivity effect of the capsule and gamma shields. A dummy capsule has also been fabricated for neutron spectral characterization of the facility. We plan to operate the prototype 4TCS capsule in the ORR in August. However, the neutron spectral characterization experiment has been postponed until anticipated changes have been made in the ORR core configuration. Preliminary calculations have indicated that these changes will have minimal effects on the HSST experiments.

3.3 Irradiated Stainless Steel Cladding

R. G. Berggren R. K. Nanstad

This task, discussed previously,[4,7,8] is to obtain fracture toughness properties for irradiated stainless steel vessel cladding. The first irradiation experiment, containing CVN and tensile specimens from type 309/308 three-layer cladding deposited by the single-wire series-arc process, was installed in the Nuclear Science and Technology Facility reactor in Buffalo, New York, in June. We expect the irradiation to be completed around the end of July. Specimens will be shipped to ORNL in September, and testing will begin in October.

References

1. R. G. Berggren et al., "Fourth HSST Irradiation Series," pp. 59–61 in *Heavy-Section Steel Technology Program Quart. Prog. Rep. October–December 1982*, NUREG/CR-2751, Vol. 4 (ORNL/TM-8369/V4), Union Carbide Corp. Nuclear Div., Oak Ridge Natl. Lab.

2. R. G. Berggren, R. K. Nanstad, and F. W. Stallman, "Second and Third 4TCS Irradiation Study," pp. 70–74 in *Heavy-Section Steel Technology Program Quart. Prog. Rep. April–June 1982*, NUREG/CR-2751, Vol. 2 (ORNL/TM-8369/V2), Union Carbide Corp. Nuclear Div., Oak Ridge Natl. Lab.

3. U.S. Nuclear Regulatory Commission, *Regulatory Guide 1.99*, Rev. 1, Washington, D.C. (April 1977).

4. R. G. Berggren, T. N. Jones, and R. K. Nanstad, "Investigation of Irradiated Materials," pp. 67–76 in *Heavy-Section Steel Technology Program Quart. Prog. Rep. January–March 1983*, NUREG/CR-3334, Vol. 1 (ORNL/TM-8787/V1), Union Carbide Corp. Nuclear Div., Oak Ridge Natl. Lab.

5. R. G. Berggren and R. K. Nanstad, "Irradiation-Induced K_{Ic} Curve Shift," pp. 74–78 in *Heavy-Section Steel Technology Program Quart. Prog. Rep. April–June 1982*, NUREG/CR-2751, Vol. 2 (ORNL/TM-8369/V2), Union Carbide Corp. Nuclear Div., Oak Ridge Natl. Lab.

6. R. G. Berggren and R. K. Nanstad, "Irradiation-Induced K_{Ic} Curve Shift," pp. 61–62 in *Heavy-Section Steel Technology Program Quart. Prog. Rep. October–December 1982*, NUREG/CR-2751, Vol. 4 (ORNL/TM-8369/V4), Union Carbide Corp. Nuclear Div., Oak Ridge Natl. Lab.

7. R. G. Berggren, R. K. Nanstad, and W. R. Corwin, "Irradiated Stainless Steel Cladding," pp. 78–80 in *Heavy-Section Steel Technology Program Quart. Prog. Rep. April–June 1982*, NUREG/CR-2751, Vol. 2 (ORNL/TM-8369/V2), Union Carbide Corp. Nuclear Div., Oak Ridge Natl. Lab.

8. R. G. Berggren, R. K. Nanstad, and W. R. Corwin, "Irradiated Stainless Steel Cladding," pp. 62–63 in *Heavy-Section Steel Technology Program Quart. Prog. Rep. October–December 1982*, NUREG/CR-2751, Vol. 4 (ORNL/TM-8369/V4), Union Carbide Corp. Nuclear Div., Oak Ridge Natl. Lab.

4. THERMAL-SHOCK INVESTIGATIONS

R. D. Cheverton

During this report period, thermal-shock experiment TSE-7 was conducted, the ORNL probabilistic fracture-mechanics code OCA-P was modified to include a new flaw-size distribution function and finite-length flaws, and OCA-P was used to analyze several Oconee postulated transients to determine the effect of cladding and to determine the benefit of using certain three-dimensional (3-D) flaws in lieu of two dimensional (2-D) flaws. Material properties and heat treatment studies were performed in support of TSE-7.

4.1 Thermal-Shock Experiment TSE-7

R. D. Cheverton D. G. Ball
S. E. Bolt

4.1.1 Introduction

Thermal-shock experiment TSE-7 was the eighth in a series of experiments conducted for the purpose of investigating the behavior of surface flaws in thick-walled steel cylinders subjected to severe thermal shock. For each of the previous experiments, except TSE-2 (Ref. 1) and to some extent TSE-5 (Ref. 2), the initial flaw extended the full length of the test cylinder, constituting a 2-D or effectively infinitely long, axially oriented, inner-surface flaw. Such flaws have been considered by some to be reasonable for use as initial flaws in the analysis of pressurized-water reactor (PWR) overcooling accidents (OCAs). However, initial flaws are much more likely to be short than effectively infinitely long, and short flaws may have less tendency for radial propagation, or because of dynamic effects they may have a greater tendency. Because of this latter possibility, TSE-2 was conducted earlier with an axially oriented short flaw (semicircular flaw with a = 19 mm). Relatively high K ratios near the inner surface resulted in some axial extension of the flaw (~100 mm), but more extensive axial extension and eventual radial propagation did not take place because of a lack of driving force; that is, the thermal-shock capability of the test facility was not adequate for further extension. The crack extension that did take place was in reasonably good agreement with a 3-D linear-elastic fracture-mechanics (LEFM) static analysis, and it was concluded that dynamic effects were not significant.

During TSE-5 (Ref. 2) a very short and shallow cross crack in the electron-beam (EB) weld, which was used to generate the intended long axial flaw, extended on the surface the full circumference and branched at many points to also extend in an axial direction to the ends of the cylinder. The depth of penetration was ~40% of the wall thickness. This event was not properly recorded because it was not expected, but it did demonstrate the ability of a short flaw to effectively become infinitely long as a result of severe thermal shock.

If a short and shallow flaw can effectively become infinitely long without propagating radially, and if dynamic effects associated with short flaws do not result in a lower critical value of RTNDT than for 2-D flaws, then in the analysis of OCAs, initial flaws should be modeled as 2-D flaws. However, if these conditions are not satisfied, it might be necessary or at least desirable to model the flaw in three dimensions. One purpose of TSE-7 was to evaluate the behavior of a finite-length surface flaw in the absence of cladding and under severe thermal-shock loading conditions.

PWR pressure vessels are, of course, clad on the inner surface with a thin layer of stainless steel. This material has a lower thermal conductivity, a higher coefficient of thermal expansion, and presumably higher fracture toughness than the base material and thus influences the behavior of flaws. Generally speaking, flaws that extend through the cladding into the base material have a greater potential for radial propagation than subclad cracks and thus are of greatest concern. If the through-clad crack is assumed to be very long, the fracture toughness of the cladding has no bearing on flaw behavior. However, if the flaw is short and the cladding toughness sufficient, surface extension and thus excessive radial propagation may be prevented. This possibility was to be investigated by first demonstrating with TSE-7 that a short flaw would extend to become a long flaw and then performing essentially the same experiment with a clad cylinder to determine the effect of the cladding. Thus, the design of TSE-7 had to be compatible with the intent of both experiments. Test conditions consistent with both of the TSE-7 objectives were achieved and are summarized in Table 4.1.

4.1.2 Design of TSE-7

TSE-7 was designed so that there would be a rather large potential for axial extension of the flaw. This required a severe thermal shock and crack initiation early in the transient when the radial gradient in toughness would be steep, thus reducing the potential for radial propagation. Furthermore, a semicircular flaw geometry was selected to obtain relatively high K_I values near the surface. This feature, combined with the steep gradient in toughness, provides relatively high values of K_I/K_{Ic} near the surface and thus a potential for axial extension without radial propagation.

As the flaw extends in length, the K ratios near the surface decrease, and those at the deepest point increase. The flaw could arrest and then extend in length again later in the transient without radial propagation. However, the free-end condition of the cylinder would tend to limit axial extension, and eventually radial propagation would take place. As it did, the tendency for axial extension would increase.

For the purpose of making experimental design calculations for TSE-7, the shape of the flaw during propagation was assumed to be semielliptical. An initial flaw depth (a) of 19 mm was selected on the basis of providing adequate driving force for axial extension and a reasonable margin to cover uncertainties.

Preliminary calculations for TSE-7 indicated that the thermal shock achieved during TSE-5 would be adequate and that the fracture toughness

Table 4.1. Test conditions for TSE-7

Test cylinder	
Identification number	TSC-4
Dimensions, mm (in.)	
Inside diameter	686 (27)
Outside diameter	991 (39)
Length	1220 (48)
Material	A508 class-2 chemistry
Tempering temperature	704°C (1300°F) for 4 h
RTNDT, °C (°F)	−1 (30)
Flaw (intended)[a]	b/a = 1, a = 19 mm
Thermal shock	
Cylinder temperature (initial), °C (°F)	93 (200)
Sink temperature, °C (°F)	−196 (−320)
Quench medium	Liquid nitrogen
Inner-surface coating	3M-34 plus 3M-NF34
Quench rate	Similar to TSE-5[b]
Duration, min	30

[a] Actual flaw shape and size not yet determined.

[b] Described in Fig. 4.5.

should be about the same as that used for TSE-5A (Ref. 3). With these conditions as input, a 3-D finite-element analysis was performed using ORVIRT (Ref. 4) for several times in the transient, for a = 19 mm and for b/a = 1, 3, 5, 10, 20, and 30. The results for times of 1.3 and 1.5 min are shown in Fig. 4.1 (*a*) and (*b*). The calculated K ratios close to the surface are exaggerated to some extent because of plane-stress conditions in that area, and as indicated by the results of TSE-2, a calculated plane-strain K ratio of unity or greater would have to extend to a depth of ~5 mm for crack propagation to actually take place. As shown in Fig. 4.1(*a*), the time in the transient corresponding to $K_I/K_{Ic} = 1$ at a′ = 5 mm was estimated to be ~1.3 min.

Figure 4.1 indicates that as the crack front advances, K_I values for locations close to the surface decrease, but elsewhere they increase. Near the inner surface the arrest K ratios drop below unity; at middepth they rise above unity; and they are less than unity along the bottom portion of the flaw, assuming retention of semielliptical geometry. The implication is that the flaw would tend to tunnel and would not grow radially. Tunneling tends to increase the K_I values near the surface and thus

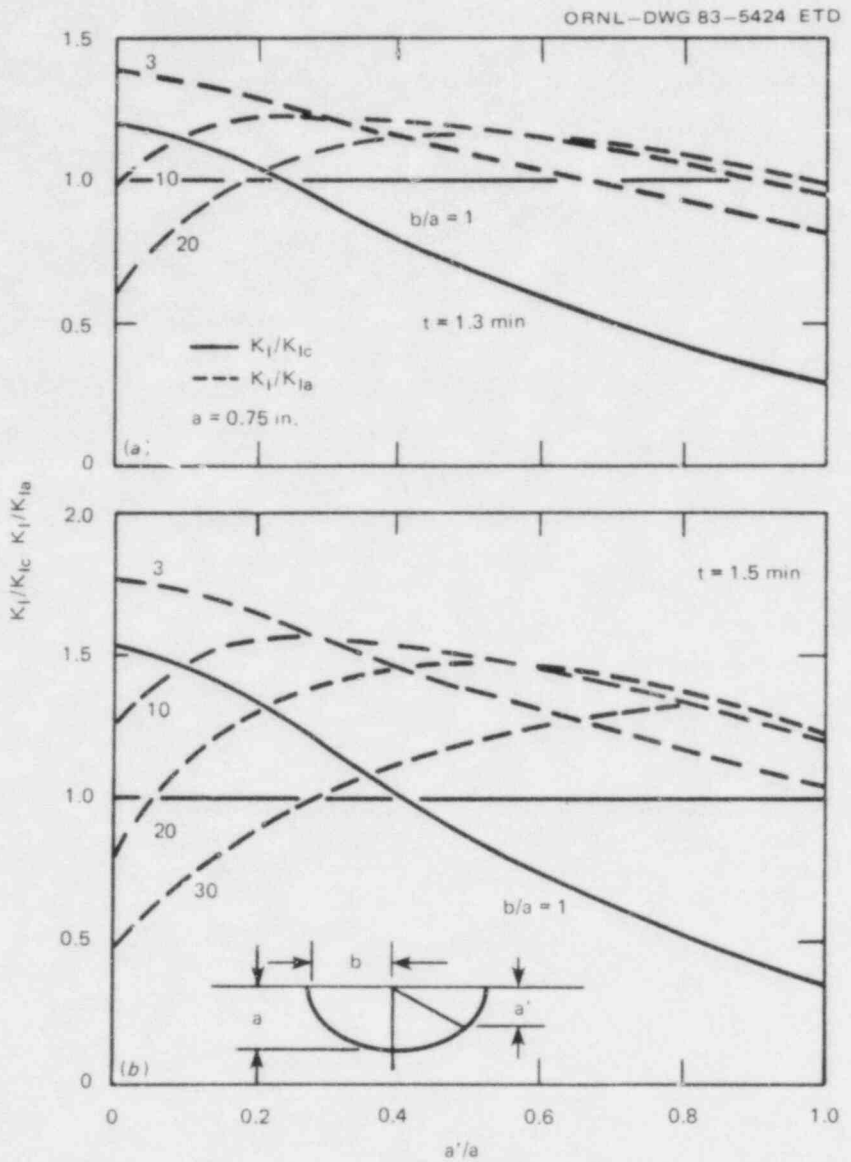

Fig. 4.1. K_I/K_{Ic} and K_I/K_{Ia} vs a'/a for (*a*) t = 1.3 min and (*b*) t = 1.5 min from TSE-7 pretest analyses.

tends to promote extension on the surface. If this did happen, as it appears to have during TSE-2, then the flaw would become quite long, as a result of the first initiation event, without the deepest point propagating radially.

Because the initial flaw was to be rather short, there was a good possibility that K_{Ic}/K_{Ia} would be greater than assumed in the previous analysis. This could result in the first initiation event occurring at a later time and thus result in a greater chance of radial propagation during the first event. If this happened, the chances of the flaw extending to the ends of the cylinder during the first event would be even greater than previously indicated, because the K ratio at the surface increases

with increasing crack depth and time. This is indicated in Fig. 4.1(*b*), which corresponds to a time of 1.5 min.

As indicated in Fig. 4.2, the selected combination of initial flaw size, thermal shock, and fracture toughness for TSE-7 was such that a substantial deviation in either would not prevent propagation of the initial flaw. Maximum values of K_I/K_{Ic} [$d/dt(K_I/K_{Ic}) = 0$] along the crack front of the initial flaw for nominal test conditions were in the range of 1.5 to 2.2, and it was expected that the actual transient would be somewhat

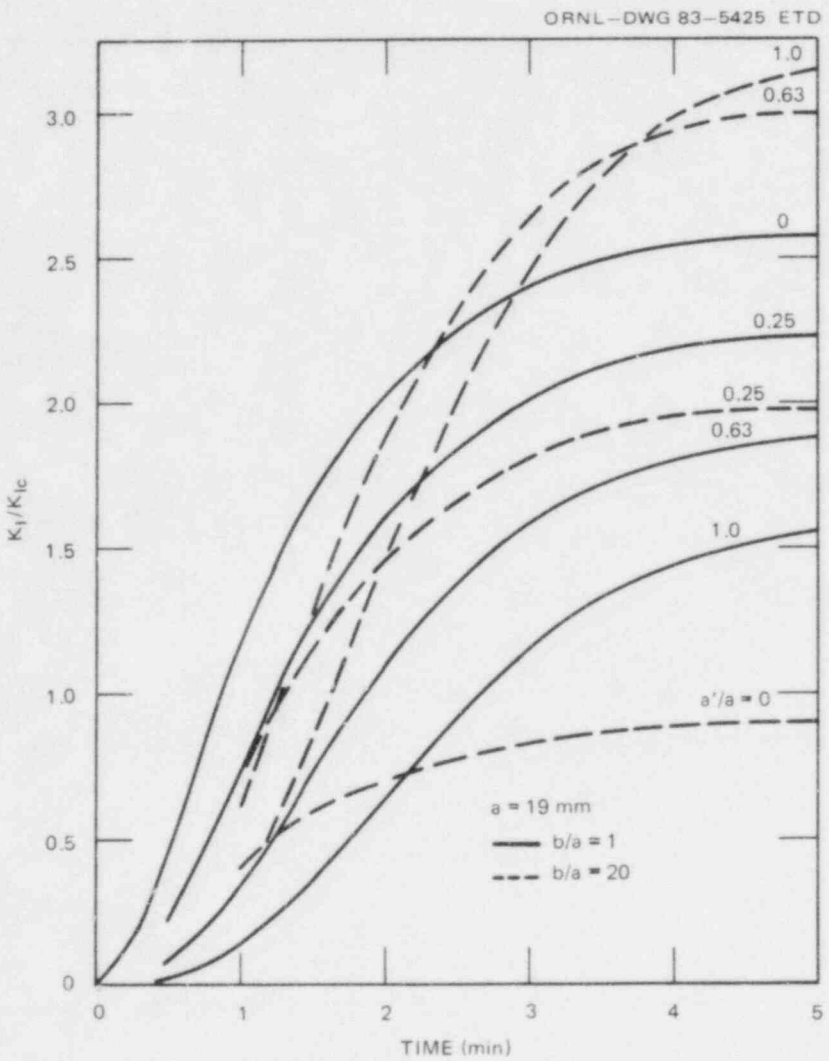

Fig. 4.2. TSE-7 pretest calculated values of K_I/K_{Ic} vs time for several points on crack front of semielliptical inner-surface flaws with b/a = 1 and 20 (approximate closed-form solution).

more severe than that assumed for the analysis. Also, Fig. 4.3 shows that warm prestress (WPS) was not likely to prevent propagation of the finite-length flaw because for all points on the crack front for b/a = 1 and b/a = 20, the stress-intensity factor did not reach a maximum until t ≃ 5 min. Crack propagation would take place well before this time, as indicated in Figs. 4.1 and 4.2.

Based on the analysis and results of TSE-5A, once the flaw became quite long it would propagate in a series of initiation-arrest events about 70% of the way through the wall, and further propagation would be prevented by WPS ($\dot{K} < 0$). This is indicated in Fig. 4.4, which is a set of critical-crack-depth curves for TSE-7, based on 2-D flaws, the same

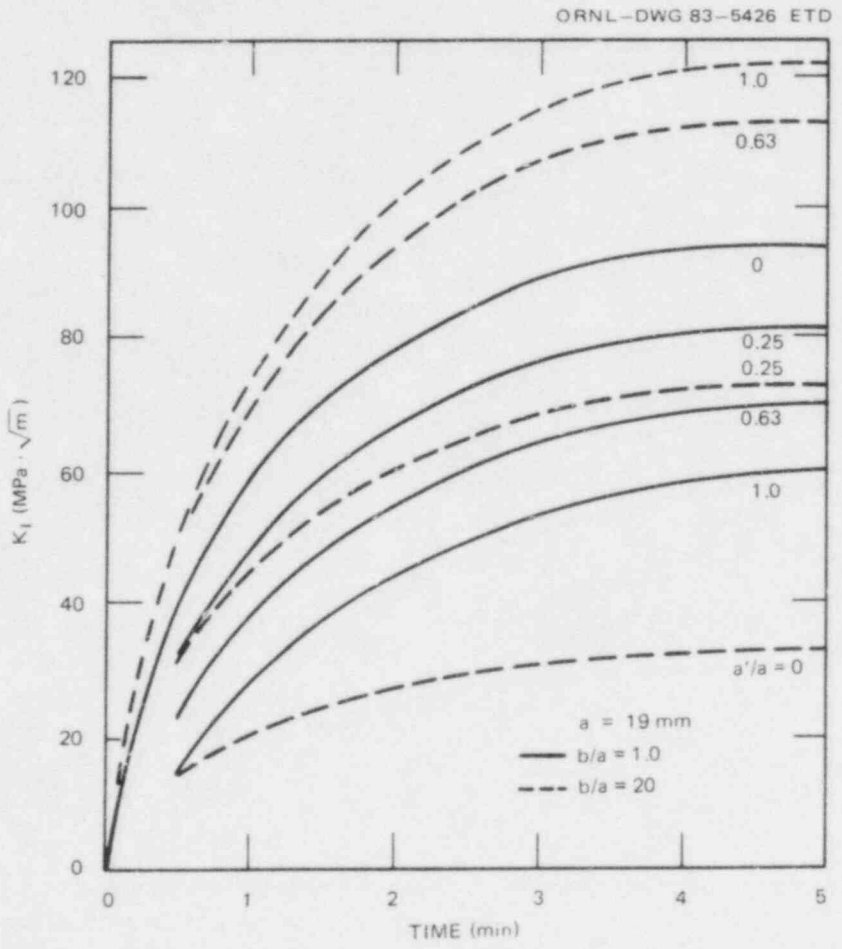

Fig. 4.3. TSE-7 pretest calculated values of K_I vs time for several points on crack front of semielliptical inner-surface flaws with b/a = 1 and 20 (approximate closed-form solution).

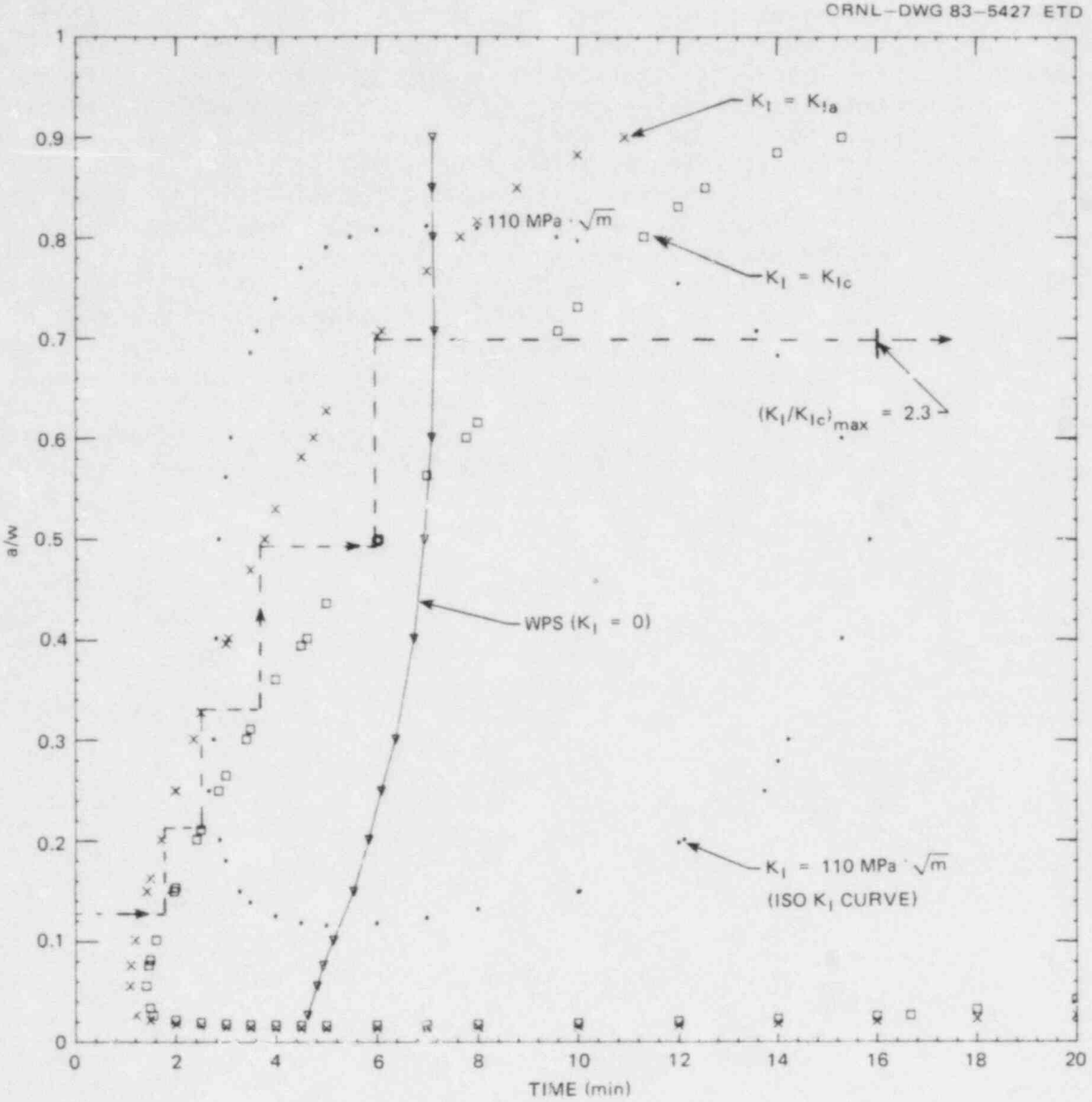

Fig. 4.4. TSE-7 pretest critical-crack-depth curves for 2-D flaws and $RTNDT_o$ = 0°F (−18°C).

thermal transient, and the same fracture toughness used for the above finite-length flaw analysis. The indicated flaw path is predicted on the assumption that the initial flaw would effectively become a long axial flaw before propagating radially.

4.1.3 Preparations for TSE-7

In preparation for TSE-7 a thermal-hydraulic experiment was conducted with the TSE-7 test cylinder to determine whether the specified inner-surface coating was appropriate. The thermal transients corresponding to a

point in the cylinder wall close to the inner surface (radial depth = 1.3 mm) are shown in Fig. 4.5 for TSE-5, -5A, and -7 thermal-hydraulic experiment (TSF-7-1). (The TSE-5 transient was used for the TSE-7 pretest analysis discussed here.) The TSF-7-1 transient was more severe than desired for TSE-7, and a correction was made for TSE-7 by increasing the thickness of the inner-surface coating by a small amount.

Also in preparation for TSE-7, material characterization studies were carried out to determine an appropriate tempering temperature for the test cylinder. The desired toughness curve was the one deduced from TSE-5A (corresponds very closely to the ASME Sect. XI curve with RTNDT = −18°C). The test cylinder for TSE-5A was A508 with class-2 chemistry, the same as for TSE-7, and it was tempered at 679°C. However, the TSE-7 test cylinder was from a different heat of material; thus, there was a good chance that the required tempering temperature would be different.

The approach to determining the appropriate tempering temperature for the TSE-7 test cylinder was to first obtain Charpy curves for tempering temperatures of 649, 677, and 704°C. These curves were then compared with

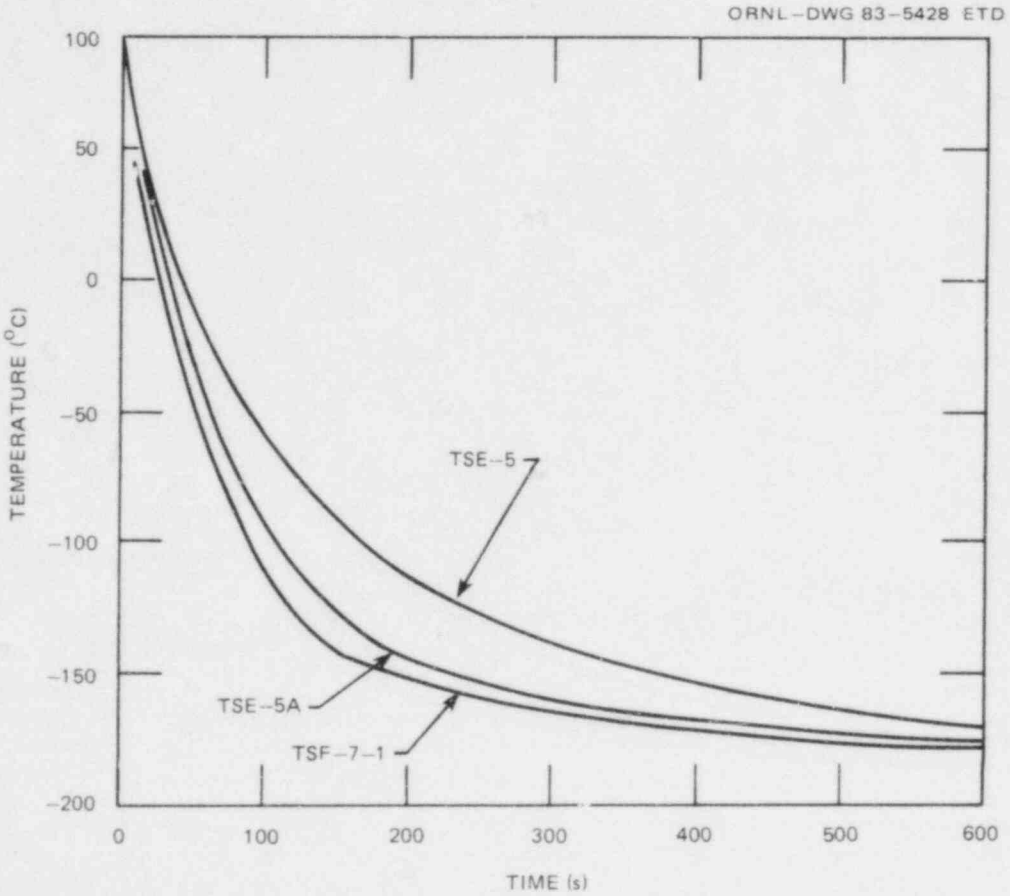

Fig. 4.5. Thermal-shock-experiment temperature transients corresponding to point in cylinder wall near inner surface (radial depth = 1.3 mm).

a similar curve for the TSE-5A test cylinder. Each of the TSE-7 curves fell to the right of the TSE-5A curve, indicating that a higher tempering temperature than 704°C would be required. This was not desirable because the yield strength could be too low. Therefore, a tempering temperature of 677°C was tentatively selected, and ten 1T-CS specimens were prepared using a portion of the TSE-7 test cylinder prolongation tempered accordingly. Each of the ten specimens was broken at room temperature, and the results are compared with the TSE-5A data in Fig. 4.6. As indicated, the TSE-7 1T-CS lowest point is ~50 MPa.$\sqrt{m}$ below the TSE-5A 1T-CS lower-bound curve. This was considered too low, and a set of 1T-CS specimens was tempered at 704°C and tested; the results are included in Fig. 4.6. This set has points slightly above the TSE-5A upper bound and slightly below the

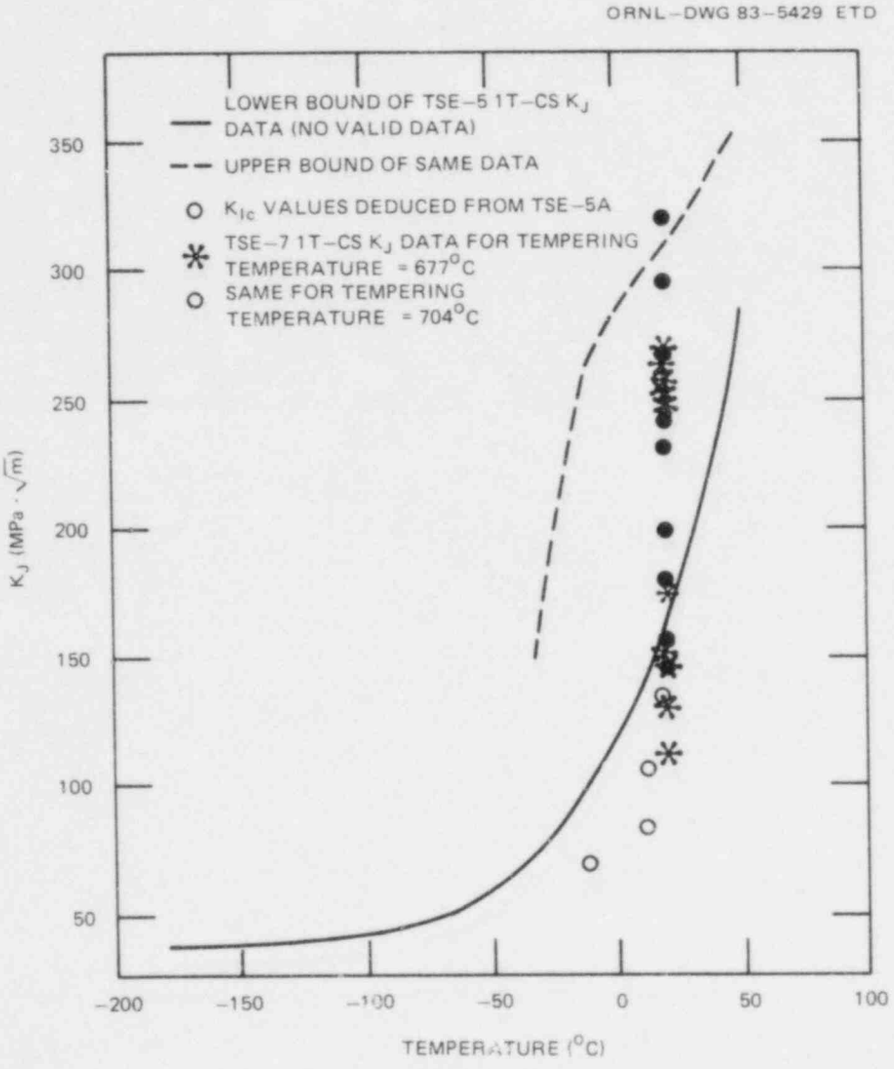

Fig. 4.6. Comparison of toughness data pertaining to TSE-7 and -5A.

lower bound. The corresponding yield strength was determined to be 450 MPa at room temperature, which was a little less than the expected maximum thermal stress during TSE-7. However, the temperature of the inner surface of the cylinder wall at the time a stress of 450 MPa was to occur was quite low (<−70°C), and this would elevate the yield strength sufficiently. All things considered, it appeared that a tempering temperature of 704°C would be satisfactory. Further characterizations of the material (K_{Ia} and additional K_J data) were to be completed after TSE-7 had been conducted (see Sect. 4.1.5.)

4.1.4 Testing technique

TSE-7 was conducted in the same manner as that for TSE-5, -5A, and -6; that is, the test cylinder, initially at a temperature of ~93°C, was submerged in liquid nitrogen (LN_2). Film boiling was suppressed and nucleate boiling promoted by coating the inner surface of the test cylinder with a thin layer of "rubber cement," and the ends and outer surface of the cylinder were well-insulated to prevent quenching of these latter surfaces. The length of the test cylinder (1.2 m) was minimized [consistent with the requirement that from a fracture-mechanics (FM) point of view the cylinder would be effectively infinitely long] to prevent excessive vapor concentration in the upper regions.

The thermal shock was administered to the inner surface by first lowering the test cylinder into a container of LN_2 and then suddenly releasing a nitrogen-gas bubble from the interior cavity, allowing LN_2 to flood the cavity. Natural convection provided circulation of liquid up through the central cavity and down over the insulation on the outside of the specimen. Nitrogen vapor exited through the top of the tank containing the LN_2, and most of the entrained liquid fell back into the tank; makeup was provided as necessary. A schematic of the test facility is shown in Fig. 4.7.

Data retrieved from the test cylinder included indications of crack initiation and arrest (COD, AE, and UT instrumentation), crack depth (UT), and radial temperature distributions in the wall as a function of time. These actual temperatures are used in the posttest FM analysis of the experiment. Temperature distributions in the wall were measured with 12 thermocouples at each of 15 different locations around the cylinder. These locations and those for the COD gages and the UT and AE transducers are shown in Fig. 4.8.

As indicated in Fig. 4.8, 33 COD gages (Ailtech weldable strain gages) were used, and with one exception they were paired at 16 locations along the expected flaw path (longitudinal line through the crack plane) to obtain an instrumented path width of ~48 mm. Any portion of the flaw that ran outside this path would not be instrumented. The unusually large number of gages was used not only to define a rather wide path but also to provide a means for following in some detail axial progression of the flaw.

Because the actual flaw path would probably deviate some from a truly longitudinal line, UT instrumentation was not expected to be useful in tracking axial progression of the flaw. Thus, only three UT crystals were used, and they were located directly opposite the initial flaw.

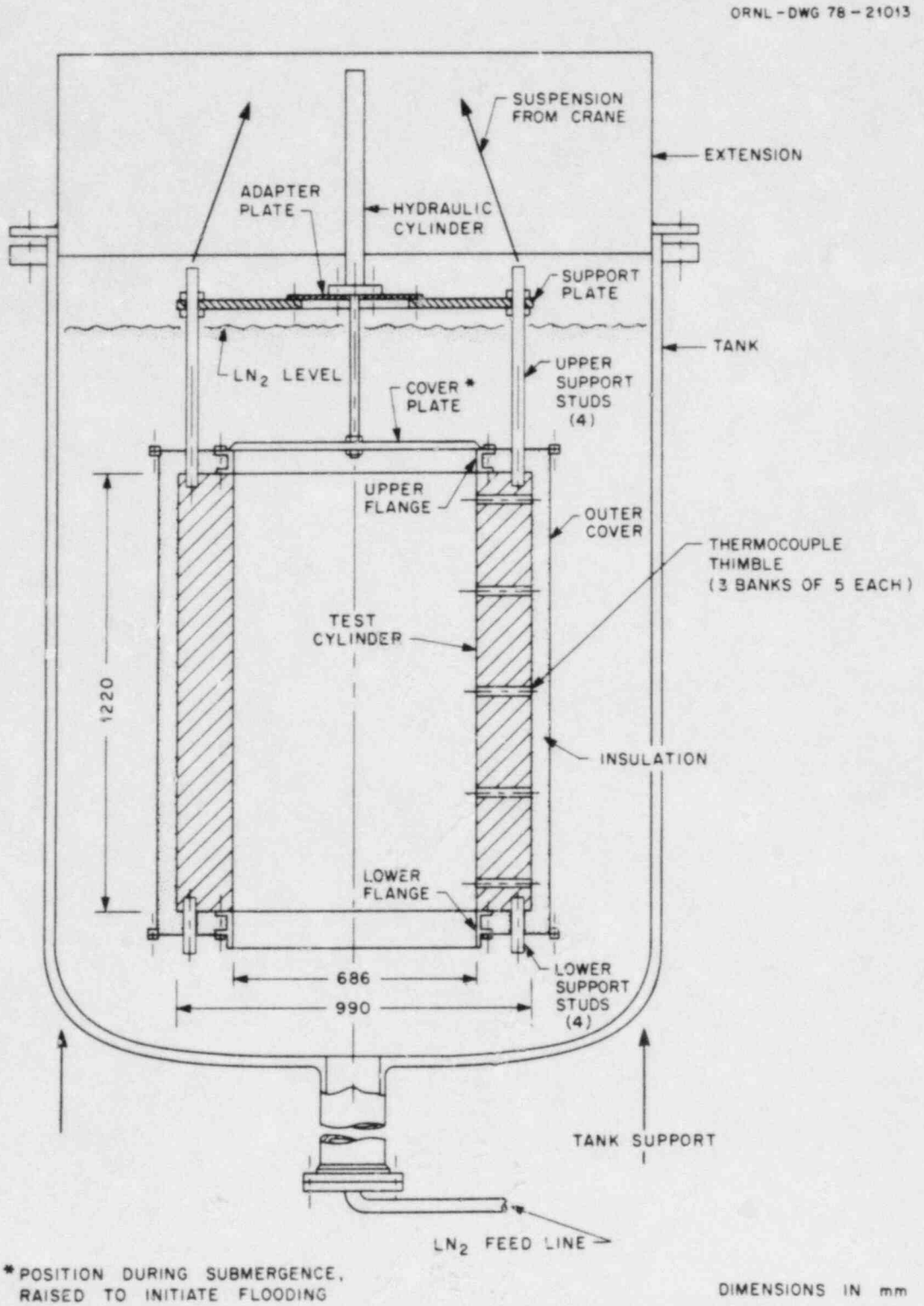

Fig. 4.7. Schematic cross section of ORNL LN_2 thermal-shock test facility.

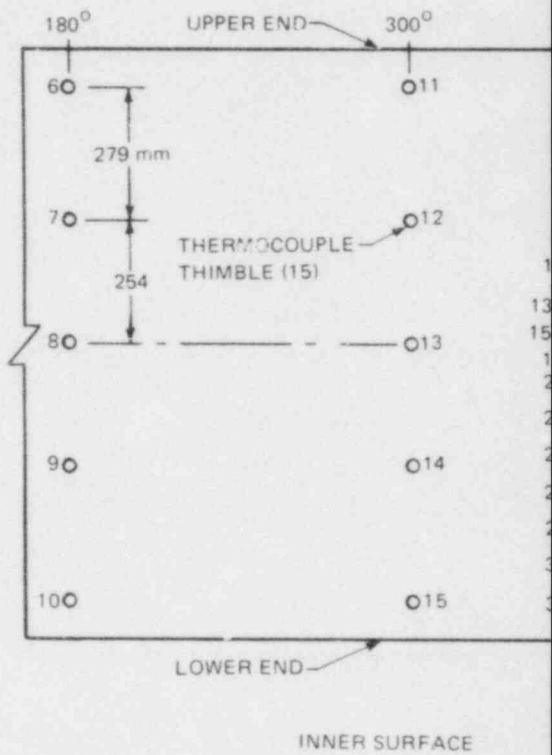

Fig. 4
instrumenta

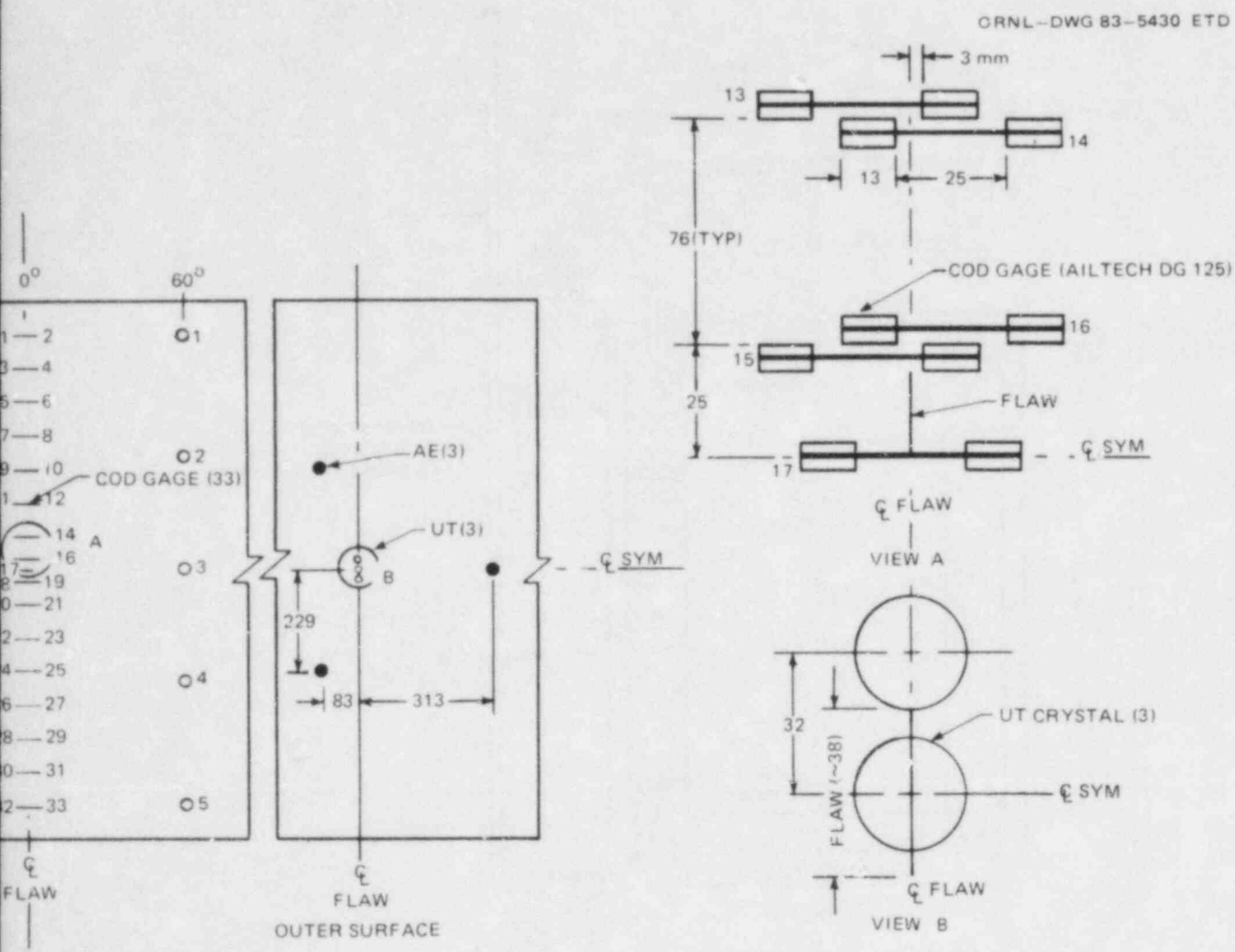

.8. Developed view of TSC-4 indicating types and locations of ation.

4.1.5 Results of TSE-7

During TSE-7 three initiation-arrest events were detected with the COD and UT instrumentation. The times, crack depths (based on UT data), and crack-tip temperatures corresponding to the events are summarized in Table 4.2. The COD data indicate that during the first event the initial flaw extended axially to or nearly to the ends of the cylinder, and visual inspection of the inner surface revealed a complex cracking pattern covering the entire inner surface and involving many bifurcation events (Fig. 4.9). Because the COD gages indicate that the axial extensions close to the initial crack plane occurred during the first event, and because the thermal shock was quite uniform in an azimuthal direction, it is believed that essentially the entire cracking pattern developed during the first event. The two subsequent events presumably resulted in some axial and radial extension, as indicated by the COD and UT instrumentation for the portion of the flaw near the crack plane. The final crack depth for a large portion of the crack pattern was measured with UT instrumentation; a summary of results is shown in Fig. 4.9 by means of recorded crack-depth values at the locations of some of the UT measurements. Away from the ends of the cylinder and for portions of the crack that extend to the ends of the cylinder, the range of recorded crack depths is about 41 to 58 mm. For the portions of the crack that do not extend all the way to the ends of the cylinder, the final depths are in the range of 25 to 30 mm. Because of free-end effects, the crack depths near the ends of the cylinder are substantially less.

At first glance, the cracking pattern in Fig. 4.9 is apparently the result of more than one initial flaw. However, each path can be traced from its terminus to the single intended initial flaw. Some of the crack branches were attracted to and terminated in the 25-mm-diam thermocouple-

Table 4.2. Summary of results for TSE-7[a]

	Event	Time (min)	a (mm)	$(T_s - RTNDT)$ (°C)	$(T_a - RTNDT)$ (°C)
1	Initiation	1.53	13	−78	−23
	Arrest		32		+39
2	Initiation	2.43	32	−100	+6
	Arrest		46		+33
3	Initiation	3.00	46	−106	+17
	Arrest		52		+33

[a] a_a = estimates based on UT,

T_s = temperature at inner surface,

RTNDT ≃ −1°C,

T_a = temperature at indicated depth of flaw.

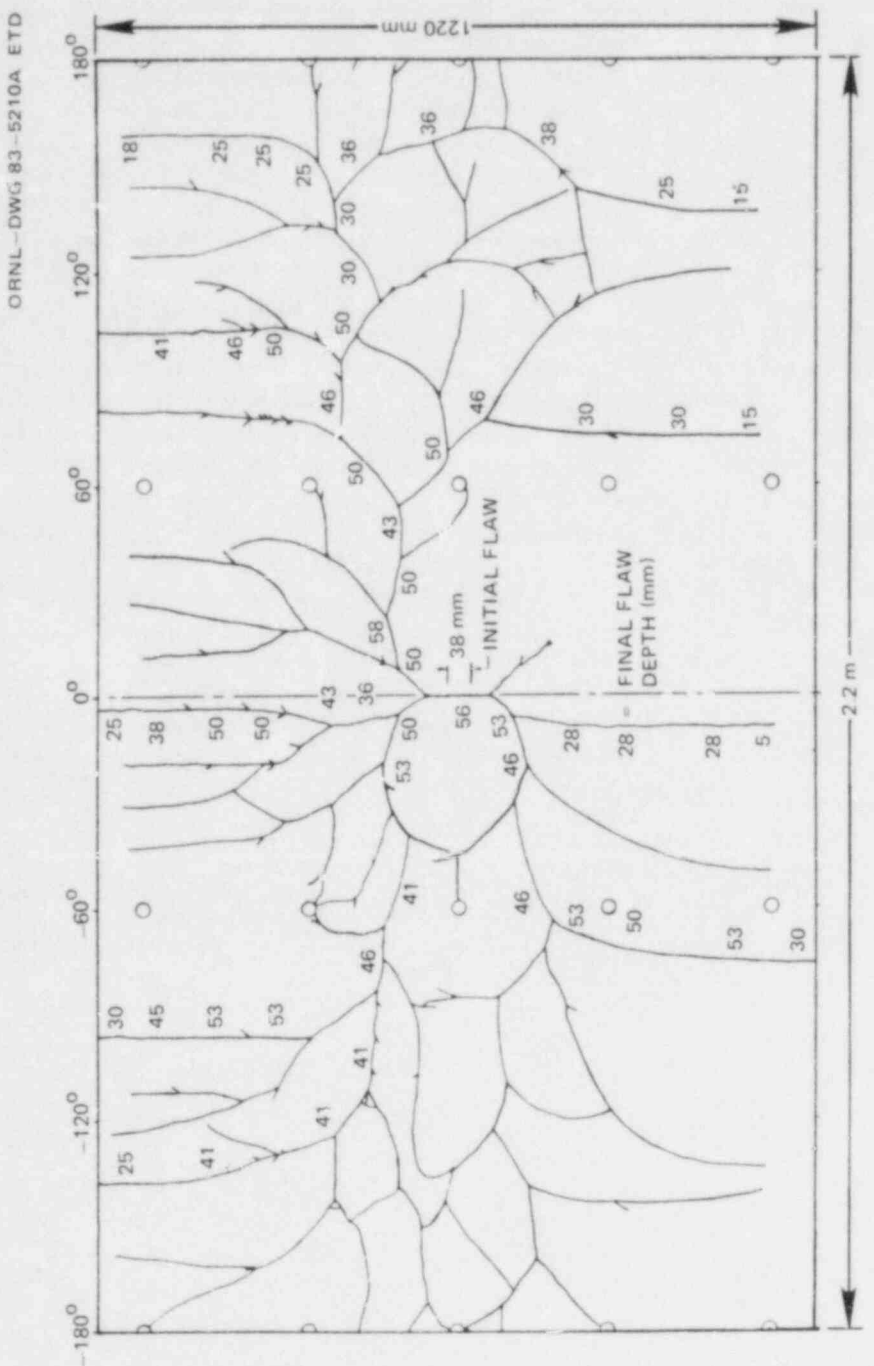

Fig. 4.9. Developed view of inner surface of TSE-7 test cylinder showing final crack pattern and UT estimates of crack depth at selected locations.

thimble holes, which constitute stress risers. One branch terminated in one of the 3-mm-diam COD-gage-lead holes, and some terminated at another branch of the crack. In the latter case the intersection was at a 90° angle because the stresses normal to the intersected crack were relieved by the presence of the crack.

For the first time in the thermal-shock program, significant difficulties were encountered with application of the inner-surface rubber-cement coating that enhances the heat transfer to LN_2. The result was an axial variation in the thickness of the coating, and this resulted in a significant axial gradient in vessel temperature. The axial gradient in temperature at several times during the transient for a radial position in the wall located 1.3 mm from the inner surface is shown in Fig. 4.10. The vertical bars in Fig. 4.10 represent the range of three temperature measurements at 120° intervals around the cylinder. As indicated, the azimuthal uniformity in temperature was satisfactory.

Figure 4.11 shows T (a = 0) vs time as measured at midlength of the test cylinder and compares it with the curve used for the pretest analysis of TSE-7. As indicated, the actual transient was somewhat more severe for times of interest than used in the pretest analysis.

Using the measured radial temperature distributions at the horizontal midplane (see Fig. 4.12), a posttest 2-D analysis of a single long axial flaw indicates, as shown in Fig. 4.13, that this flaw would experience

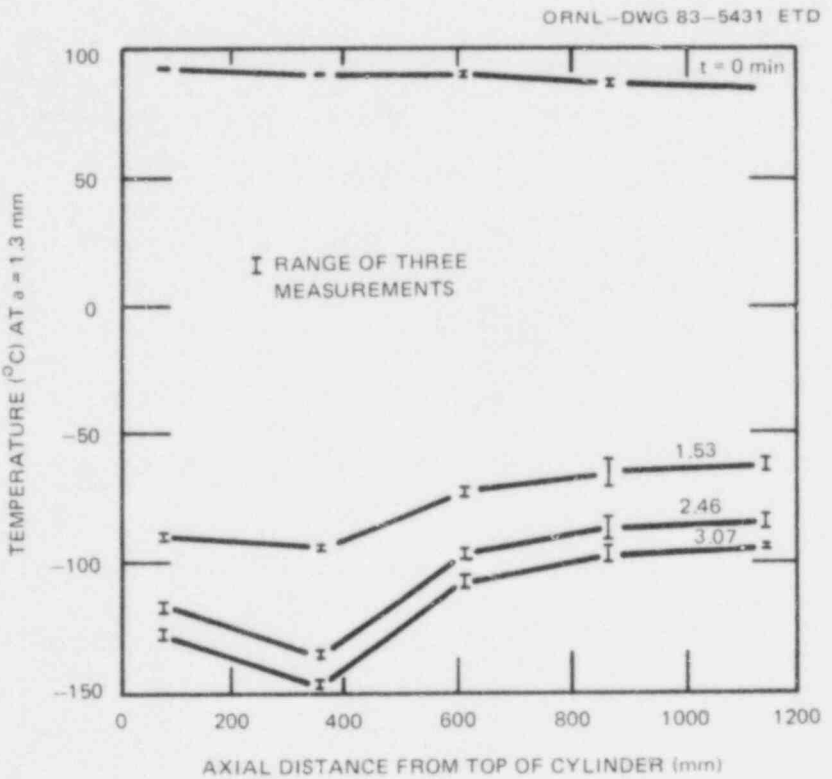

Fig. 4.10. Axial temperature profiles for several times during TSE-7 at radial position of 1.3 mm from inner surface of test cylinder.

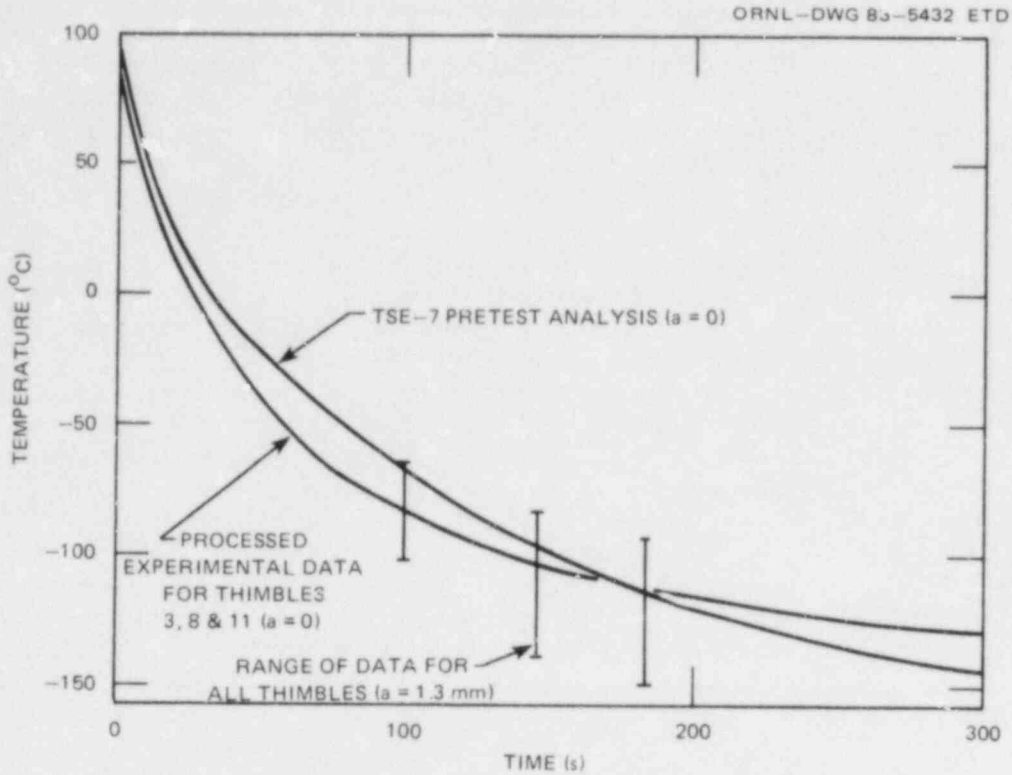

Fig. 4.11. Temperature transients at inner surface.

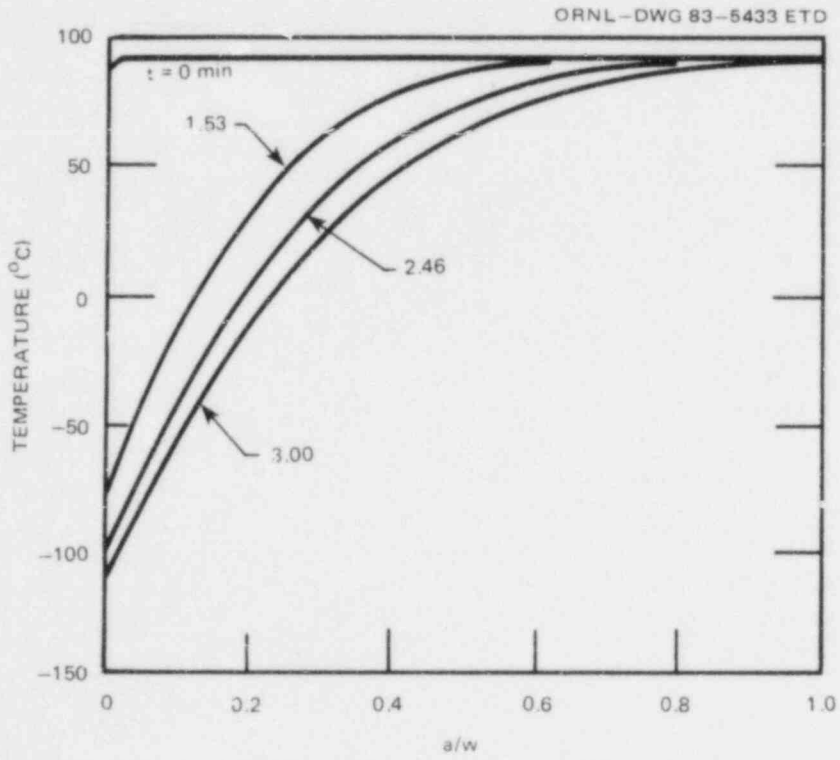

Fig. 4.12. Test-cylinder midlength radial temperature distribution for several times in TSE-7 transient.

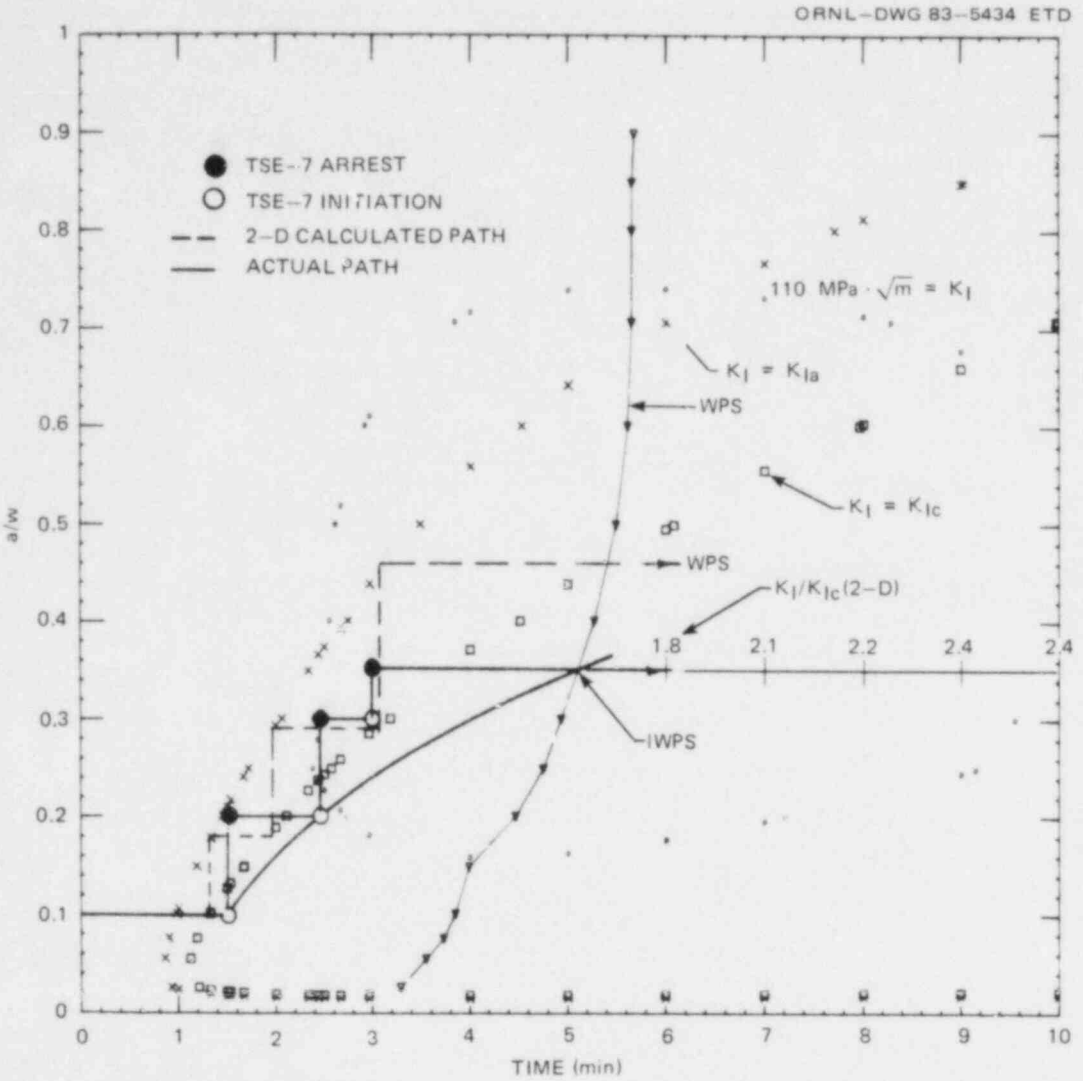

Fig. 4.13. Critical-crack-depth curves for TSE-7 based on measured temperature distributions at cylinder midlength and fracture-toughness data deduced from TSE-5A.

three initiation-arrest events; a fourth event would be prevented by WPS; and the final arrested depth would be ~76 mm (a/w = 0.5). The actual final crack depth was less because of stress relief caused by the many axial branches, and because none of the axially oriented branches extended the full length of the cylinder without a significant diversion from a straight line. Nonvertical segments tend to reduce the COD of the vertical segments and thus, in effect, reduce the lengths of the vertical segments, in which case they are not effectively 2-D flaws, and their K_I values are less. This results in less radial propagation than calculated for a single 2-D flaw.

Figure 4.13 also includes the "actual" path of events based on UT estimates of crack depth at the location of the initial flaw. The lower

K_I values that resulted from the extensive cracking pattern are evident from the general shift in the initiation and arrest curves to the right of the 2-D curves. The incipient WPS point (IWPS) was estimated based on (1) the knowledge that a fourth event did not take place and (2) the assumptions that the WPS curve would be essentially the same for the 2-D and actual flaws and that $(K_I/K_{Ic})_{max}$ for the final crack depth would be greater than unity and would occur to the right of the WPS curve.

Figures 4.14–4.16 include plots of K_I, K_{Ic}, K_{Ia}, σ, and T vs a/w for the times corresponding to the three events during TSE-7. These data were obtained from the posttest analysis and thus are based on the measured temperatures at midlength of the cylinder. The K_I values are for a 2-D axial flaw.

4.1.6 Conclusions

The results of TSE-7 indicate once again that under severe thermal-shock loading conditions the potential exists for a short flaw to extend in length to effectively become a long flaw. Furthermore, TSE-7 is a satisfactory prelude to a similar experiment designed to help investigate the effects of cladding on the surface extension of short flaws.

4.2 Thermal-Shock Materials Characterization

W. J. Stelzman R. K. Nanstad
R. L. Swain

Properties characterization continued for prolongation TSP-4 of test cylinder TSC-4 that was used in experiment TSE-7. Tensile properties at 21°C were determined from segments of "as-quenched" TSP-4 after tempering for 4 h at 676 or 702°C followed by cooling in air. The results from compact tension (CT)-oriented tensile specimens from the 0.84t depth from the inner surface of the 203-mm-thick prolongation are listed in Table 4.3. Specimens with a gage diameter of 4.52 mm and a gage length of 31.8 mm were used, resulting in a length-to-diameter ratio of 1:7. The total elongation results have been adjusted mathematically to the more common ratio of 1:4.

Increasing the temper temperature from 676 to 702°C decreased the yield and ultimate stress values and increased the ductility. The average yield and ultimate stresses were 500 and 645 MPa after 4 h at 676°C and decreased to 449 and 589 MPa, respectively, after 4 h at 702°C. The average total elongation and reduction of area (ductility) for the same tempers increased from 25.8 and 69.2% to 26.7 and 71.7%, respectively, after the 702°C temper.

Charpy-V impact (CVN) results were also obtained after the 4-h temper at 704°C. CT-oriented specimens from depths ranging from 0.20 to 0.34t from the inner surface of the 203-mm-thick prolongation were used, and the results are shown in Figs. 4.17 and 4.18. The two segments from which the CVN specimens were machined had been processed slightly differently. One

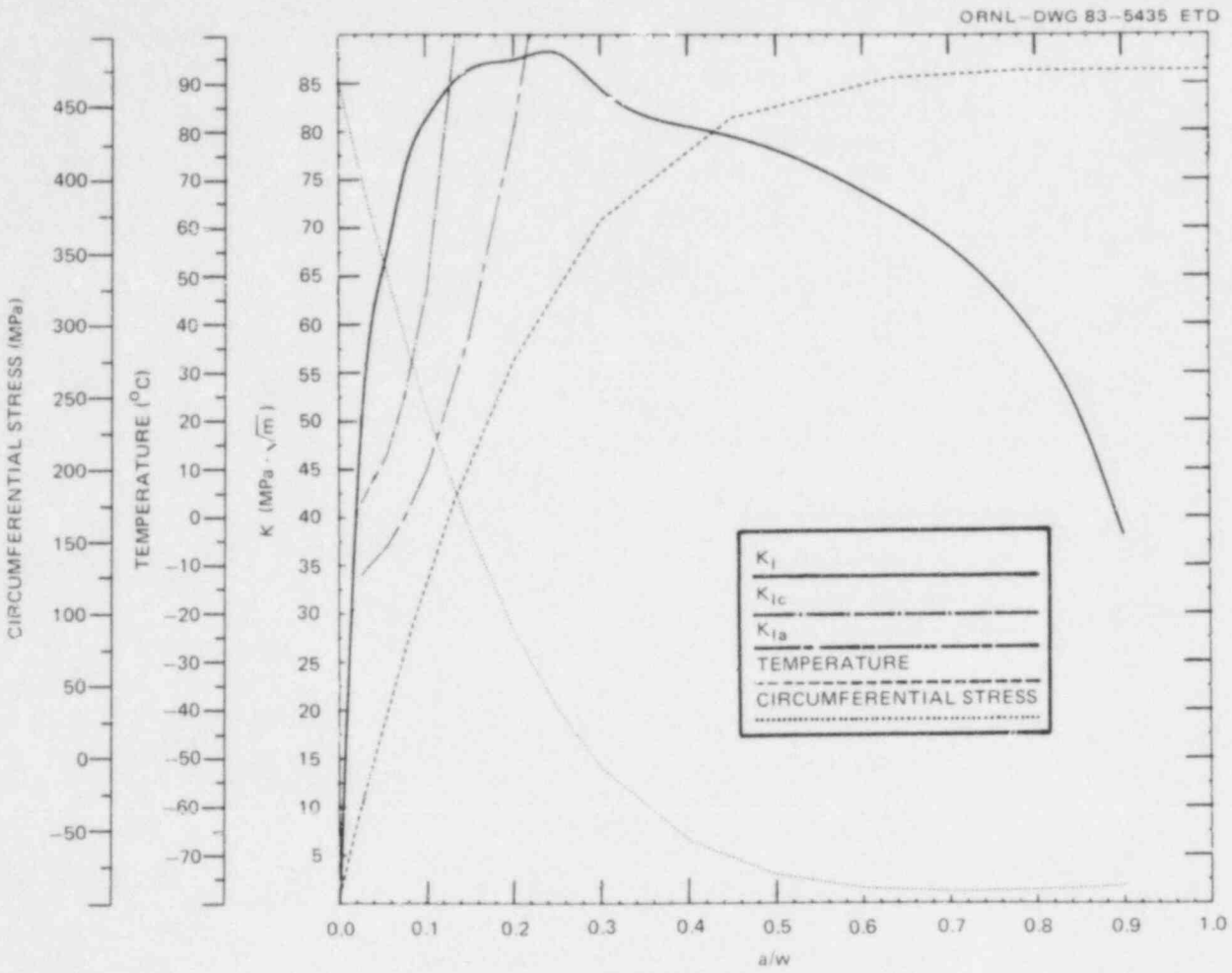

Fig. 4.14. TSE-7 posttest-analysis five-curve plot for t = 1.53 min.

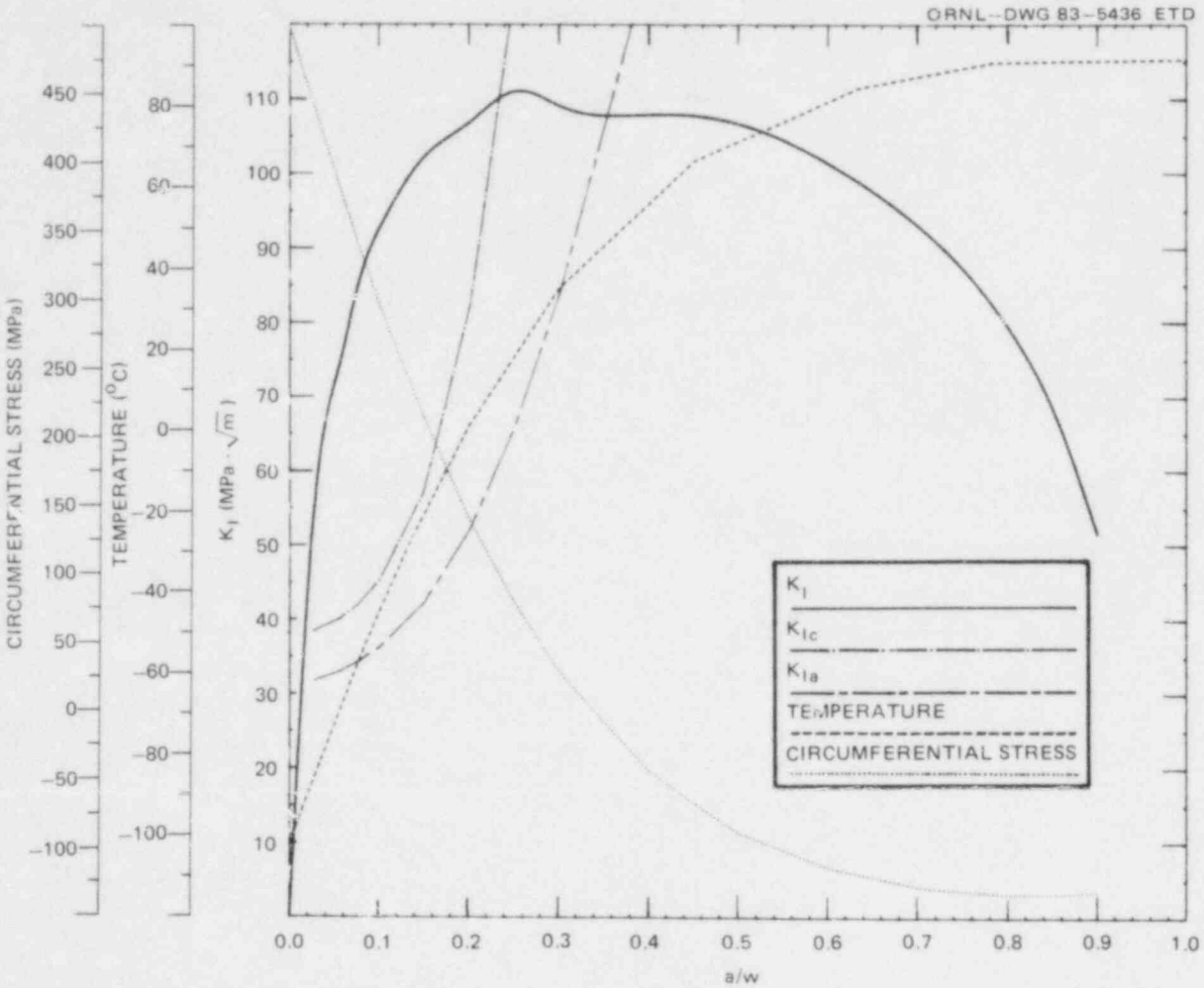

Fig. 4.15. TSE-7 posttest-analysis five-curve plot for t = 2.43 min.

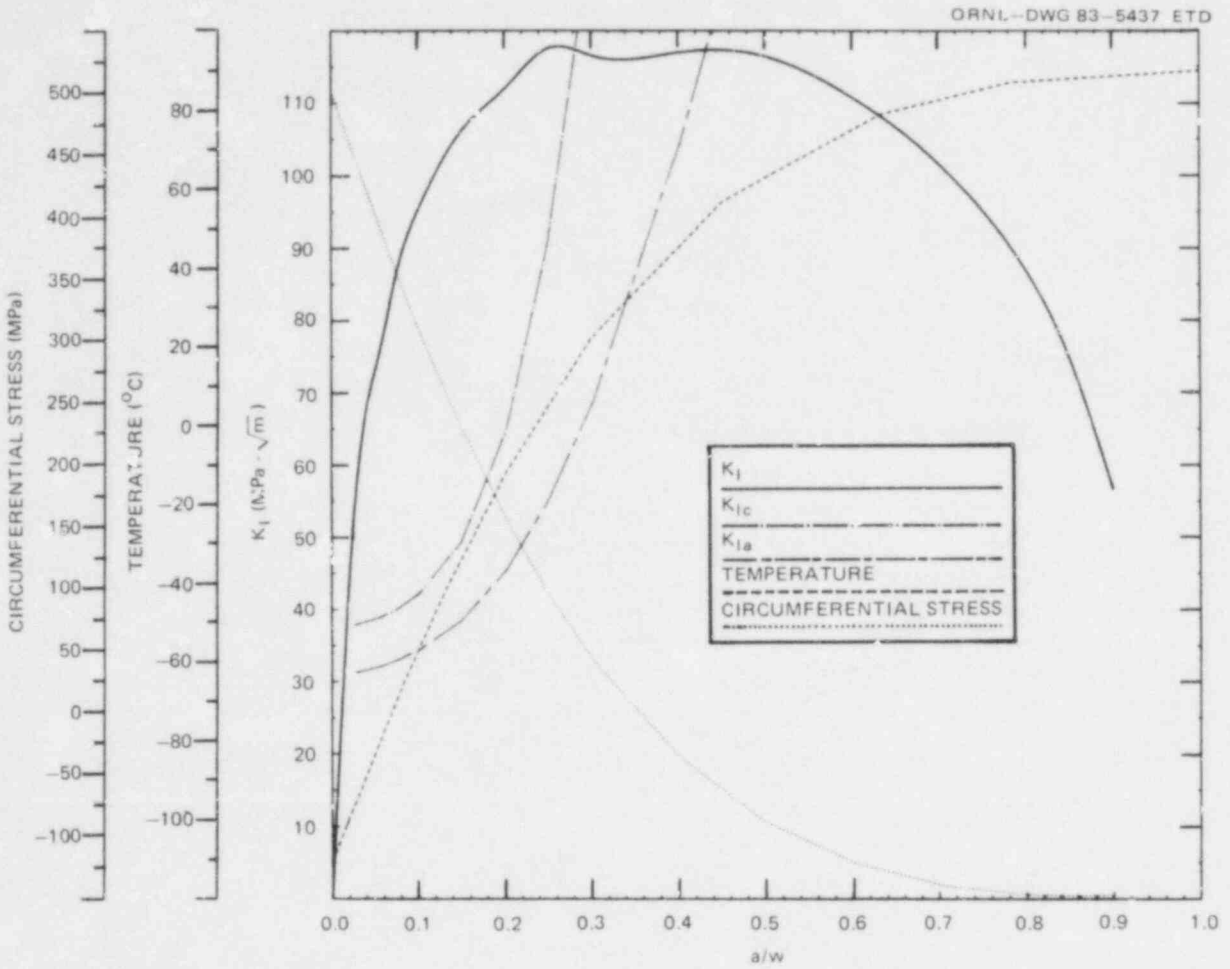

Fig. 4.16. TSE-7 posttest-analysis five-curve plot for t = 2.97 min.

Table 4.3. Tensile properties of "as-quenched" 203-mm-thick thermal-shock prolongation TSP-4 at 21°C after tempering for 4 h at 676 and 702°C

Stresses[a] (MPa)		Ductility (%)	
Yield[b]	Ultimate	Total elongation[c]	Reduction of area
4 h at 676°C temper			
501	647	25.9	69.0
499	644	26.5	70.5
501	643	24.9	68.2
4 h at 702°C temper			
450	571	25.0	70.8
449	497	28.1	71.4
447	599	26.9	70.0

[a] 4.52-mm-diam CT-oriented specimens, strain rate 0.016/min.

[b] 0.2% offset.

[c] Gage length to gage diameter = 4.

segment was tempered by itself for 4 h at 702°C and cooled in air; the remainder of the prolongation was then tempered with the test cylinder TSC-4 for 4 h at 704°C and cooled in air, after which the segment for the CVN specimens was removed. The results from the single segment (702°C temper) have been reported[5] and are combined with the 704°C temper CVN energy results in Fig. 4.17 and the lateral expansion and fracture appearance in Fig. 4.18. No difference between the CVN results was noted. The criteria for the RT_{NDT} set forth in the *ASME Boiler and Pressure Vessel Code*[6,7] at the 68-J energy level and the 0.89-mm lateral expansion level are met at T_{CV} = 27°C and (T_{CV} − 33°C) = −6°C. The drop-weight NDT from type P3 specimens (T_{NDT}) after the 702°C temper has been determined previously[8] to be −1°C. Therefore, the RT_{NDT} is determined by the drop-weight NDT and $RT_{NDT} = T_{NDT} = -1°C$.

Fracture toughness characterization has also been continued with CT-oriented 1T compact specimens (1TCS) machined from segments tempered for 4 h at 702 or 704°C followed by cooling in air. The segments were treated similar to the CVN specimen segments. 1TCS specimens were machined so the fatigue crack tip would be located at the 0.58 and 0.83t depth location from the inner surface of the 203-mm-thick prolongation. All specimens

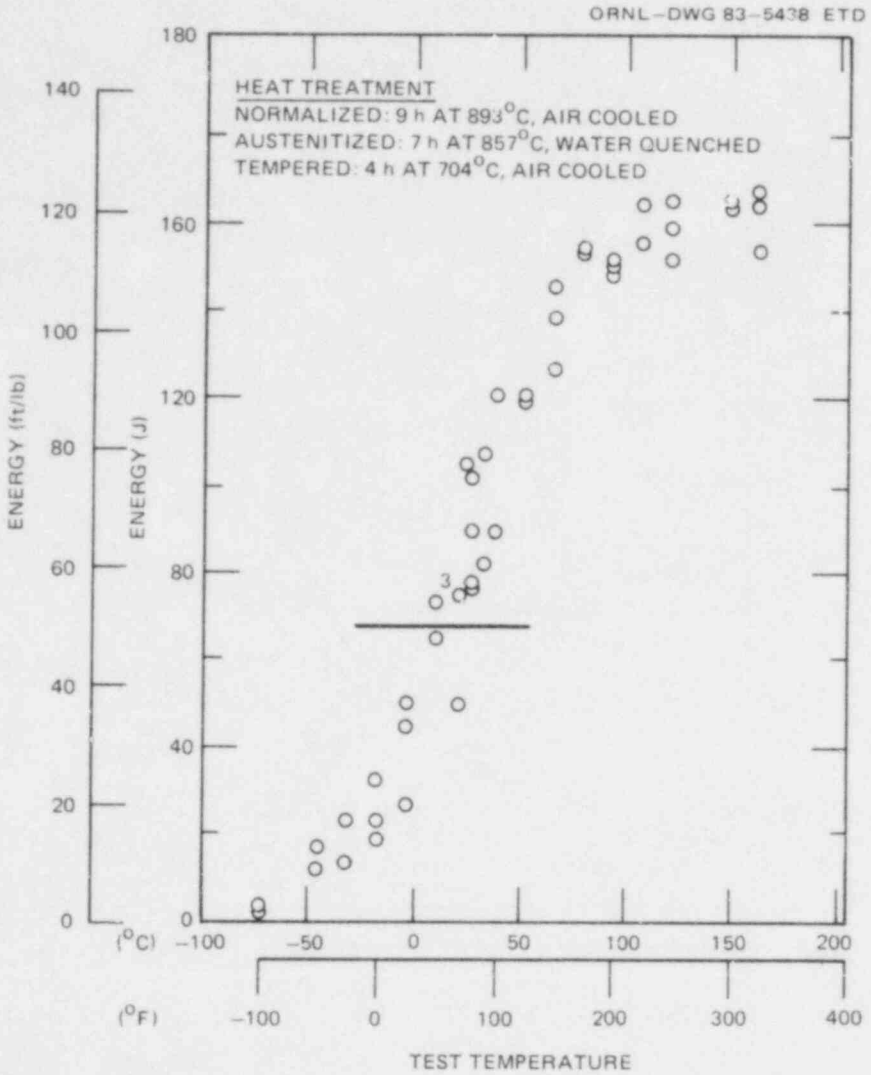

Fig. 4.17. Charpy-V impact energy of "as-quenched" 203-mm-thick thermal-shock prolongation TSP-4 after tempering for 4 h at 704°C and cooling in air.

were precracked to an average crack length-to-width ratio (a/w) of 0.558 and were tested to failure in a stroke control mode. The COD was measured at the specimen load line, and the J-integral calculation was made using the area-to-maximum load and the Merkle-Corten correction for the tensile component.[9] The static fracture toughness K_J was then calculated from $K_J^2 = EJ$, where E = 201 GPa at 21°C and 203 GPa at −18°C. The β_{Ic} adjustment was made using the Merkle method.[10] The results are given in Table 4.4 and are shown in Fig. 4.19. Ten 1TCS specimens were tested at each of two test temperatures, 21 and −18°C. K_J at 21°C varied from 147 to 321 MPa·$\sqrt{m}$ and from 80.9 to 109 MPa·$\sqrt{m}$ after the β_{Ic} adjustment. The J-integral ranged from 107 to 511 kJ/m². At −18°C, K_J ranged from 94.7 to

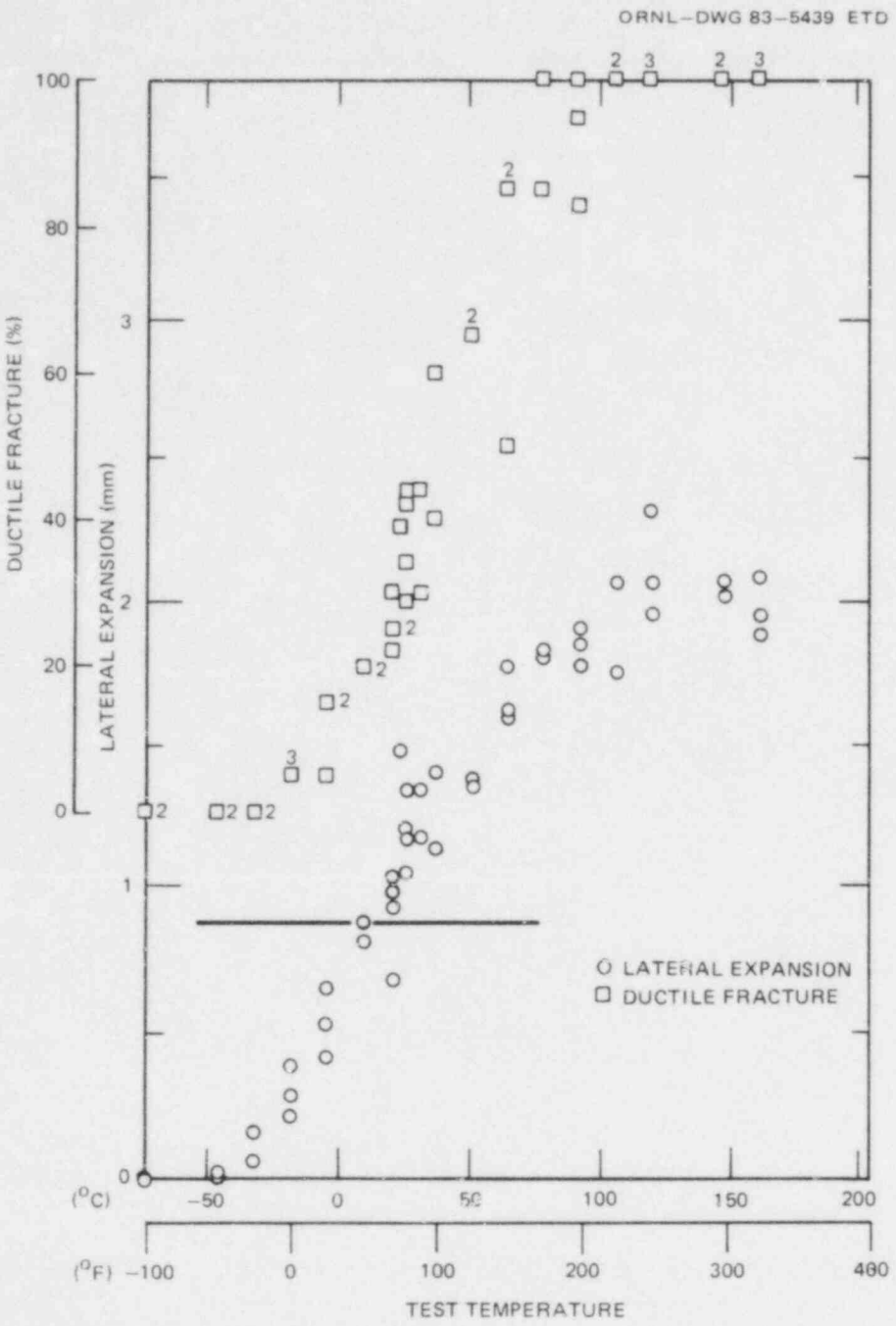

Fig. 4.18. Fracture appearance and lateral expansion for Charpy-V impact test of "as-quenched" 203-mm-thick thermal-shock prolongation TSP-4 after tempering for 4 h at 704°C and cooling in air.

Table 4.4. Static fracture toughness (K_J) from CT-oriented 1T compact specimens from prolongation TSP-4 (SA-508) after tempering at 704°C for 4 h and cooling in air

Test temperature (°C)	Static fracture toughness (MPa·√m)		J-integral (kJ/m²)	Average ductile crack extension (mm)
	K_J	β_{Ic} adjusted		
21	199	91.4	196	0.251
	321[a]	109[a]	511	0.828
	230	96.8	263	0.251
	246	99.0	299	0.310
	179[b]	87.7[b]	159	0.114
	147[b]	80.9[b]	107	0.099
	241	98.4	289	0.325
	268	102	355	0.457
	295	106	433	0.584
	156	83.0	121	0.117
−18	197	93.1	191	0.140
	106	71.3	55	0.051
	201[a]	93.8[a]	199	0.163
	94.7[b]	67.6[b]	44	0.036
	164	86.5	132	0.089
	105	71.1	54	0.038
	162	86.0	128	0.119
	144	82.1	102	0.069
	125	77.1	77	0.051
	96.0	68.0	45	0.064

[a]Maximum fracture toughness.

[b]Minimum fracture toughness.

201 MPa·√m before the β_{Ic} adjustment and from 67.6 to 93.8 MPa·√m after the adjustment. The J-integral ranged from 44 to 199 kJ/m². All the specimens experienced some stable ductile crack extension prior to failure. The ductile crack extension values, determined using a nine-point averaging method, are presented in Table 4.4. All specimens failed prior to attainment of limit load.

Precracking is presently under way for 30 additional specimens made of TSP-4 material tempered for 4 h at 704°C followed by air cooling. The specimens will be tested at three test temperatures, one of which will be −46°C.

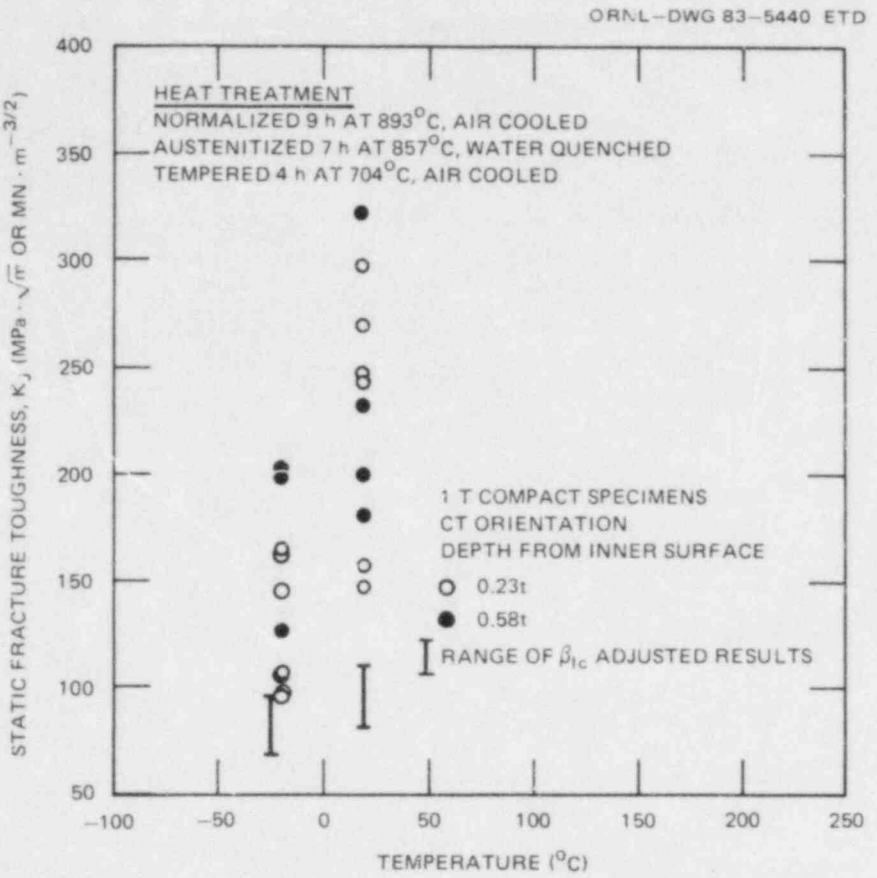

Fig. 4.19. Static fracture toughness (K_J) of "as-quenched" 203-mm-thick thermal-shock prolongation TSP-4 after tempering at 704°C for 4 h and cooling in air.

4.3 Probabilistic Fracture Mechanics

R. D. Cheverton D. G. Ball

A probabilistic fracture-mechanics (FM) code, OCA-P, has been developed that is a combination of OCA-II (Ref. 11) and a Monte Carlo routine similar to that included in VISA (Ref. 12). The Monte Carlo portion of the code generates a large number of vessels (10^6 more or less), each with a different combination of values of the various parameters that are susceptible to significant uncertainties [K_{Ic}, K_{Ia}, $RTNDT_o$, $\Delta RTNDT$ = f (fluence, Cu, Ni), Cu, Ni, F]. A deterministic FM analysis is then performed with OCA-II for each of these vessels for a specific transient to determine how many of the vessels would fail. The conditional probability of failure [P(F/E)], that is, the probability of failure assuming the transient event occurs, is calculated as the number of vessels that fail divided by the total number generated.

A necessary ingredient in OCA-P is the flaw-size distribution function, and the one selected for use in OCA-P at this time was obtained from the Marshall Report[13] and is discussed in Ref. 14. The particular relation, described in Eq. (4.1) and shown in Fig. 4.20, describes the flaw-depth distribution prior to preservice inspection and weld repair. To obtain the flaw-depth distribution corresponding to the time at which the

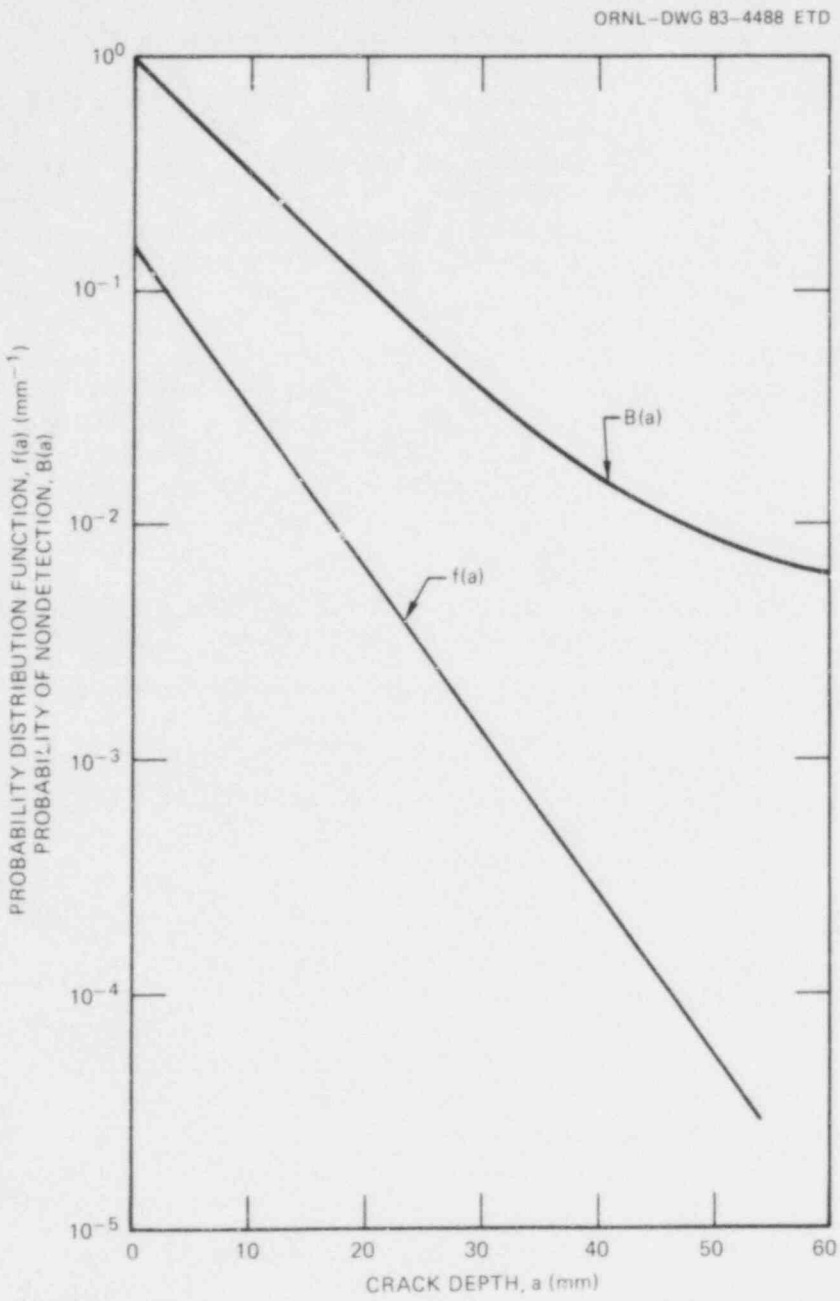

Fig. 4.20. Crack-size distribution and crack-nondetection probability functions.

vessel goes into operation, Eq. (4.1) must be multiplied by the probability of nondetection, assuming that all detected flaws are removed by one means or another. This probability is described in Eq. (4.2) and was also taken from the Marshall Report.

$$f(a) = 0.16\ e^{0.16a},\ mm^{-1} \tag{4.1}$$

$$B(a) = 0.005 + 0.995\ e^{-0.113a}\ mm^{-1} \tag{4.2}$$

The uncertainties in Eqs. (4.1) and (4.2) are orders of magnitude. The data upon which they are based were taken from unclad nonnuclear vessels, and Eq. (4.1) does not distinguish between surface and buried flaws or various orientations. The flaws of concern to the PTS issue are those that extend through the cladding into the base material, and there are no data for such flaws. Furthermore, if OCA-P is to be used in an absolute sense, it is necessary to include the flaw density N, as discussed in Ref. 14. The uncertainty in N is also very large for the same reason.

Because OCA-P makes use of OCA-II, it is possible to include certain 3-D flaws in the OCA-P analysis. The 3-D flaws available in OCA-II at this time are the 6/1 and 2-m semielliptical flaws described in Ref. 15.

OCA-P has been used recently to calculate several postulated transients for Oconee-I. Table 4.5 lists all of the pertinent input data for

Table 4.5. Input data for OCA-P analysis of Oconee postulated transient: probabilistic parameters

Parameter	Mean value (μ)	Standard[a] deviation (σ)	Truncation
Fluence (F)	*b*	0.3 (f)	F = 0
Copper	*b*	0.025%	
Nickel	*b*	0.0	
$RTNDT_o$	−7°C	9°C[c]	*c*
ΔRTNDT	*d*	13°C[c]	*c*
K_{Ic}	ASME XI + 18.5 MPa·$\sqrt{m}$	0.15 μ (K_{Ic})	$\pm 3\sigma$
K_{Ia}	ASME XI	0.10 μ (K_{Ia})	$\pm 2\sigma$

[a] Normal distribution used for each parameter.

[b] Proprietary information.

[c] $\sigma(RTNDT_o + \Delta RTNDT) = [\sigma^2(RTNDT_o) + \sigma^2(\Delta RTNDT)]^{1/2}$, truncated at $\pm 3\sigma$.

[d] $\Delta RTNDT = 0.56\ [-10 + 470\ Cu + 350\ Ni\ Cu][F \times 10^{-19}]^{0.27}$ or $= 0.56\ [283\ (F \times 10^{-19})^{0.194} - 48]$, °C, whichever is least.

the analysis, and Fig. 4.21 describes the downcomer coolant temperature and pressure transients for the most severe case. This particular transient, referred to as TBVF(4), is the result of all four turbine bypass valves failing to close once they have opened.

Results of the OCA-P analysis for TBVF(4) are shown in Fig. 4.22, which is a plot of P(F/E) vs the number of effective full-power years of service (EFPY). Because of the accumulative effect of radiation damage, P(F/E) increases with EFPY but tends to level off as the radiation effect saturates. For most PWRs the plant design lifetime is 32 EFPY. As indicated in Fig. 4.22, at 32 EFPY, P(F/E) is 1.2×10^{-3} and 1.6×10^{-4} for t_{max} (duration of transient) = 120 and 60 min, respectively. (For this analysis the transient was terminated by a large step decrease in pressure at t_{max}.)

Additional studies were conducted to determine the sensitivity of P(F/E) to the value of one standard deviation σ in K_{Ic} and the concentration of copper. The results are shown in Fig. 4.23 for t_{max} = 120 min, and as indicated the sensitivity of P(F/E) to $\sigma(K_{Ic})$ and σ(Cu) is not large.

In the above analysis the (2-D 2-m) axial flaw combination[15] was used, and cladding was not included. To determine the benefit of using the (2-D 2-m) flaw combination as opposed to the (2-D 2-D) combination and also to determine the effects of cladding, OCA-P calculations were made

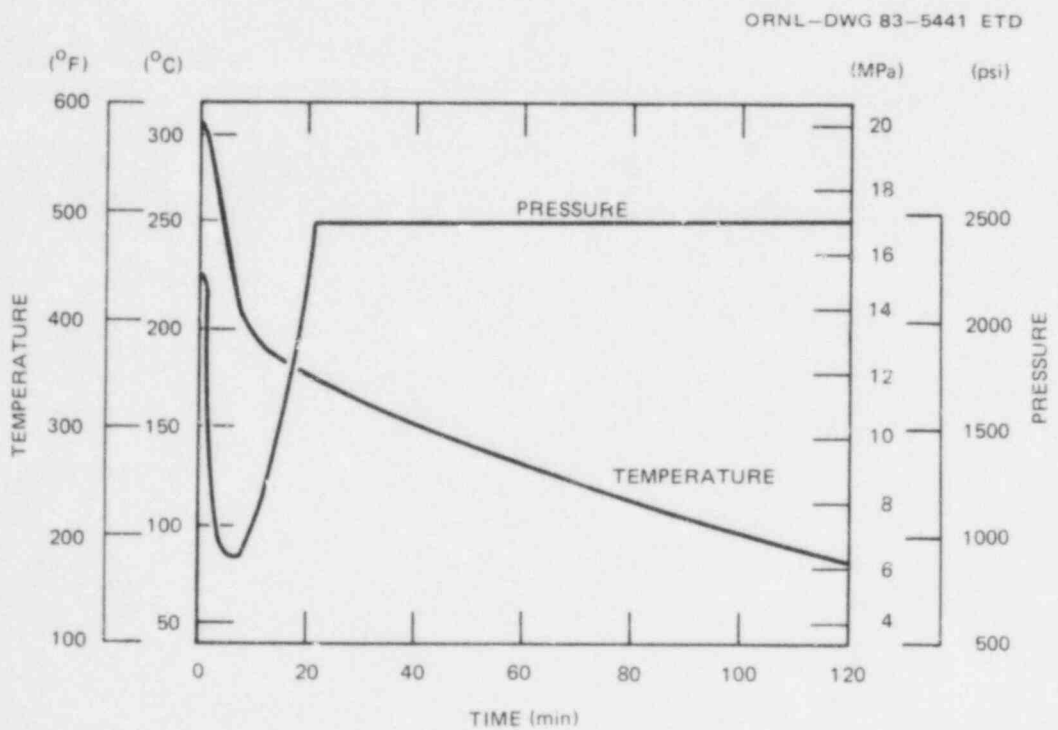

Fig. 4.21. Oconee postulated TBVF(4) transient.

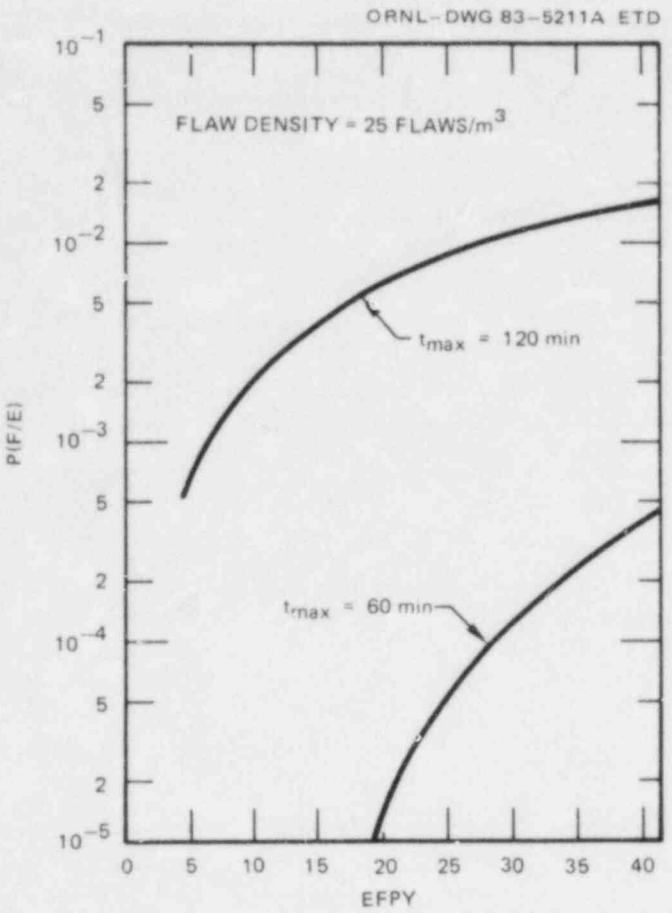

Fig. 4.22. OCA-P analysis of Oconee TBVF(4) case showing sensitivity of conditional probability of failure to fluence and duration of transient.

for the following transient:

$$T_c = 66 + 222\ e^{-0.1s\ t\ min^{-1}}\ {}^{\circ}C\ ,$$

$$p = \text{constant},$$

$$t_{max} = 45\ \text{min},$$

$$F = 1.1 \times 10^{19}\ \text{neutrons/cm}^2\ ,$$

where

T_c = temperature of coolant in downcomer,
t = time in transient,
t_{max} = duration of transient,
p = primary-system pressure.

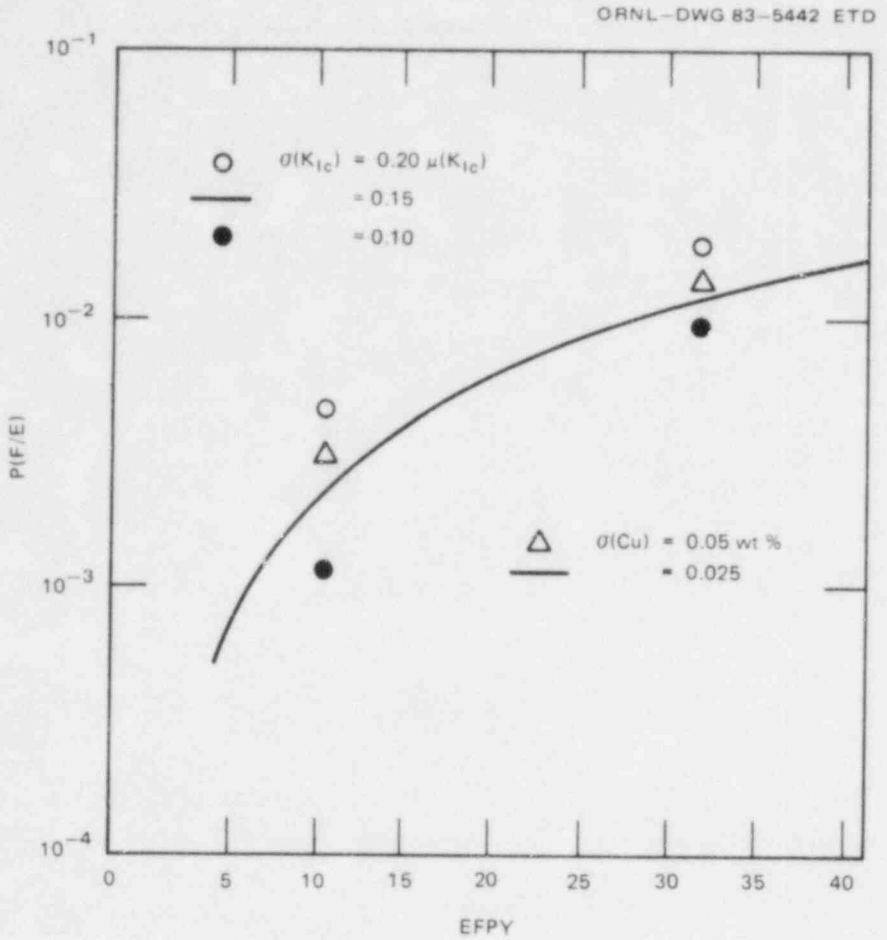

Fig. 4.23. Sensitivity of P(F/E) to $\sigma(K_{Ic})$ and σ(Cu) for Oconee TBVF(4) with t_{max} = 120 min.

As indicated in Fig. 4.24, the benefit of the (2-D 2-m) flaw combination decreases with increasing pressure, and there is none for $p \geq 12.4$ MPa. On the basis of previous studies[14] this trend would be expected.

The two curves in Fig. 4.24 were calculated ignoring the effects of cladding. Two additional calculations were made with cladding included for the (2-D 2-D) flaw combination and for a pressure of 13.8 MPa. One calculation was made assuming that shallow flaws in the cladding could not propagate ($K_{Ic} = \infty$), and for the other the toughness properties of the cladding were assumed to be the same as for the base material. As indicated in Fig. 4.24, inclusion of the cladding in the FM model increases P(F/E) but not by much. For K_{Ic} (cladding) = ∞, the increase in P(F/E) is from 0.14 to 0.17, and for K_{Ic} (cladding) = K_{Ic} (base metal) the increase is from 0.14 to 0.37.

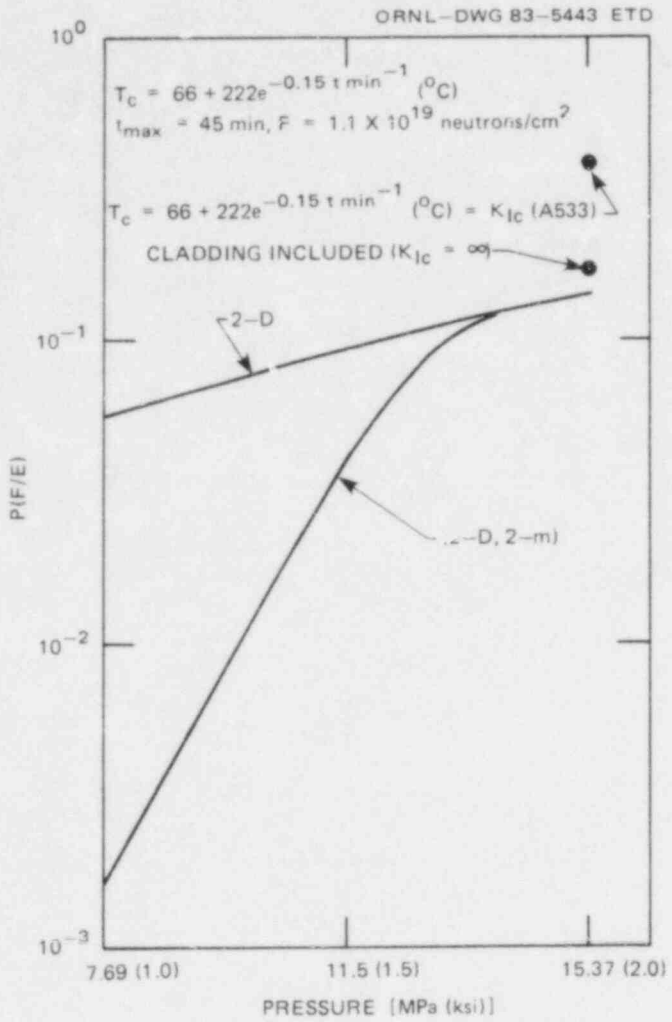

Fig. 4.24. Sensitivity of P(F/E) to 3-D vs 2-D flaws and to inclusion of cladding.

References

1. R. D. Cheverton and S. E. Bolt, *Pressure Vessel Fracture Studies Pertaining to a PWR LOCA-ECC Thermal Shock: Experiments TSE-3 and TSE-4 and Update of TSE-1 and TSE-2 Analysis*, ORNL/NUREG-22, Union Carbide Corp. Nuclear Div., Oak Ridge Natl. Lab., December 1977.

2. R. D. Cheverton et al., "Thermal-Shock Investigations," pp. 62-70 in *Heavy-Section Steel Technology Program Quart. Prog. Rep. October-December 1979*, ORNL/NUREG/TM-380, Union Carbide Corp. Nuclear Div., Oak Ridge Natl. Lab., May 1980.

3. R. D. Cheverton et al., "Thermal-Shock Investigations," pp. 37–49 in *Heavy-Section Steel Technology Program Quart. Prog. Rep. October–December 1980*, ORNL/NUREG/TM-437, Union Carbide Corp. Nuclear Div., Oak Ridge Natl. Lab., March 1981.

4. B. R. Bass and J. W. Bryson, *Applications of Energy Release Rate Techniques to Part-Through Cracks in Plates and Cylinders. Vol. 2. ORVIRT: A Finite-Element Program for Energy Release Rate Calculations for 2-Dimensional and 3-Dimensional Crack Models*, NUREG/CR-2997, Vol. 2 (ORNL/TM-8527/V2), Union Carbide Corp. Nuclear Div., Oak Ridge Natl. Lab., February 1983.

5. W. J. Stelzman, R. K. Nanstad, and R. L. Swain, "Thermal Shock Materials Characterization," pp. 93–94 in *Heavy-Section Steel Technology Program Quart. Prog. Rep. January–March 1983*, NUREG/CR-3334, Vol. 1 (ORNL/TM-8787/V1), Union Carbide Corp. Nuclear Div., Oak Ridge Natl. Lab.

6. *ASME Boiler and Pressure Vessel Code*, Sect. III, Division 1, Nuclear Power Plant Components, 1977 Ed. and Addenda, American Society of Mechanical Engineers, New York.

7. W. J. Stelzman and D. A. Canonico, "Characterization of the V-9 Prolongation," pp. 40–43 in *Heavy-Section Steel Technology Program Quart. Prog. Rep. October–December 1978*, NUREG/CR-0656 (ORNL/NUREG/TM-298), Union Carbide Corp. Nuclear Div., Oak Ridge Natl. Lab.

8. W. J. Stelzman and R. K. Nanstad, "Thermal Shock Characterization," pp. 71–76 in *Heavy-Section Steel Technology Program Quart. Prog. Rep. October–December 1982*, NUREG/CR-2751, Vol. 4 (ORNL/TM-8369/V4), Union Carbide Corp. Nuclear Div., Oak Ridge Natl. Lab.

9. J. G. Merkle and H. T. Corten, "A J-Integral Analysis for the Compact Specimen, Considering Axial Force as Well as Bending Effects," *J. Press. Vessel Technol., Series J. Trans. ASME* 96(4), 286–92 (1974).

10. J. G. Merkle, "New Method for Analyzing Small Scale Fracture Specimen Data in the Transition Zone," pp. 307–15 in *Proc. U.S. Nuclear Regulatory Commission 10th Water Reactor Safety Research Information Meeting*, NUREG/CP-0041, Vol. 4, 1982.

11. D. G. Ball, R. D. Cheverton, and S. K. Iskander, *OCA-II, A Code for Calculating the Behavior of 2-D and 3-D Surface Flaws in a Pressure Vessel Subjected to Temperature and Pressure Transients*, ORNL-5934, Union Carbide Corp. Nuclear Div., Oak Ridge Natl. Lab. (to be published).

12. NRC Staff Evaluation of PTS, Report to the Commission, Appendix H, Sept. 13, 1982 (draft).

13. W. Marshall, *An Assessment of the Integrity of PWR Pressure Vessels*, United Kingdom Atomic Energy Authority, Second Report, March 1982.

14. R. D. Cheverton et al., "Thermal-Shock Investigations," pp. 69–71 in *Heavy-Section Steel Technology Program Quart. Prog. Rep. October–December 1982*, NUREG/CR-2751, Vol. 4 (ORNL/TM-8369/V4), Union Carbide Corp. Nuclear Div., Oak Ridge Natl. Lab.

15. R. D. Cheverton and D. G. Ball, "Thermal-Shock Investigations," pp. 77–97 in *Heavy-Section Steel Technology Program Quart. Prog. Rep. January–March 1983*, NUREG/CR-3334, Vol. 1 (ORNL/TM-8787/V1), Union Carbide Corp. Nuclear Div., Oak Ridge Natl. Lab.

5. PRESSURE VESSEL INVESTIGATIONS

R. H. Bryan

Investigations during this report period were concentrated on various preparations for the first pressurized-thermal-shock experiment (PTSE-1). Fabrication of two test vessels was completed, and a series of material characterization tests for PTSE-1 was begun. The major facility construction phase was completed, and testing on the completed systems was undertaken while further facility modification was in progress. An instrumented but unflawed vessel was prepared for preliminary tests (PTSE-0) to determine the test facility operating characteristics and to rehearse pressure-temperature transients for the fracture test PTSE-1.

A new computer code OCA/USA was developed to combine the capabilities of the OCA-II code[1] for linear-elastic fracture analysis and the PTSUSA code[2] for upper-shelf ductile tearing analysis. Improvements to both original codes were made to facilitate evaluation of PTSEs and to incorporate elastic-plastic fracture analysis and ligament tensile instability.[3] OCA/USA is being used in conjunction with the results of material characterization tests for planning PTSE-1.

5.1 PTS Studies

5.1.1 Test vessel fabrication and material characterization (K. R. Thoms)

The Babcock and Wilcox Company (B&W) prepared two intermediate test vessels (ITVs), V-7 and V-8, for use in PTSE-0 and the first fracture-mechanics experiment PTSE-1, respectively. The preparation was accomplished by welding a 1320-mm-long plug fabricated from TSC-6 into each of the vessels. B&W is performing material characterization tests with specimens taken from cylinder TSC-6, which received the same heat treatments as the inserts in the vessels. These characterization data will be used in the pretest analysis for PTSE-1.

Following welding of the plugs into the vessels, magnetic-particle test inspections and repair of some indications were made. The two vessels along with the remainder of TSC-6 then went through a postweld heat treatment, which was performed at 561°C for 12.3 h. The vessels were subsequently radiographed and machined to the required outside diameter of 981.08 mm, and inspections showed that both are well within the specified $\pm$0.25-mm tolerance. Oak Ridge National Laboratory (ORNL) accepted the weldment in vessel V-8 with a radiographic indication of a slag inclusion that exceeds the limits of the specification. It was decided that the size, location, orientation, and nature of the defect make it innocuous. The two vessels and the remnant of TSC-6 were delivered to ORNL in June, and since then further preparations for testing have been under way.

B&W completed the Charpy-V impact specimen testing on the material from TSC-6. The data indicate that the effective RT_{NDT} is ~50°C, which

is slightly higher than previously estimated. The fully ductile upper-shelf temperature T_D is ~175°C.

5.1.2 PTS test facility construction (R. W. McCulloch)

Design and construction of the coolant system[4] (Fig. 5.1) in the PTS Facility (PTSTF) were accomplished under Department of Energy (DOE) Directive CL-523. Union Carbide Corporation-Nuclear Division (UCC-ND) furnished titles I, II, and III engineering; procured the ITV shroud or outer test vessel (OTV); provided instrumentation and controls (I&C) design, component procurement, and fabrication; performed utility tie-ins, instrument calibration, and preoperational testing; and provided support to the construction contractor. Mechanical components procurement and construction were performed by the Rust Engineering Company, the DOE construction contractor.

Site construction of the coolant system was completed during this report period. Original plans called for completion of major construction and beneficial occupancy of the facility by UCC-ND on April 15, 1983. Then UCC-ND would have performed instrumentation checkout prior to Rust Engineering completing construction on June 17, 1983. A DOE, UCC-ND, and Rust Engineering agreement was reached that allowed Rust Engineering to complete all construction on April 15. Instrumentation and mechanical checkouts were immediately initiated, and the coolant system was completed on May 20, 1983, ~1 month ahead of the original schedule. Construction costs were $1.14 million, and this was $60 thousand less than budgeted.

In addition to directive-controlled design and construction tasks, several peripheral facility-related tasks are in progress to enable PTSE testing. These include upgrading the data acquisition and pressurization systems; determining and installing needed test instrumentation; and providing reliable high-pressure, high-temperature seals for instrumentation and pressurization penetrations of the test vessels.

The data acquisition system (DAS) was completed by ORNL's I&C Division personnel and delivered to the test facility on June 28, 1983. The system will be integrated into facility and test instrumentation and checked out prior to start of shakedown tests.

Figure 5.2 shows a simplified block diagram of the DAS. The PDP 11/34 central processing unit receives up to 195 thermocouple, 136 strain gage and crack-opening displacement (COD), and 30 miscellaneous inputs from facility and ITV sensors. Data are stored, manipulated, and made available through three separate terminals. One terminal is dedicated to operation instructions and calibration; the other two provide plotting of selected test data. A graphics copier is available for hard-copy printout. A separate data logger independently records critical data from test and facility instrumentation as a safeguard against the loss of main DAS records.

Figure 5.3 summarizes instrumentation for both the PTSE-0 and PTSE-1 vessels. Cables from sensors on the test vessel will be connected to the DAS cables in two junction boxes installed adjacent to the OTV. Cables and cable trays from the junction boxes to the DAS have been installed. Design, procurement, and fabrication of test instrumentation and control

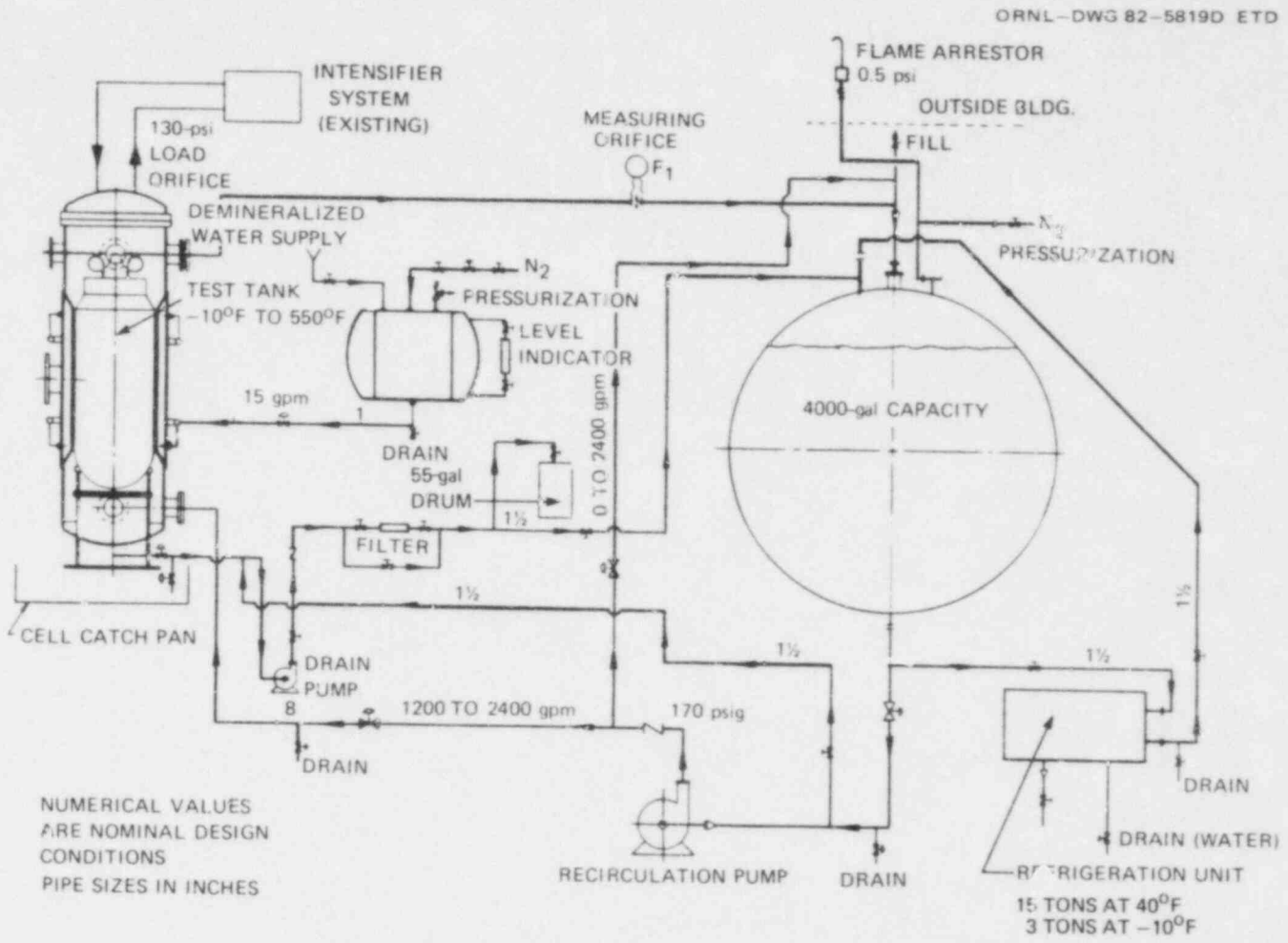

Fig. 5.1. Flow diagram of the coolant system of the PTSTF.

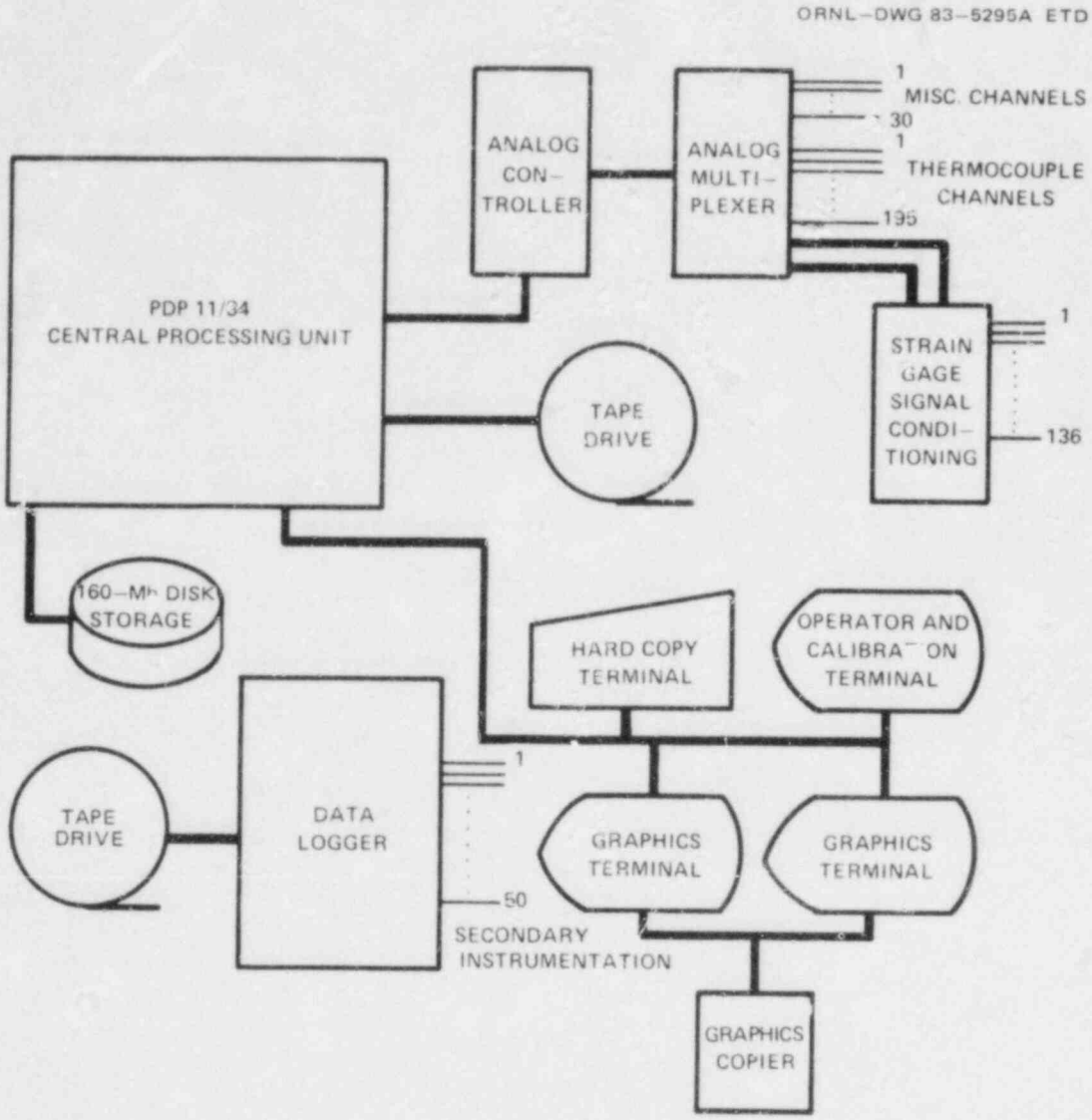

Fig. 5.2. Data acquisition system in the PTSTF.

cables to connect the ITV to the DAS, data logger, pressurization system, and control room were completed.

5.1.3 ITV preparation (R. W. McCulloch)

Both test vessels have been machined for installation of thermocouple thimbles. One test vessel (V-7) is being instrumented for facility shakedown tests (PTSE-0), while the other (V-8) is being prepared for PTSE-1. Figure 5.4 shows thermocouple instrumentation locations for the two vessels. Crack-mouth-opening displacement (CMOD) gage locations are shown in Fig. 5.3. The two vessels will be identically instrumented with thermocouples, but only the second will contain a flaw and associated CMOD instrumentation.

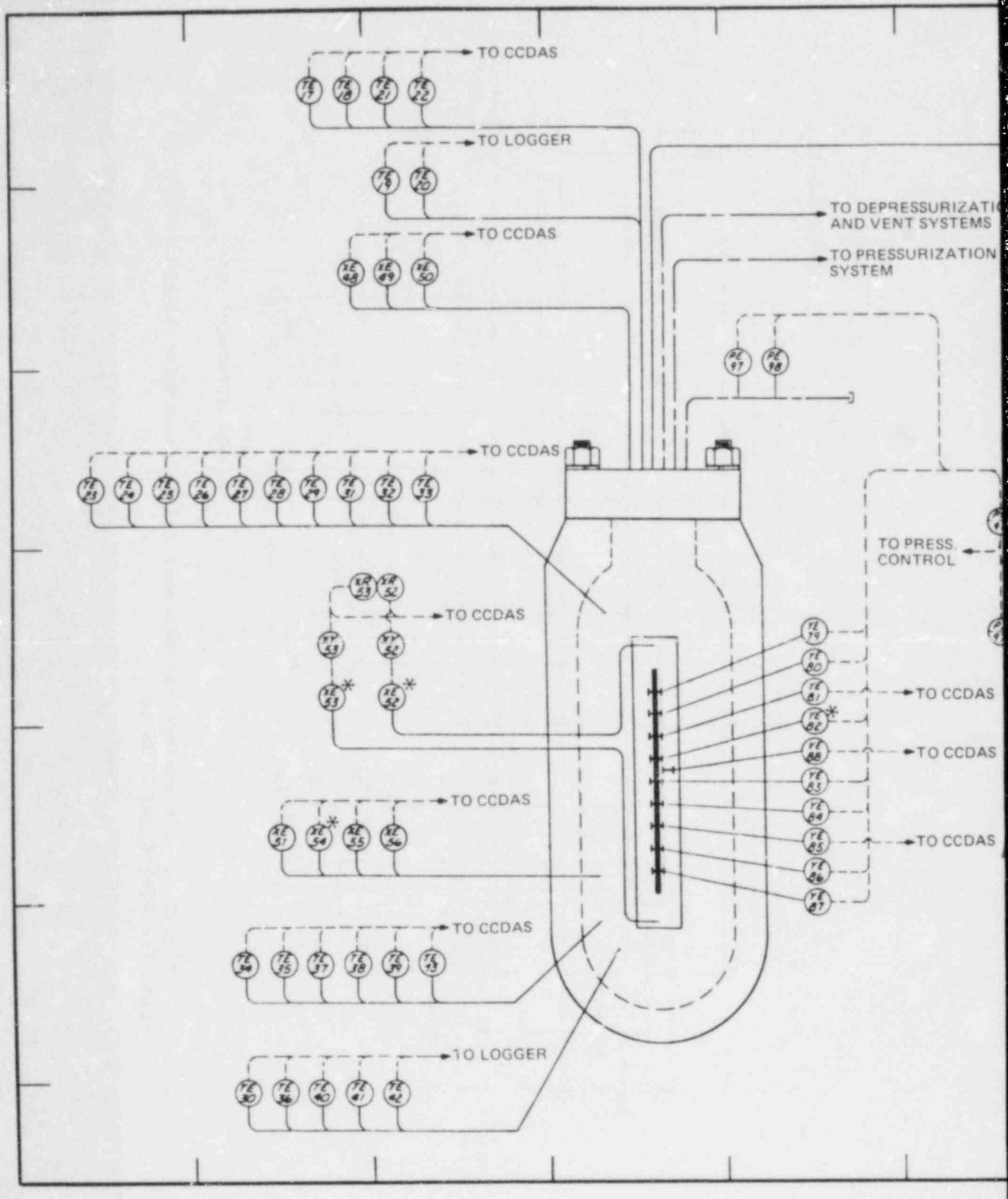

Fig. 5.3. ITV instrumentation for PTSE-
will be essentially the same as PTSE-1.

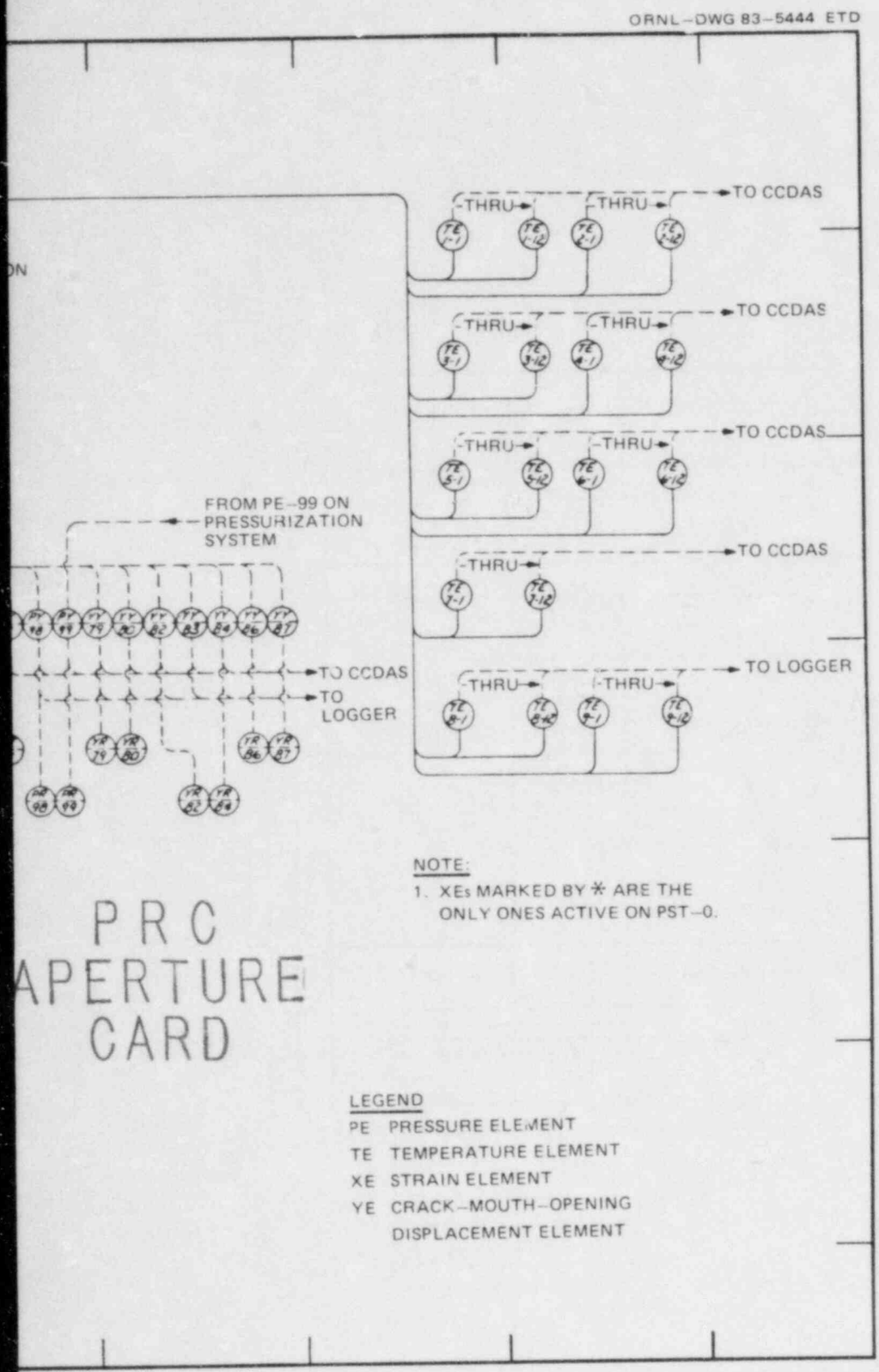

-1. Thermometry for PTSE-0

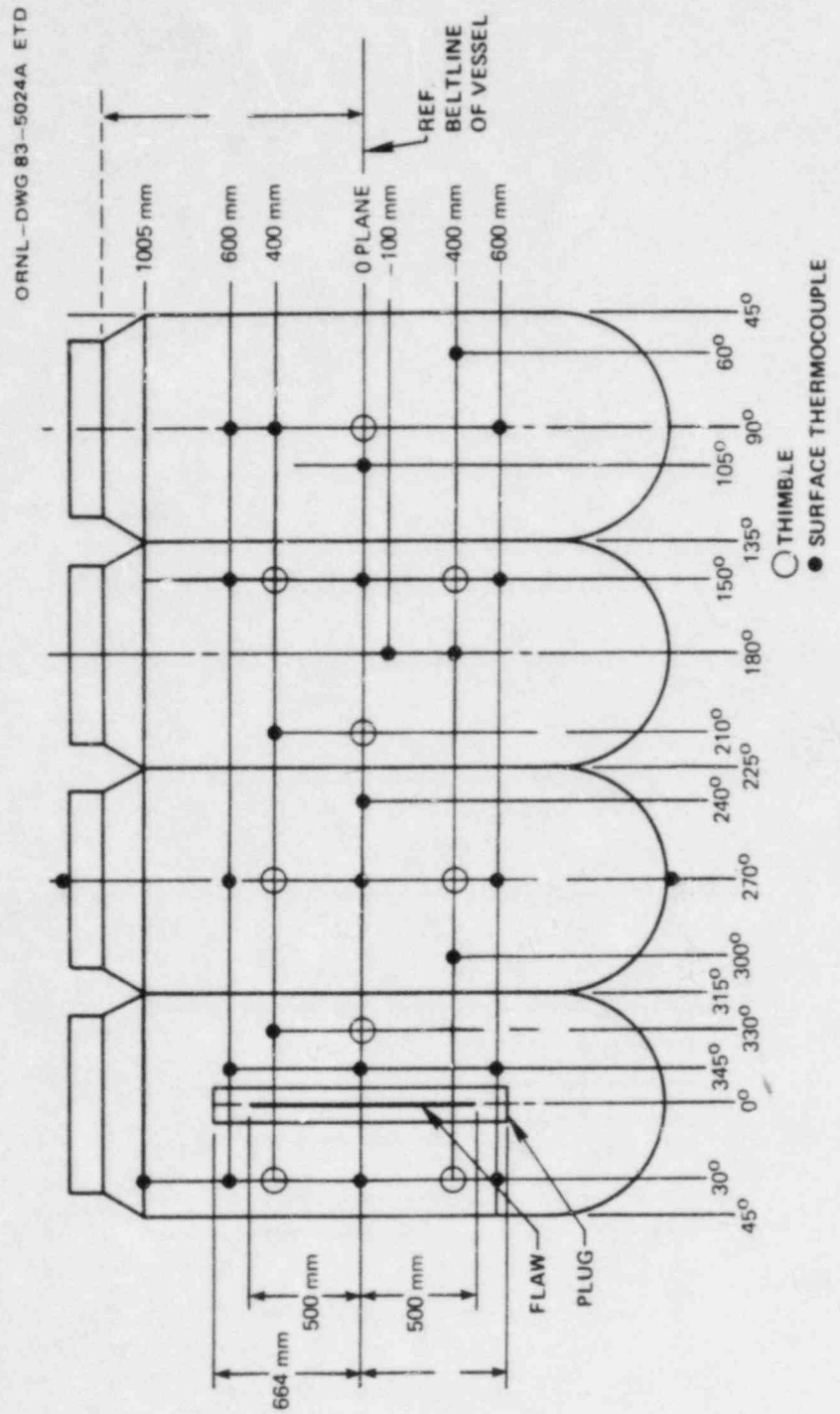

Fig. 5.4. ITV surface thermocouple and thermocouple thimble locations for PTSE-0 and PTSE-1.

Each vessel will contain twenty-five 1.2-mm-diam sheathed thermocouples on the outer surface with their thermoelements welded to form intrinsic junctions with the vessel surface. The thermocouple insulation at the junction is protected from the coolant with a high-temperature room-temperature vulcanizing (RTV) sealant.

Nine thermocouple thimbles (Fig. 5.4), each with twelve 0.5-mm-diam sheathed insulated junction thermocouples, measure temperature profiles in the vessel wall. Figure 5.5 schematically represents the thermocouple thimble.

The center of the thimble contains the 12 small-diameter thermocouples encased within a 3.2-mm-OD carbon steel tube, which surrounds a 1.4-mm-OD carbon steel rod. This assembly, after being assembled and swaged, is inserted into a 15.9-mm carbon steel thimble. The entire assembly is then swaged to obtain intimate contact of the inner assembly with the thimble. Thermocouple junctions are positioned from as shallow as 5.1 mm from the vessel outer surface to as deep as 91 mm within the 148-mm-thick wall. The central carbon steel rod terminates near the inner end of the 105-mm thimble, and the 12 thermocouples are encased beyond that point within a stainless steel tube. The tube is routed

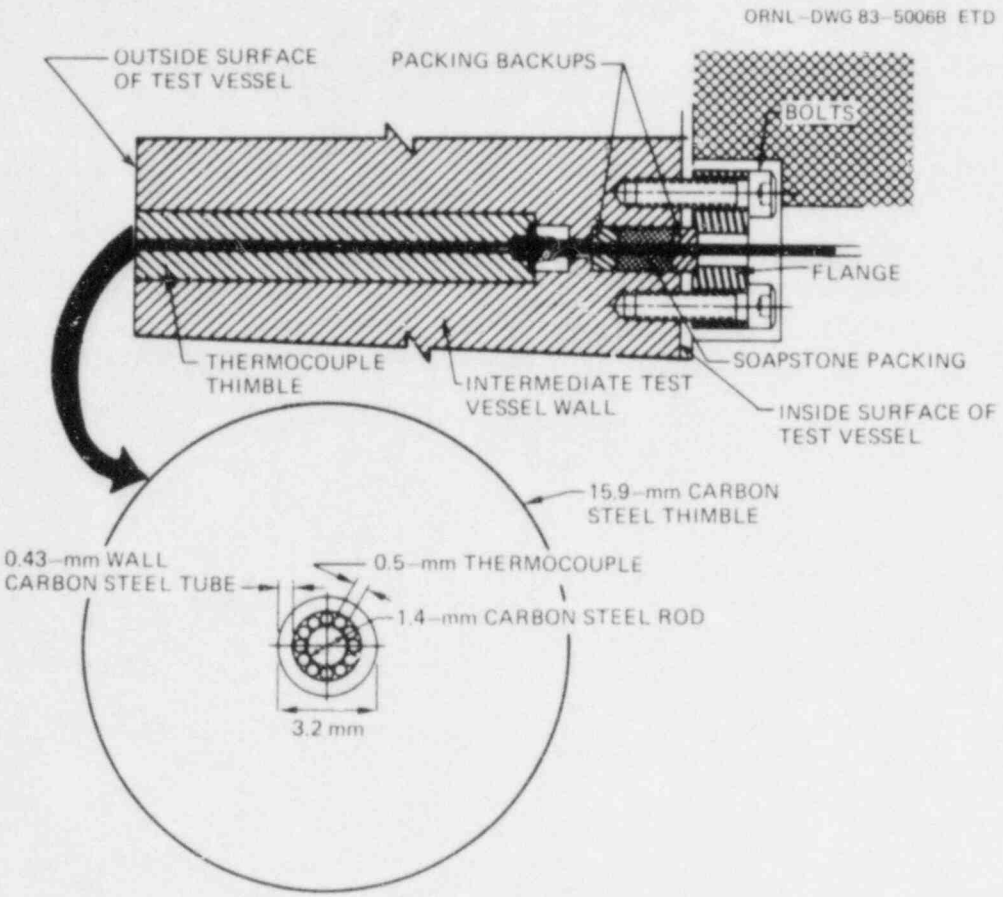

Fig. 5.5. Thermocouple thimble for measurement of temperature profile in wall of ITV.

through a seal at the inner wall of the vessel, then through the interior of the vessel, through a head seal into the OTV, and through a seal in an OTV flange to an instrumentation junction box within the containment cell. The small-diameter thermocouples exit the stainless steel protection tube within the instrumentation junction box. The 0.08-mm-diam thermoelements of each thermocouple are then attached to a miniature terminal strip for connection to the instrumentation cables to the DAS.

Handling and connection of the small thermoelements to the miniature terminal strip necessitated that a device be developed to allow long lengths (20 mm) to be easily stripped. Figure 5.6 shows this device, and Fig. 5.7 shows thermocouples with their thermoelements stripped. The device consists of a fixed lower and a moveable upper electrode, each of which is connected to a 250-J capacitance discharge welder. The sheath of the 0.5-mm thermocouple is placed between the electrodes as shown in the figure. A short time-constant 200-J pulse then supplies enough energy to vaporize the sheath, while the thermocouple insulation protects the thermoelements. Copper shim stock is used on both electrodes to prevent electrode contamination.

All thermocouples installed in test vessels for PTSE-0 and PTSE-1 are calibrated to National Bureau of Standards standards by the Metrology Laboratory of the ORNL I&C Division. In addition, a prototype thimble and two of the nine thimbles used in the first vessel were given thermal transient tests. In these tests the thimble was inserted in the center of a 102-mm-diam carbon steel cylinder that contained surface intrinsic junction thermocouples. The cylinder was insulated and heated to ~260°C. The face of the cylinder was then sprayed with cold water, while the thimble and cylinder thermocouples were monitored. Comparison of temperatures from thimble and intrinsic junction thermocouples indicated that both profiles and transient response of the thimbles accurately represented that of the surrounding carbon steel.

5.2 Vessel V-8A Posttest Materials Characterizations

W. J. Stelzman R. K. Nanstad
T. D. Owings, Jr.

A posttest characterization of the weld metal from the low-upper-shelf longitudinal seam weld in vessel V-8A was begun. Tensile and CVN specimens were machined from the weld metal. The results of tests of W- and L-oriented tensile specimens are presented in Table 5.1. Orientation has a slight effect on the yield and ultimate stresses. The average values ranged from 402 to 423 MPa and 502 to 525 MPa for the yield and ultimate stresses, respectively. The ductility values show little effect of orientation. Average ductility values ranged from 17.1 to 18.6% for total elongation and 53.6 to 54.8% for the reduction of area. The elastic modulus results showed greater scatter from the L-oriented specimens.

The results of WL-oriented weld metal CVN specimens also tested over a temperature range of −73 to 260°C are shown in Fig. 5.8. Salient transition temperatures were 48°C at 34 J, 44°C at 0.64-mm lateral expansion, and 47°C at 50% ductile fracture. The onset of upper shelf (100% ductile fracture) occurred at 107°C, and the upper-shelf energy is ~57 J.

ORNL–PHOTO 7012–83

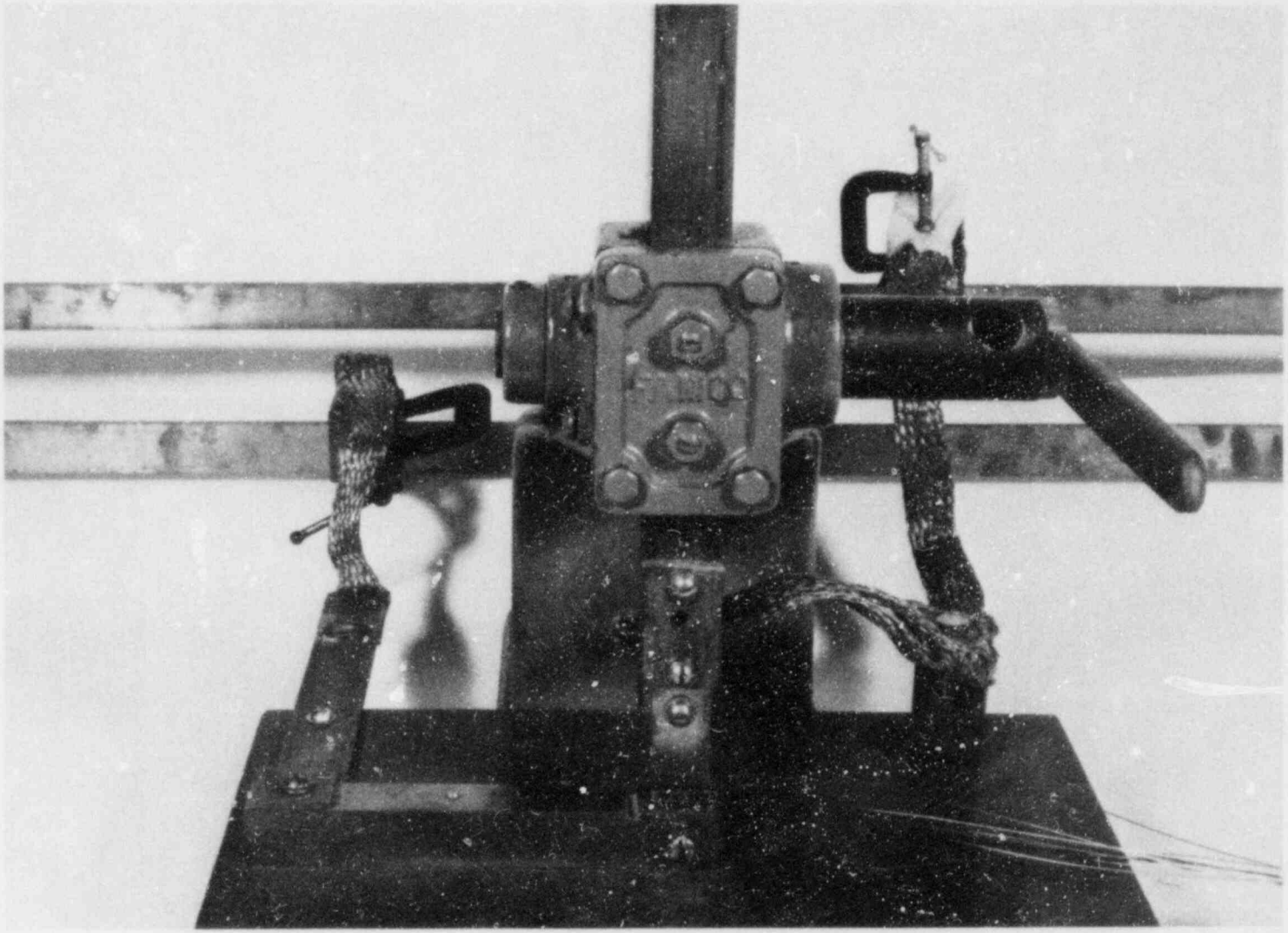

Fig. 5.6. Thermocouple stripping device.

ORNL–PHOTO 7011–83

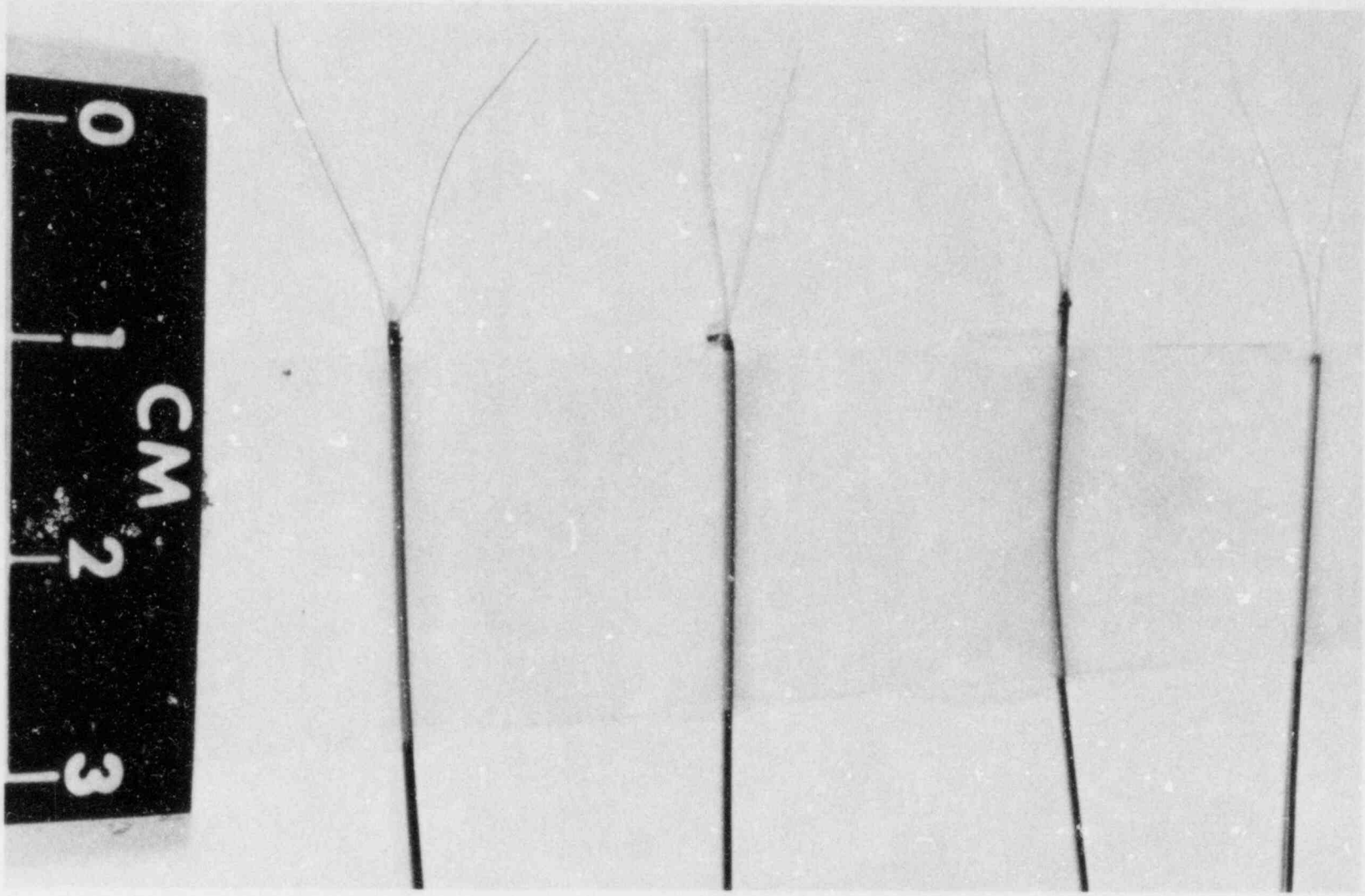

Fig. 5.7. Small-diameter thermocouples with their thermoelements stripped.

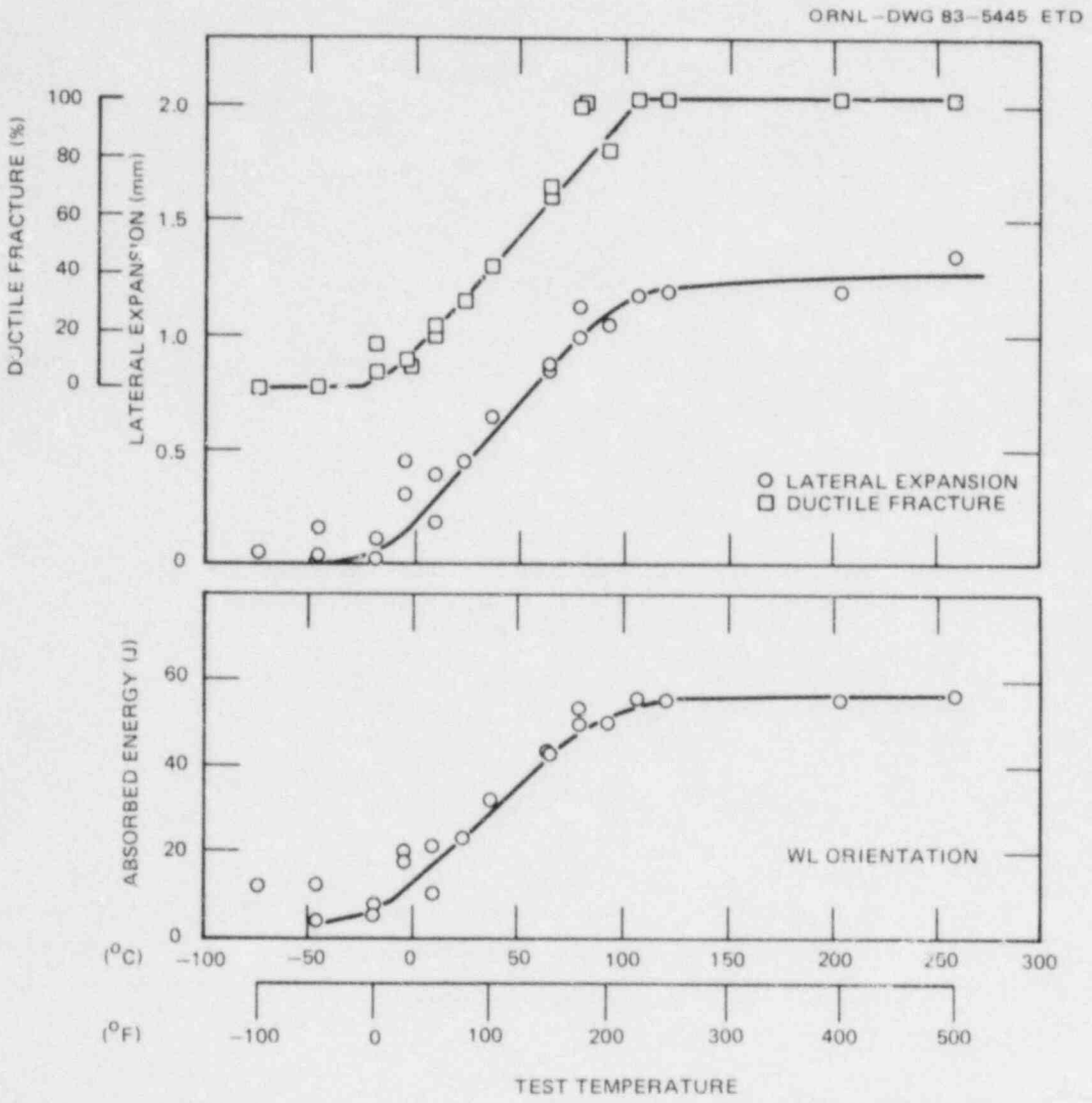

Fig. 5.8. Posttest through-thickness Charpy V-notch impact properties of weld metal from 152-mm-thick submerged-arc weld in test vessel V-8A.

Table 5.1. Tensile properties (6.4-mm-diam specimens, strain rate 0.016/min) of weld metal from the submerged-arc repair weld in vessel V-8A at 149°C

Stresses (MPa)		Ductility (%)		Elastic modulus (GPa)
Yield[a]	Ultimate	Total elongation[b]	Reduction of area	
		L orientation[c]		
429	525	18.7	54.3	205
417	525	18.6	53.0	187
		W orientation[d]		
403	502	16.9	52.9	234
401	502	17.3	56.7	231

[a] 0.2% offset.

[b] Gage length to gage diameter = 5.

[c] Specimen length parallel to welding direction L; fracture transverse to L.

[d] Specimen length perpendicular to L; fracture along centerline of weld.

References

1. D. G. Ball, R. D. Cheverton, and S. K. Iskander, *OCA-II, A Code for Calculating the Behavior of 2-D and 3-D Surface Flaws in a Pressure Vessel Subjected to Temperature and Pressure Transients*, ORNL-5934, Union Carbide Corp. Nuclear Div., Oak Ridge Natl. Lab., to be published.

2. R. H. Bryan and J. G. Merkle, "Upper-Shelf Arrest Analysis Based on J_R-Controlled Tearing," *Heavy-Section Steel Technology Program Quart. Prog. Rep. January-March 1983*, NUREG/CR-3334, Vol. 1 (ORNL/TM-8727/V1), Union Carbide Corp. Nuclear Div., Oak Ridge Natl. Lab.

3. J. G. Merkle, "Elastic-Ideally Plastic Pressurized Thermal Shock Analysis for a Deep Continuous External Longitudinal Crack in a Cylinder," *Heavy-Section Steel Technology Program Quart. Prog. Rep. January-March 1983*, NUREG/CR-3334, Vol. 1 (ORNL/TM-8787/V1), Union Carbide Corp. Nuclear Div., Oak Ridge Natl. Lab.

4. G. C. Robinson and R. W. McCulloch, "Pressurized Thermal-Shock Studies," *Heavy-Section Steel Technology Program Quart. Prog. Rep. January-March 1982*, NUREG/CR-2751, Vol. 1 (ORNL/TM-8369/V1), Union Carbide Corp. Nuclear Div., Oak Ridge Nat. Lab.

6. STAINLESS STEEL CLADDING INVESTIGATIONS

The study of stainless steel cladding has been mostly centered around a series of clad plate tests. The purpose of these tests was to investigate the influence of the cladding on crack initiation, growth, and arrest. Further testing has been suspended until additional information is available on the influences that irradiation has on the fracture characteristics of the cladding. (Those investigations are reported in Chap. 3 of this report.) However, in preparation for testing of a more prototypical cladding in the future, a contract was finalized with Combustion Engineering Company to prepare stainless steel clad plate material using a series-arc three-wire process. The plates are to be delivered early in FY-1984.

7. ENVIRONMENTALLY ASSISTED CRACK GROWTH STUDIES*

W. H. Bamford† L. J. Ceschini†

7.1 Introduction

The objective of this task is to characterize the crack growth rate properties of light-water reactor (LWR) materials exposed to primary-coolant environments. The work now being conducted falls into four major areas:

- corrosion fatigue crack growth tests in simulated pressurized-water reactor (PWR) environment,
- static load K_{ISCC} tests in simulated PWR environment,
- fractographic examination of specimen fracture surfaces, and
- characterization of environment by measurement of electrochemical potential.

7.2 Fatigue Crack Growth Results

Recent results have shown that different levels of environmental enhancement can occur in the crack growth rate properties of pressure vessel steels in water environments. These levels of enhancement have been found to be related to two main factors, the chemistry of the material and the water environment conditions. Both of these factors are under active investigation in this program, the former having been carefully considered through completion of a test matrix reviewed in the previous progress report[1] and reported in detail in Ref. 2. The effects of water chemistry and environmental conditions on environmental enhancement have been recently reviewed by Scott[3] and will be further investigated in this program in future work.

Fatigue crack growth tests during this report period have concentrated on two areas. The first involved participation in the round robin test program for corrosion fatigue at high R ratio, which is being coordinated by the International Cyclic Crack Growth Rate (ICCGR) Review Group, and the second is a new thrust toward better characterizing the effect of materials chemistry on environmental enhancement.

The round robin test program is being carried out by approximately 12 different laboratories throughout the world. The test conditions are very straightforward and were designed to be carefully followed by each

---

*Work sponsored by HSST Program under Union Carbide Corporation-Nuclear Division (UCC-ND) Subcontract 11X-21598C between UCC-ND and Westinghouse Electric Corporation, Nuclear Technology Division.

†Westinghouse Electric Corporation, Power Systems, Nuclear Technology Division, Pittsburgh, Pa. 15230.

laboratory. Specifically, the test loading conditions are as follows:

Initial ΔK	11 MPa·$\sqrt{m}$
Frequency	17 mHz
Load form	sine wave
R	0.7

The material chosen for the test specimens is an older heat of A533B class 1 steel, expected to have a reasonable sensitivity to environmental effects on crack growth, having a sulfur content of 0.013 wt %. The specimen was tested under constant load amplitude conditions as specified, and the following water chemistry was maintained:

Conductivity	1 μmho/cm
ph	9 at room temperature
Dissolved oxygen	5 ppb
Hydrogen	50 standard cm^3/kg H_2O
Temperature	288°C

Figure 7.1 shows that the crack growth rate results displayed the expected degree of environmental enhancement. The crack growth rate increased quickly from the beginning of the test and then began to increase at a slower rate once the rate reached 10^{-3} mm/cycle at $\Delta K \cong 15$ MPa·$\sqrt{m}$. The observed growth rates followed the ASME Sect. XI reference law[4] for high R ratio very well.

The crack growth rate behavior observed in this test is similar to that observed for another heat of A533B class 1 plate (designated PN), which was tested earlier[1] and contained 0.016 wt % sulfur. The crack growth rate results for this plate are shown in Fig. 7.2. Another example of similar behavior is heat "IN," which had 0.026 wt % sulfur and is shown in Fig. 7.3. Thus, the behavior observed in the round robin specimen was typical of other results obtained for similar materials in this program. For reference, the material chemistry of all the materials discussed in this report is summarized in Table 7.1.

Table 7.1. Material chemistries – matrix study of sulfur effects

Specimen	Elements										
	C	Mn	P	S	Si	Ni	Cr	Mo	Cu	V	Co
A533B class 1											
Heat IN	0.21	1.26	0.012	0.026	0.25	0.47		0.47	0.19		
Heat TW	0.21	1.38	0.008	0.004	0.21	0.67		0.56	0.08		
Heat W7	0.23	1.40	0.005	0.004	0.25	0.70		0.57			
Heat PN	0.21	1.33	0.012	0.016	0.22	0.56		0.54	0.13		
Heat CQ2	0.21	1.28	0.006	0.025	0.24	0.56		0.53	0.12		
Round robin material	0.17	1.32	0.008	0.013	0.23	0.59	0.05	0.55	0.10	0.004	

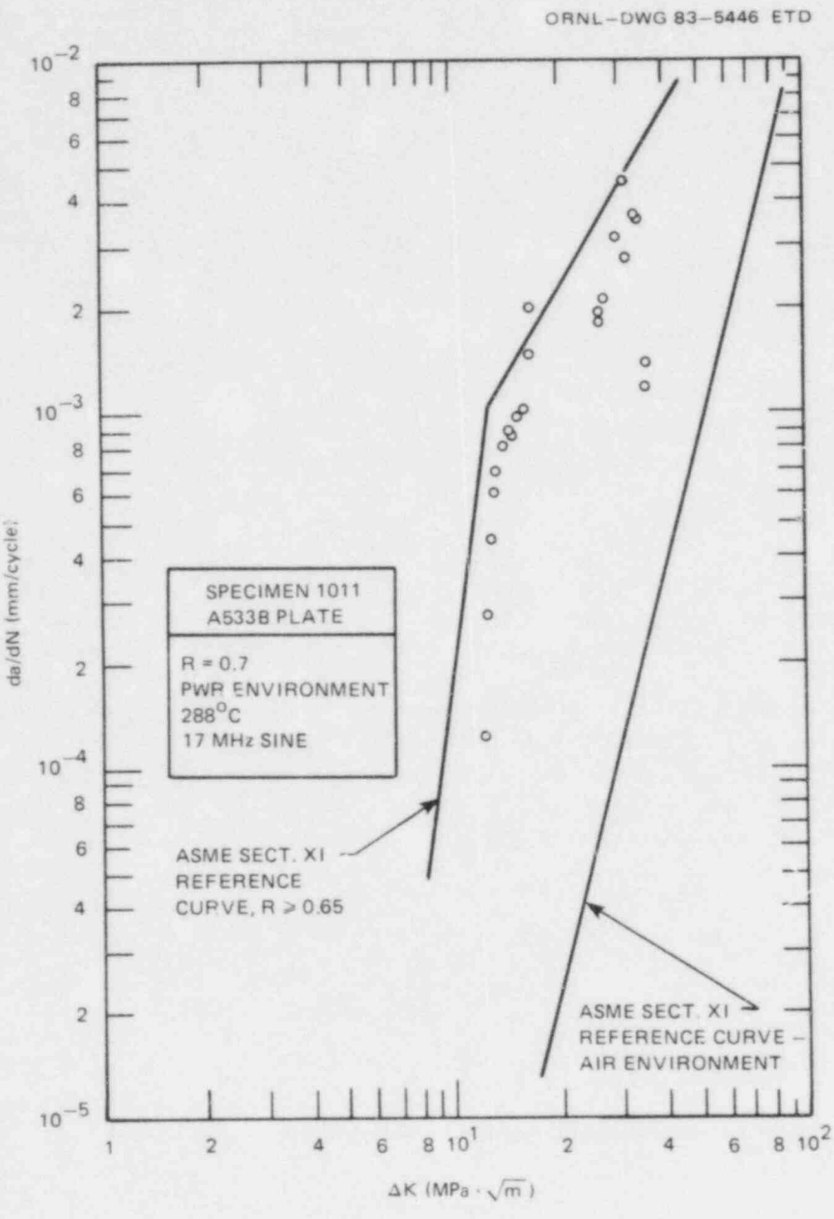

Fig. 7.1. Crack growth rate results to specimen 1011, tested in PWR environment at R = 0.7, as part of ICCGR review group round robin.

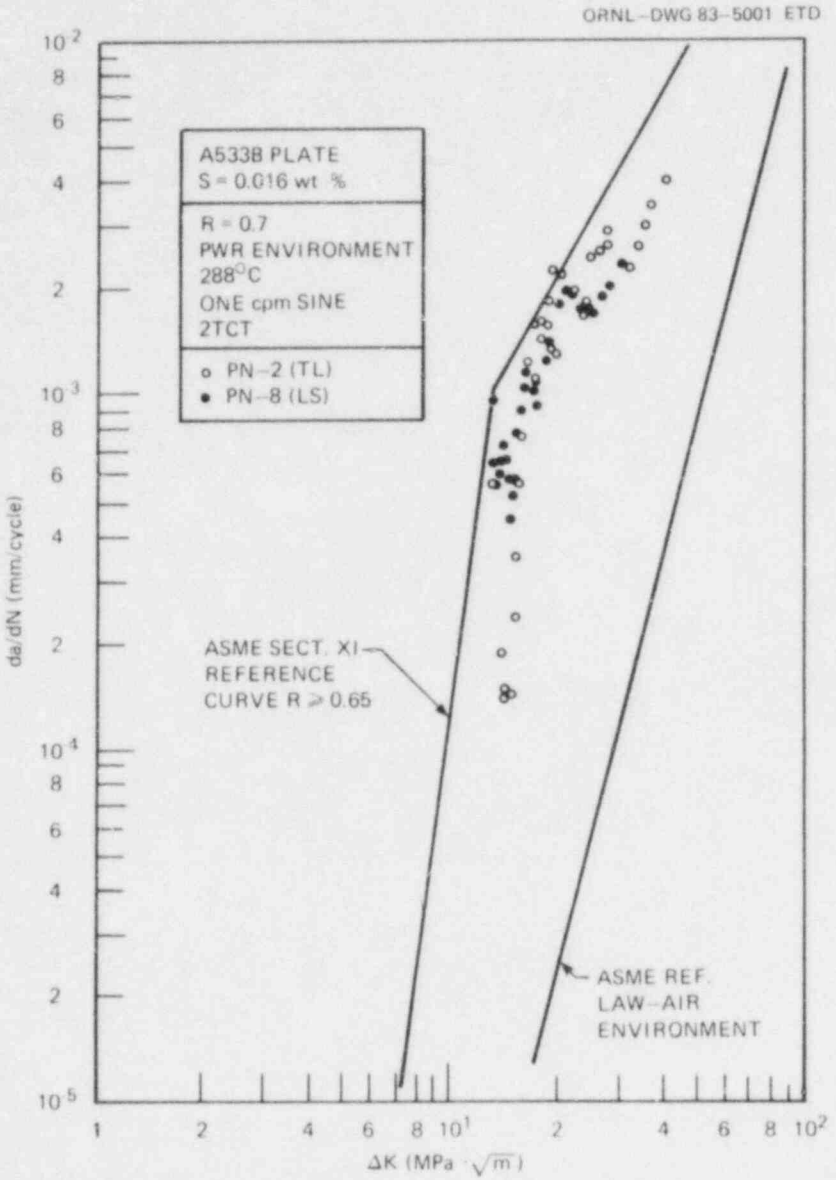

Fig. 7.2. Effect of specimen orientation on crack growth, medium-sulfur plate PN, R = 0.7. *Source:* W. H. Bamford and L. J. Ceschini, "Environmentally Assisted Crack Growth in Light Water Reactors," *Heavy Section Steel Technology Progam Quart. Prog. Rep. January-March 1983*, NUREG/CR-3334, Vol. 1 (ORNL/TM-8787/V1), Union Carbide Corp. Nuclear Div., Oak Ridge Natl. Lab.

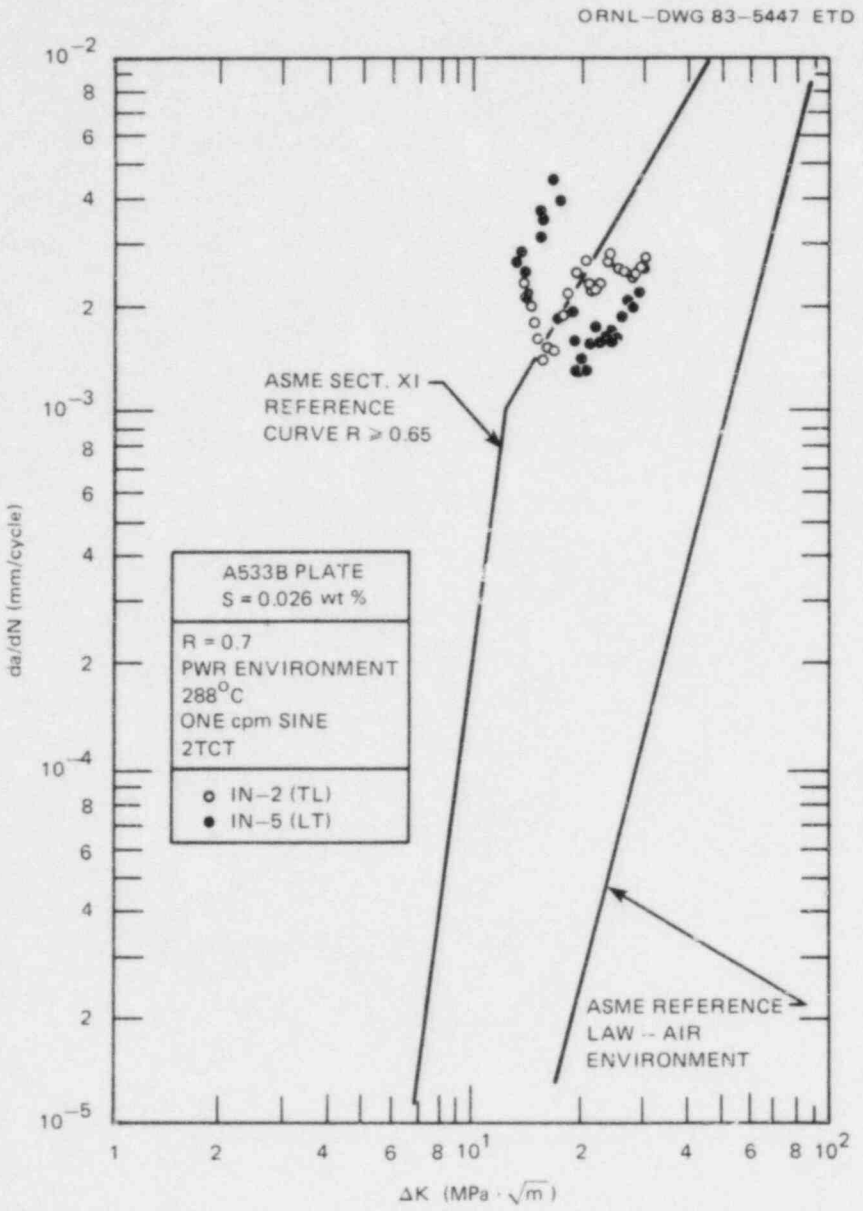

Fig. 7.3. Effect of specimen orientation at high-sulfur heat, R = 0.7.

The second area of emphasis during this report period was the beginning of a new investigation into the effect of material chemistry on environment enhancement of crack growth. This work will involve detailed study of a heat of high-sulfur plate material, typical of the oldest materials in service in operating plants. The crack growth characteristics will be studied as a function of temperature and frequency of loading. This behavior will be evaluated relative to the propensity of the material to exhibit cracking under static loading, as measured through bolt-load static-loaded specimens and constant extension rate tests.

To provide a basic characterization, the first of two tests on this heat, labeled "CQ2," was completed during this report period. The test was carried out at one cycle per minute with a sine wave loading and R ratio equal to 0.2 to provide a base for comparison with the wide variety of materials that have now been tested under this identical set of conditions. The results are shown in Fig. 7.4 and demonstate that this heat has at least as much environmental enhancement as any heat tested to date. The crack growth results for this test show rates somewhat in excess of the Sect. XI reference growth law at high values of applied stress-intensity factor range ΔK.

For comparison, crack growth results previously reported for another high-sulfur heat, plate "IN," tested under the same loading conditions, are shown in Fig. 7.5. The next tests of this new heat CQ2 will be performed at R = 0.7, after which the frequency and temperature dependence will be studied. Fracture surface study as well as metallography will be done to help in understanding the mechanism of environmental enhancement.

7.3 Crack Growth Behavior in Static Tests

The behavior of cracks in the steels and welds of interest in a water environment has been under investigation using bolt-loaded specimens since 1974. The specimens are WOL-type, 2.54 cm thick and loaded to a fixed displacement by a bolt of the same material. The specimens are positioned in the bottom of two of the operating corrosion fatigue autoclaves.

Crack propagation under static load has been observed in several samples of the 19 specimens that have been tested thus far. Thirteen remain in testing, including specimens of A508 Class 2, A533B Class 1, a Linde 124 weld, and two heat-affected zones. No further crack propagation was observed in this report period.

7.4 Characterization of Water Environment Through Potential Measurement

The effects of environmental conditions on the level of enhancement of fatigue crack growth for pressure vessel steels have been studied in considerable depth in the past several years. A good reference on this subject is the work of Scott.[3] It has been proposed that the environment interacts with the material in the crack-tip region in a manner dependent

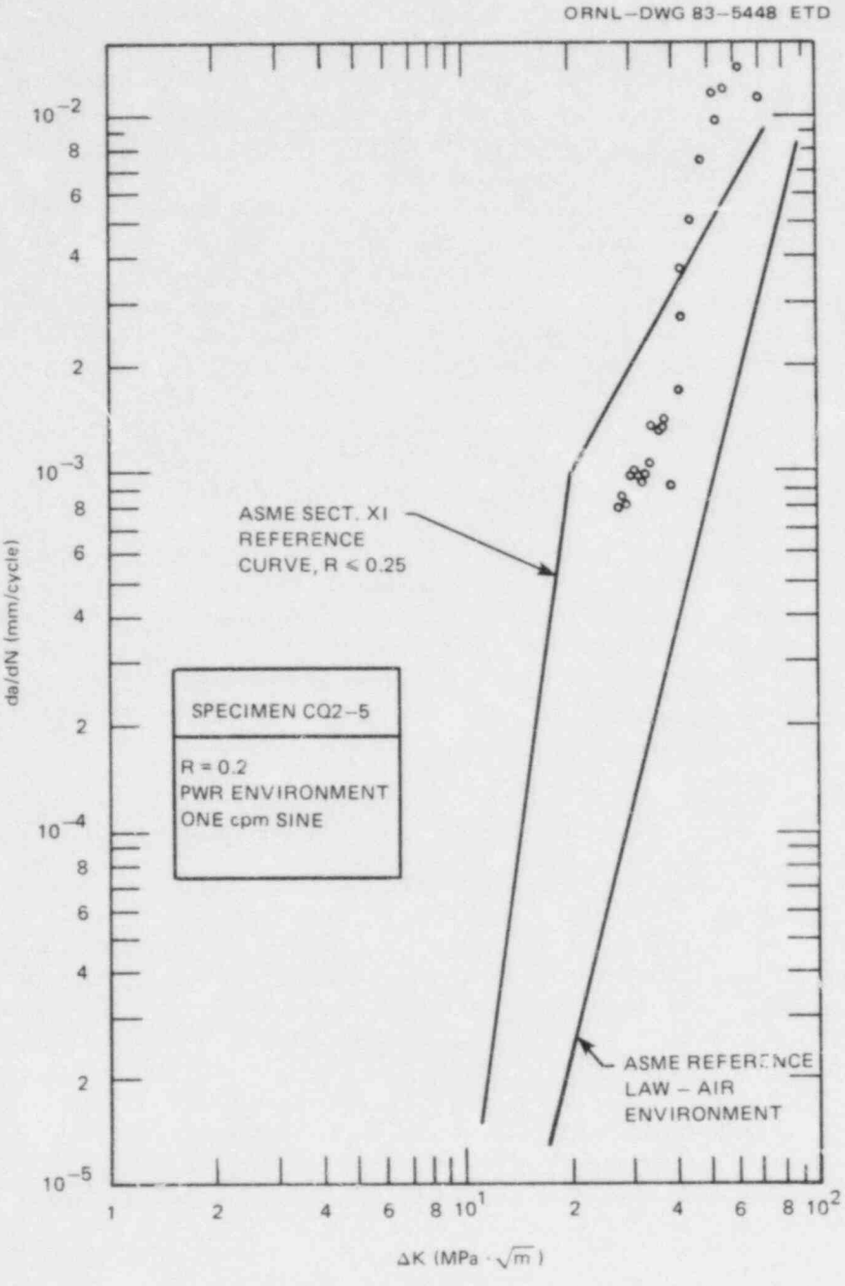

Fig. 7.4. Crack growth rate results for specimen CQ2-5, tested in PWR environment at R = 0.2.

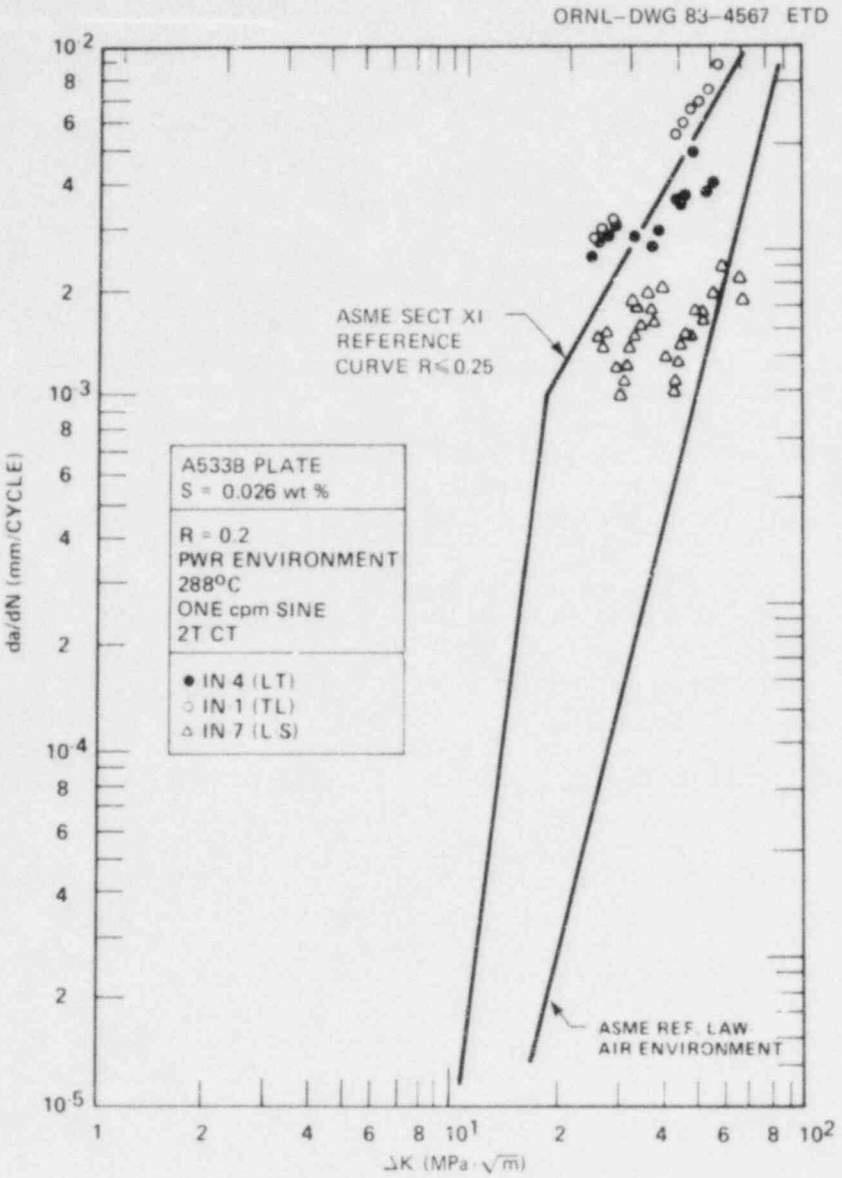

Fig. 7.5. Effect of specimen orientation on crack growth, high-sulfur plate material, R = 0.2.

on the crack-tip strain rate. It has been suggested, and there is some experimental evidence to show, that small amounts of oxygen in the water can have a marked influence on the amount of environmental enhancement. The experimental evidence of this behavior has come primarily from constant extension rate tests (CERT)[5] with very carefully controlled oxygen levels. The precise level of oxygen in the water in a large autoclave is difficult to determine, because it can change as a result of the many oxidizing reactions taking place both on the test specimen and the autoclave itself.

The most reliable way of characterizing the environment as it could influence corrosion fatigue has been found to be measurement of the electrochemical potential of the system. This measurement technique has been used for many years in low-temperature pressurized environments, and in the last few years, attempts have been made to develop means for its application to the LWR environment. Efforts in this area have been aided immeasurably by the work of the ICCGR Review Group.

During the past 2 years, the available measurement methods have been discussed in depth within this group, and virtually every method has been tried by at least one laboratory. Experience with the various electrodes has been collected through a detailed survey conducted of the members, and results showed that the two most reliable systems are the silver-silver chloride (Ag-AgCl) system developed by Andresen,[6] and the hydrogen reference electrode. Both these systems are being developed for installation on the Westinghouse autoclaves.

The Andresen Ag-AgCl electrode is mounted externally on the environmental chamber and is shown in Fig. 7.6. The device consists primarily of a 0.32-cm-diam silver rod in a solution of 0.1-M potassium chloride, which acts as a bridge. Porous zirconia is used as a separator between the liquid bridge and the environment. The reference electrode must be kept cool and pressurized, and horizontal installation is preferred. Experience with this apparatus by other laboratories has been relatively good, with some reporting long service times before the electrolyte was dispersed through the porous plug and the operability impaired. A second problem associated with the failure of this electrode is the contamination of the environment with chlorides. For this reason, and to extend service life, this electrode will first be installed in a separate chamber at the exit of the chamber, which may be isolated.

A hydrogen electrode will be installed in this small chamber as well and will also be installed in the autoclave itself near the specimen. A cross-sectional sketch of this electrode is shown in Fig. 7.7. The electrode is formed from a closed-end tube of palladium-silver alloy pressurized on the inside with pure hydrogen. The alloy tube is encased in a perforated sleeve that allows water to be trapped between the alloy tube and the sleeve, where it is saturated with hydrogen permeating through the wall of the alloy tube. The electrode acts as a hydrogen reference electrode. The advantage of this system is that its failure does not result in any contamination of the autoclave environment, because there is a hydrogen overpressure at all times.

These systems have been designed and built, and they are currently in the final stages of installation on one autoclave system. Checkout of the system is expected to be completed during the next report period, and operational results should become available during that time frame.

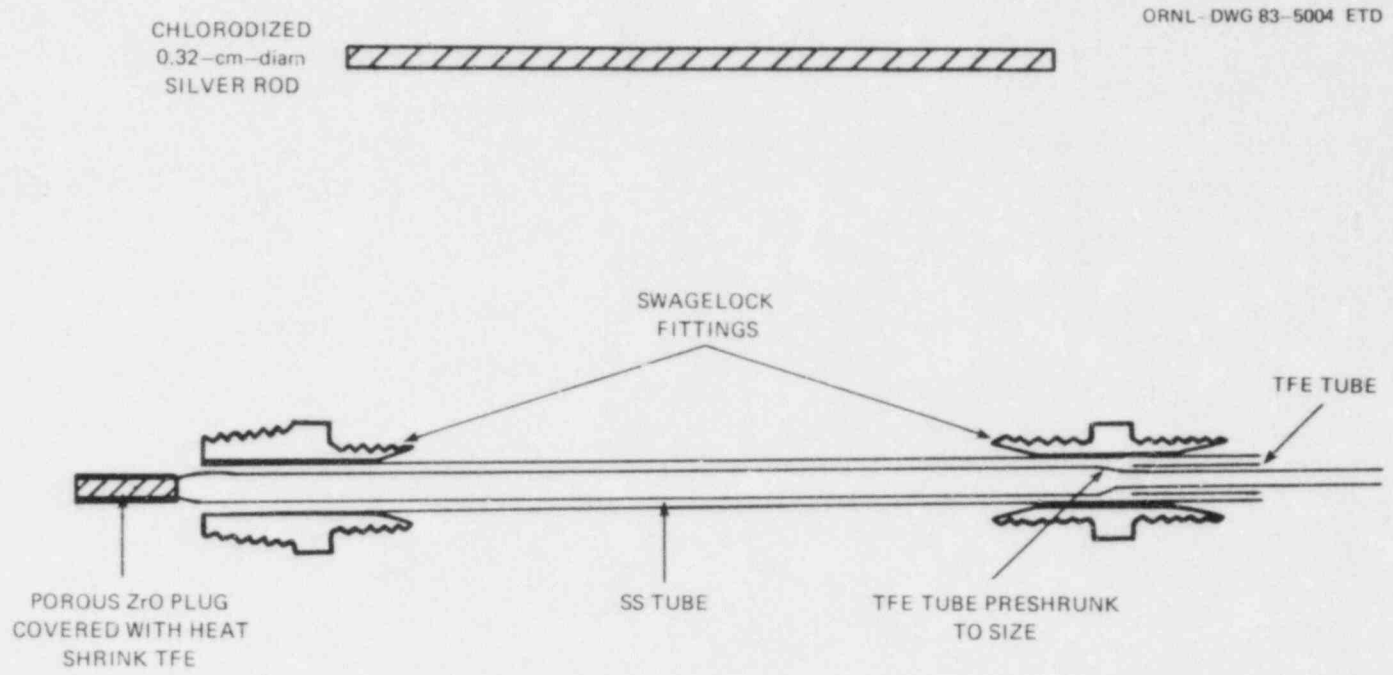

Fig. 7.6. Cross-sectional view of Andresen electrode parts.

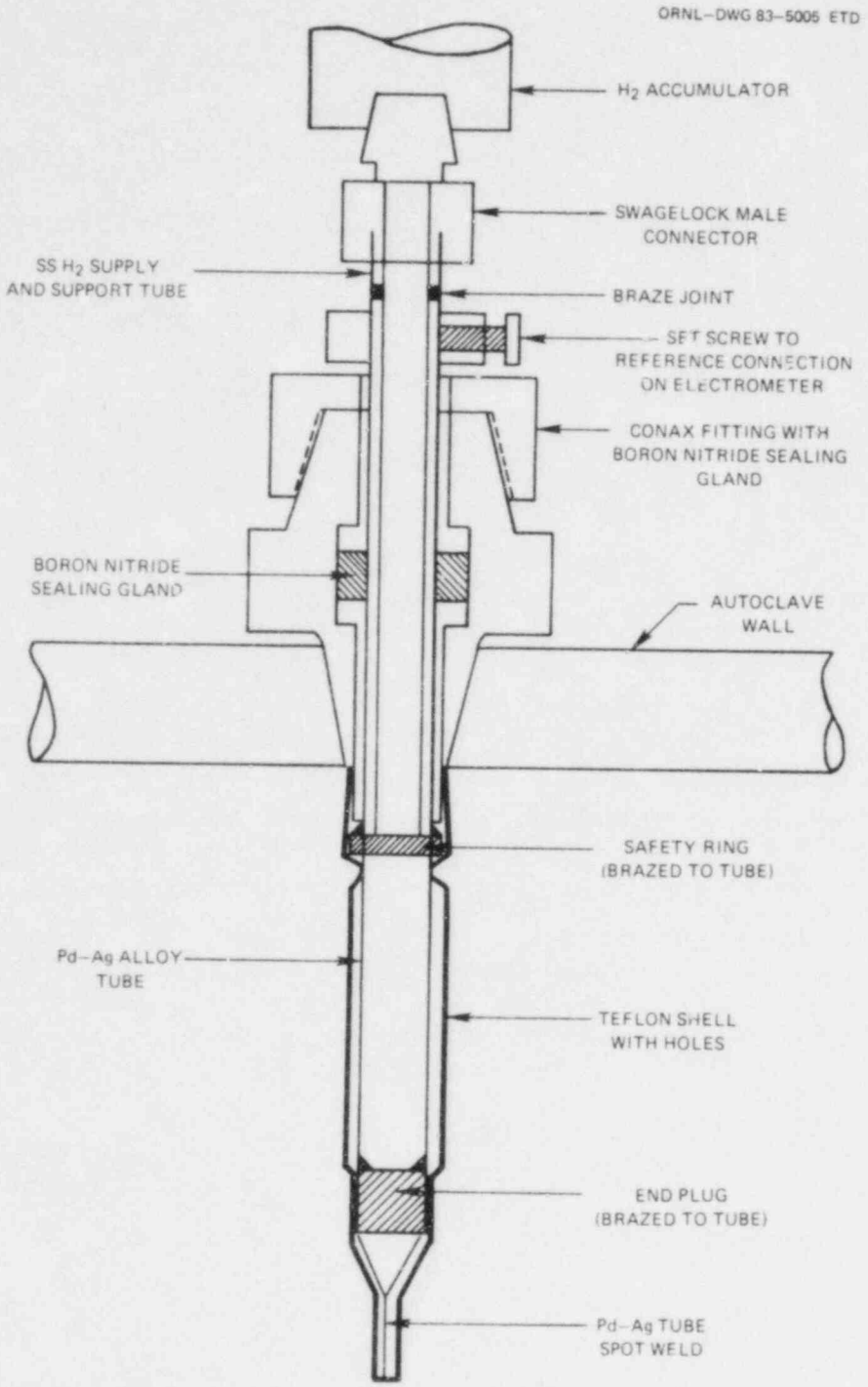

Fig. 7.7. Sketch of hydrogen reference electrode.

Another survey is now being conducted by the ICCGR group, and results are expected to form the basis for the reliable comparison of different autoclave systems and for accurate characterization of water environments.

References

1. W. H. Bamford and L. J. Ceschini, "Environmentally Assisted Crack Growth in Light Water Reactors," *Heavy-Section Steel Technology Program Quart. Prog. Rep. January-March 1983*, NUREG/CR-3334, Vol. 1 (ORNL/TM-8787/V1), Union Carbide Corp. Nuclear Div., Oak Ridge Natl. Lab.

2. W. H. Bamford, "Environmental Cracking of Pressure Boundary Materials and the Importance of Metallurgical Considerations," *Aspects of Fracture in Pressure Vessels and Piping*, ASME Publication PVP 58, American Society of Mechanical Engineers, New York, 1982.

3. P. M. Scott, "Chemistry Effects in Corrosion Fatigue," *Proceedings of the ASTM Conference on Corrosion Fatigue, St. Louis, Mo., October 1981*, to be published by American Society for Testing and Materials, 1983.

4. *ASME Boiler and Pressure Vessel Code*, Sect. XI, 1980 ed., Winter 1980 Addendum, American Society of Mechanical Engineers, New York.

5. F. P. Ford, Principal Investigator, *Mechanisms of Environmental Cracking in Systems Peculiar to the Power Generation Industry*, Electric Power Research Institute Report NP-2589 (Final Report), prepared by General Electric Company, September 1982.

6. P. L. Andresen, *Innovations in Experimental Techniques for Testing in High Temperature Aqueous Environments*, Report 81CRD088, General Electric Company, Schenectady, N.Y., May 1981.

CONVERSION FACTORS[a]

SI unit	English unit	Factor
mm	in.	0.0393701
cm	in.	0.393701
m	ft	3.28084
m/s	ft/s	3.28084
kN	lb_f	224.809
kPa	psi	0.145038
MPa	ksi	0.145038
$MPa \cdot \sqrt{m}$	$ksi \cdot \sqrt{in.}$	0.910048
J	ft·lb	0.737562
K	°F or °R	1.8
kJ/m^2	$in.-lb/in.^2$	5.71015
$W \cdot m^{-2} \cdot K^{-1}$	$Btu/h-ft^2-°F$	0.176110
kg	lb	2.20462
kg/m^3	$lb/in.^3$	3.61273×10^{-5}
mm/N	$in./lb_f$	0.175127
$T(°F) = 1.8\ T(°C) + 32$		

[a]Multiply SI quantity by given factor to obtain English quantity.

NUREG/CR-3334
Volume 2
ORNL/TM-8787/V2
Dist. Category RF

Internal Distribution

1. D. G. Ball
2. B. R. Bass
3. R. G. Berggren
4. S. E. Bolt
5. R. H. Bryan
6. J. W. Bryson
7. R. D. Cheverton
8. J. M. Corum
9. W. R. Corwin
10-11. D. S. Griffith
12. R. C. Gwaltney
13. F. J. Homan
14. S. K. Iskander
15. K. K. Klindt
16. A. P. Malinauskas
17. S. S. Manson
18. R. W. McCulloch
19. J. J. McGowan
20. J. G. Merkle
21-22. R. K. Nanstad
23. D. J. Naus
24-28. C. E. Pugh
29. G. C. Robinson
30. J. W. Roddy
31. G. M. Slaughter
32. J. E. Smith
33. W. J. Stelzman
34. K. R. Thoms
35. H. E. Trammell
36. C. D. West
37-40. G. D. Whitman
41. G. T. Yahr
42. ORNL Patent Office
43. Central Research Library
44. Document Reference Section
45-46. Laboratory Records Department
47. Laboratory Records (RC)

External Distribution

48. C. Z. Serpan, Division of Engineering Technology, Nuclear Regulatory Commission, Washington, DC 20555
49. M. Vagins, Division of Engineering Technology, Nuclear Regulatory Commission, Washington, DC 20555
50. Office of Assistant Manager for Energy Research and Development, DOE, ORO, Oak Ridge, TN 37830
51-52. Technical Information Center, DOE, Oak Ridge, TN 37830
53-327. Given distribution as shown in category RF (NTIS - 10)

☆U.S. GOVERNMENT PRINTING OFFICE: 1983-646-055/209

NRC FORM 335 (11-81)

U.S. NUCLEAR REGULATORY COMMISSION

BIBLIOGRAPHIC DATA SHEET

1. REPORT NUMBER (Assigned by DDC)
NUREG/CR-3334, Vol. 2
ORNL/TM-8787/V2

4. TITLE AND SUBTITLE (Add Volume No., if appropriate)
Heavy-Section Steel Technology Program Quarterly Progress Report for April-June 1983

2. (Leave blank)

3. RECIPIENT'S ACCESSION NO.

7. AUTHOR(S)
C. E. Pugh

5. DATE REPORT COMPLETED
MONTH: October | YEAR: 1983

9. PERFORMING ORGANIZATION NAME AND MAILING ADDRESS (Include Zip Code)
Oak Ridge National Laboratory
P.O. Box X
Oak Ridge, TN 37830

DATE REPORT ISSUED
MONTH | YEAR

6. (Leave blank)

8. (Leave blank)

12. SPONSORING ORGANIZATION NAME AND MAILING ADDRESS (Include Zip Code)
Division of Engineering Technology
Office of Nuclear Regulatory Research
U.S. Nuclear Regulatory Commission
Washington, DC 20555

10. PROJECT/TASK/WORK UNIT NO.

11. FIN NO.
B0119

13. TYPE OF REPORT
Quarterly

PERIOD COVERED (Inclusive dates)
April through June 1983

15. SUPPLEMENTARY NOTES

14. (Leave blank)

16. ABSTRACT (200 words or less)

The Heavy-Section Steel Technology (HSST) Program is an engineering research activity conducted by the Oak Ridge National Laboratory for the Nuclear Regulatory Commission. The program comprises studies related to all areas of the technology of materials fabricated into thick-section primary-coolant containment systems of light-water-cooled nuclear power reactors. The investigation focuses on the behavior and structural integrity of steel pressure vessels containing cracklike flaws. Current work is organized into seven tasks: (1) program administration and procurement, (2) fracture-mechanics analyses and investigations, (3) investigations of irradiated materials, (4) thermal-shock investigations, (5) pressure vessel investigations, (6) stainless steel cladding investigations, and (7) environmentally assisted crack growth studies.

17. KEY WORDS AND DOCUMENT ANALYSIS

17a. DESCRIPTORS

Pressure vessels
Ferritic steels
Weldments
Irradiation
Cladding
Flaws
Thermal shock
Fracture mechanics
Toughness
Crack arrest
Crack growth

17b. IDENTIFIERS/OPEN-ENDED TERMS

18. AVAILABILITY STATEMENT
Unlimited

19. SECURITY CLASS (This report)
Unclassified

21. NO. OF PAGES

20. SECURITY CLASS (This page)
Unclassified

22. PRICE
$

NRC FORM 335 (11-81)